U.S.N.A - - - Trident Scholar project report; no. 373 (2008)

# The Effect of Diameter on Dynamic Seabed Penetration

by

Midshipman 1/c Catherine M. Ortman
United States Naval Academy
Annapolis, Maryland

_____
(signature)

Certification of Adviser Approval

CDR Patrick J. Hudson, USN
Naval Architecture and Ocean Engineering Department

_____
(signature)

_____
(date)

Acceptance for the Trident Scholar Committee

Professor Joyce E. Shade
Deputy Director of Research & Scholarship

_____
(signature)

_____
(date)

USNA-1531-2

# REPORT DOCUMENTATION PAGE

Form Approved
OMB No. 074-0188



| 1. AGENCY USE ONLY (Leave blank) | 2. REPORT DATE | 3. REPORT TYPE AND DATE COVERED |
|---|---|---|
| | 2 May 2008 | |

**4. TITLE AND SUBTITLE**
Effect of Diameter on Dynamic Seabed Penetration

**5. FUNDING NUMBERS**

**6. AUTHOR(S)**
**Ortman, Catherine M.**

| 7. PERFORMING ORGANIZATION NAME(S) AND ADDRESS(ES) | | 8. PERFORMING ORGANIZATION REPORT NUMBER |
|---|---|---|
| | | |

| 9. SPONSORING/MONITORING AGENCY NAME(S) AND ADDRESS(ES) | | 10. SPONSORING/MONITORING AGENCY REPORT NUMBER |
|---|---|---|
| **US Naval Academy<br>Annapolis, MD 21402** | | **Trident Scholar project report no. 373 (2008)** |

**11. SUPPLEMENTARY NOTES**

| 12a. DISTRIBUTION/AVAILABILITY STATEMENT | 12b. DISTRIBUTION CODE |
|---|---|
| **This document has been approved for public release; its distribution is UNLIMITED.** | |

**13. ABSTRACT** (cont from p. 1) have indicated these algorithms tend to under predict the penetration of objects which are larger than three inches in diameter. To improve the current algorithms, a numerical and experimental study of the seabed penetration event was conducted. A computational analysis of the seabed penetration problem was conducted using the LS-DYNA finite element analysis (FEA) code. LS-DYNA was used to model the experiments, and then the model predictions were compared with experimental results. The penetration depths predicted by the model showed good agreement with experimental results for cohesionless soils. Using the USNA Oceanography Research Vessel (YP-686), three and nine inch penetrometers were repeatedly dropped off the stern and allowed to free fall to the seabed. An accelerometer attached to each penetrometer measured acceleration output beginning before release and continually throughout the drop. By integrating the acceleration data twice, the penetration depth could be calculated. Using this experimental data and equations available in the *Handbook for Marine Geotechnical Engineering*, new values were calculated for the strain rate factors of objects larger than three inches in diameter.

| 14. SUBJECT TERMS | 15. NUMBER OF PAGES |
|---|---|
| seabed mechanics, sediment, shear strength, penetrometer, strain rate | **135** |
| | 16. PRICE CODE |

| 17. SECURITY CLASSIFICATION OF REPORT | 18. SECURITY CLASSIFICATION OF THIS PAGE | 19. SECURITY CLASSIFICATION OF ABSTRACT | 20. LIMITATION OF ABSTRACT |
|---|---|---|---|
| | | | |

## Abstract

An accurate estimate of the undrained shear strength of seabed sediments is critical to the design of foundations and anchors of offshore structures. Naval mine warfare and undersea salvage also depend on the prediction of seafloor embedment depth, which is primarily a function of sediment strength. Direct measurement of *in-situ* sediment strengths in the offshore environment is often difficult using conventional methods, especially where depths prohibit the use of divers. Sediment core samples can be analyzed using various laboratory methods, including tri-axial and vane-shear testing, but sample disturbance during collection may introduce inaccuracy into these measurements.

Dynamic soil penetrometers have been increasingly employed in recent years to profile seafloor sediment strength. These penetrometers are normally deployed from the sea surface, with either the velocity or acceleration measured throughout the fall to the seafloor. Total embedment and undrained shear strength are estimated from the resulting measured velocity profile, using an algorithm first described by True and later refined by Rocker in the *Handbook for Marine Geotechnical Engineering*.

The method in the *Handbook* is a quasi-static approach, where work done on the penetrometer is calculated at each time step, and subtracted from the total kinetic energy before advancing to the next step. The empirical strain rate factors used in the calculations to modify the static bearing and shear strengths of the sediment are based on a best fit to penetration test data using long, cylindrical penetrometers of three inches or less in diameter. Although there are current algorithms for predicting dynamic penetration of the seafloor in the *Handbook*, recent experiments have indicated these algorithms tend to under predict the penetration of objects which are larger than three inches in diameter.

To improve the current algorithms, a numerical and experimental study of the seabed penetration event was conducted. A computational analysis of the seabed penetration problem was conducted using the LS-DYNA finite element analysis (FEA) code. LS-DYNA was used to model the experiments, and then the model predictions were compared with experimental results. The penetration depths predicted by the model showed good agreement with experimental results for cohesionless soils.

Using the USNA Oceanography Research Vessel (YP-686), three and nine inch penetrometers were repeatedly dropped off the stern and allowed to free fall to the seabed. An accelerometer attached to each penetrometer measured acceleration output beginning before release and continually throughout the drop. By integrating the acceleration data twice, the penetration depth could be calculated. Using this experimental data and equations available in the *Handbook for Marine Geotechnical Engineering*, new values were calculated for the strain rate factors of objects larger than three inches in diameter.



## Keywords

seabed mechanics, sediment, shear strength, penetrometer, strain rate

## Acknowledgments

First and foremost I want to thank CDR Patrick Hudson, my advisor, who agreed to guide me for an entire year of my first attempt at independent research. I am thankful for his counsel, patience, faith, and confidence in me. Generous amounts of his time and commitment went into helping me develop my research skills. His words of encouragement, quiet urgings, and careful reading of all of my writing will never be forgotten. His valuable advice and criticism much improved the quality of the final report.

I am also extremely grateful for the assistance, advice, and encouragement I received from Emily Ward at Johns Hopkins Applied Physics Lab where I worked for a very short duration at the beginning of my research. Emily not only is responsible for initially teaching me how to use LS-DYNA, she supported me through all of my LS-DYNA challenges. She found me resources, offered to trouble-shoot my keyword files, and stood by to make sure her suggestions worked. I cannot thank her enough.

I would like to thank the members of the Trident Scholar Committee, especially my point of contact, Professor Sarah Mouring, and my readers, Professor Deborah Konkowski and Professor Daryl Boden, for their time and guidance. I have benefited greatly from their comments and suggestions. A special thanks to Professor Mouring for lending a sympathetic ear and putting my toils in perspective. The support of the Trident Scholar Committee Co-chair, Professor Joyce Shade, was also greatly appreciated. Without Professor Shade, none of this research would have been possible or as well organized. A special thanks also to the Oceanography YP and Kenneth Zepp.

I thank my parents and sister for their persistent belief that despite their incomprehension about what I do, I must be saving the world. I am indebted to my parents for instilling in me the dedication and discipline to do whatever I undertake well. I cannot thank my sister enough for her support, encouragement, and advise to relax every now and then.

Of course, my studies would not have been the same without the social and academic challenges and diversions provided by all my student-colleagues in the Ocean Engineering major. A special thanks to my Capstone Design Team for allowing me to make our project a secondary priority.

Finally, I am thankful for the many distractions I have enjoyed during my time at the Naval Academy. Without them, crossing over to the realms of insanity would have been entirely within reach. My various hobbies, my wonderful sponsor parents, and the crew team have conspired to ensure that the road to my goal was not as bumpy as it could have been.

## Table of Contents

## List of Figures and Tables

# The Effect of Diameter on Seabed Penetrometer Dynamic Performance

MIDN 1/C Cate Ortman, USN

## Introduction

An accurate estimate of the undrained shear strength of seabed sediments is critical to the design of foundations and anchors of offshore structures. For many Navy applications, including Intelligence, Surveillance, and Reconnaissance (ISR) missions, mine countermeasures, and undersea salvage, accurate prediction of seafloor embedment depth, which is primarily a function of sediment strength, is critical to mission success. Direct measurement of *in-situ* sediment strengths in the offshore environment is often difficult using conventional methods, especially where depths prohibit the use of divers. Sediment core samples can be analyzed using various laboratory methods, including tri-axial and vane-shear testing, but sample disturbance during collection may introduce inaccuracy into these measurements. More recently, the Navy has used a dropped penetrometer called the eXpendable Doppler Penetrometer (XDP) to measure the undrained soil strength of seafloor sediments.

The XDP estimates sediment shear strength by measuring the instantaneous velocity of a sound source probe as it descends through the water and penetrates the seafloor. Soil strength is determined from the rate of velocity change of the penetrometer as it enters the seafloor and comes to rest. The research that the Navy has conducted was originally prompted by the requirement for a design of direct embedment anchor (Bowman, 1995). However, the XDP is now widely used by the Navy to characterize deep sea and littoral sediments worldwide.

**Background**

Cone penetrometers, as shown in Figure 1, are commonly used in civil engineering to measure soil strength properties (Das, 2005). Dynamic soil penetrometers have been increasingly employed in recent years to profile seafloor sediment strength. The U.S. Navy has developed the XDP to determine *in-situ* soil strength in deep water depths. Penetrometers are normally deployed from the sea surface, with either the velocity or acceleration measured throughout their fall to the seafloor. Total embedment and undrained shear strength are estimated from the resulting measured velocity profile, using an algorithm first described by True (1976) and later refined by Rocker (1985). Using the XDP, cohesive soil strengths were studied in three different sites in Alaska and Washington State by the Naval Facilities Engineering Command (NFESC) in 2001 (Thompson, 2002). Also, cohesionless soil strengths were studied by NFESC using a calcareous sand site off the coast of Key West, FL and a denser quartz/mineral sand off the coast of Biloxi, MS (Orenberg, 1996). In the Gulf of Mexico, reasonable values for the undrained shear strength of soft clays were obtained using the acceleration measurements of an expendable penetrometer (Aubeny and Shi, 2006).

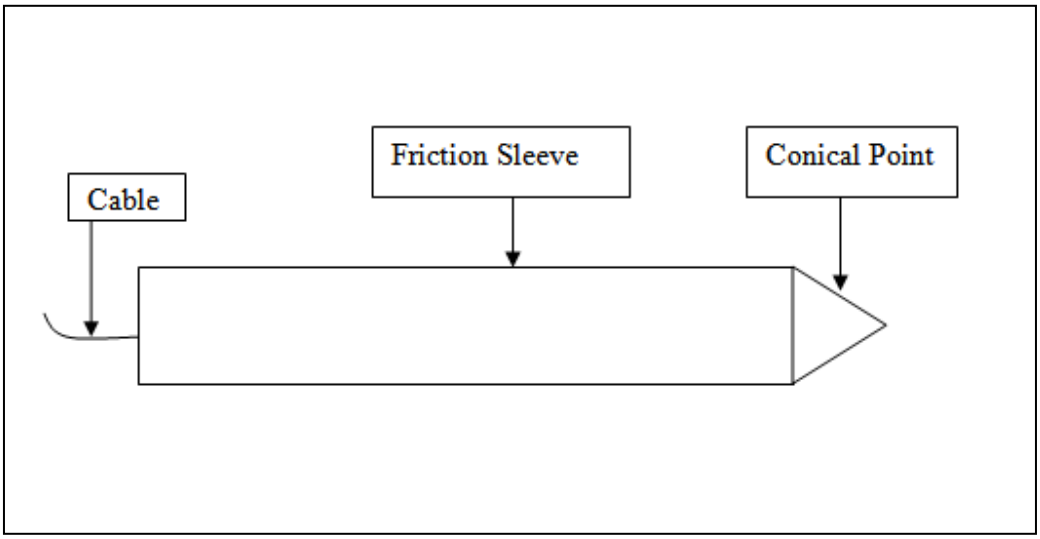


**Figure 1.** Basic penetrometer profile

Although there are current algorithms for predicting dynamic penetration of the seafloor already in use, recent experiments have indicated that these algorithms tend to under-predict the penetration of objects which are larger than three inches in diameter. One possible source of prediction error may be in the empirical strain rate constants developed by the Navy using experimental data. These previous Navy experiments used long, slender penetrators with diameters of 3.5 inches or less. When objects with diameters of 3 inches or more impact the seafloor, the strain rate effects may not scale linearly with diameter as the original Navy algorithms assume (Rocker, 1985).

For many Navy and civilian applications, accurate predictions of penetration depth is critical to mission success. Very few experiments have been conducted using penetrometers with larger diameters. For the purpose of mine burial prediction, experimentation using various size penetrometers was used to obtain bearing strength profiles of seafloor sediments in Australia (Mulhearn, 2002). As the diameter of the penetrometer increased, bearing strength decreased less rapidly, but still provided accurate penetration depth prediction. In agreement with his

results, Mulhearn recommended the use of the 190 mm (7.48 in) AUSSI (Australian Sediment Strength Instrument) and the 70 mm (2.76 in) STING (Seabed Terminal Impact Naval Gauge) for obtaining accurate bearing strength profiles. One method to improve current algorithms is to experimentally determine the effect of larger diameters on the empirical strain rate constants. Numerical modeling of the seabed penetration event may also be employed to better understand the dependence of diameter on sediment strain rates.

Engineering design has been using finite element analysis for over 30 years, but the accuracy of results for large deformation problems is still of concern. A finite element analysis of a penetrometer three inches in diameter or greater penetrating the seabed is considered large deformation because the penetrometer's vertical displacement is several times the diameter of the penetrometer. More recently, it has become possible to use finite element (FE) analysis to model large deformation problems because of improvements which allow for remeshing to avoid element distortion. In 2001, penetration in normally consolidated and heavily overconsolidated cohesive soils was modeled using the finite element program, elastoplastic-viscoplastic coupled system-soil (EPVPCS-S) by Voyiadjis and Kim. The results of the finite element analysis were compared with experimental data and very good agreement was shown for the profiles of cone resistance and excess pore water pressure. In 2004, the penetration of two soils, a sandy loam and clay loam, was modeled using MSC/DYTRAN, a commercially available finite element software (Foster et al., 2004). When compared to existing penetration data, the results of the FE analysis agreed with existing data for the sandy loam and under predicted penetration in the clay loam. Also in 2004, cone penetration of a cohesionless soil was modeled using ABAQUS, a commercial finite element program (Huang et al., 2004). The soil was modeled as an elastic-perfect-plastic obeying the Mohr-Coulomb criterion and penetrometer was assumed to be rigid.

Penetration depth in the model was found to be dependent on soil properties and the cone resistances calculated through FE analysis showed agreement with empirical correlations based on cavity-expansion theory. In 2007, cone penetration of a Norfolk sandy loam soil that varied in soil moisture content and bulk density was modeled using ABAQUS to predict the location of the hardpan in the soil (Tekeste et al., 2007). The finite element analysis was found to predict the hardpan to be located at depths shallower than experimental results. The main parameters found to be affecting the finite element analysis were soil moisture, bulk density, and cone surface conditions.

Currently, dynamic penetration of objects into the seafloor is typically predicted using a quasi-static approach described in the *Handbook for Marine Geotechnical Engineering* (Rocker, 1985). In this method, the work done on the penetrometer is calculated at each time step, and subtracted from the total kinetic energy before advancing to the next step. The empirical strain-rate constants used in the calculations to modify the static bearing and shear strengths of the sediment are based on a best-fit to penetration experiments conducted by True (1976) using long, cylindrical penetrometers of 90 mm (3.54 in) or less in diameter. Rocker also offers broad predictions of parameter values for all other object shapes (see Table 1) because little field data exists for objects of larger diameter. However, these parameter values for larger diameters are not based on experimental data. Rocker (1985) presents Equation 1 to calculate the strain rate factor, $S_{\dot{e}i}$.

**Table 1.** Values of strain rate constants based on object shape (Rocker, 1985)

| **Condition for Use in Rapid Penetration Problems** | **Parameter Value** | | |
|---|---|---|---|
| | **$S_{\dot{e}}$*** | **$C_e$** | **$C_o$** |
| Problems with long, cylindrical penetrators | 4 | 4 | 0.11 |
| All other object shapes where inadequate penetration is of concern | 3 | 10 | 0.25 |
| All other object shapes where excess penetration is of primary concern | 2 | 40 | 1 |

$$S_{\dot{e}i} = \frac{S_{\dot{e}}^{*}}{1 + \frac{1}{\left[ C_{\dot{e}} \frac{v_{i-1}}{(s_{ui} D)} + C_o \right]^{0.5}}} \qquad (1)$$

Where:

$S_{\dot{e}}^{*}$ = maximum strain rate factor, from Table 1

$C_{\dot{e}}$ = empirical strain rate coefficient from Table 1

$v_{i\text{-}1}$ = velocity entering the *i*th layer

$C_o$ = empirical strain rate constant, from Table 1

$s_{ui}$ = soil undrained shear strength equal to $s_{ui(\text{nose})}$ or $s_{ui(\text{side})}$, depending on which of these that $S_{\dot{e}i}$ is modifying

$D$ = equivalent diameter of penetrator

**Sediment Shear Strength**

Shear strength is the measurement of a soil's ability "to resist failure and sliding along any plane inside it" (Das, 2005). In structural and mechanical engineering, a soil's shear strength determines the design of structures and selection of materials. To determine when a material will fail, the Mohr-Coulomb failure criteria is used (Equation 2).

$$\tau_f = c + \sigma \tan\phi \qquad (2)$$

Where:

$\tau_f$ = shear stress on the failure plane
$\sigma$ = normal stress on the failure plane
$c$ = cohesion
$\phi$ = angle of internal friction

According to Equation 2, a material fulfills the criteria for failure when a "critical combination of normal and shear stress" is reached (Das, 2005). In saturated soil, such as the kind used in this research, the normal stress is a combination of effective stress and pore water pressure at a point in the soil. The effective stress is the average stress carried by the solids in the soil. The angle of internal friction, $\phi$, is the angle between the failure plane and the major principal plane, which can be determined by plotting Mohr's circles (Das, 2005).

Two types of laboratory tests are used to determine the shear strength of a soil, the direct shear test and triaxial shear test. The direct shear test uses a shear box which contains the specimen. The box is horizontally split, forming two halves. A normal force is applied to the top of the box while a shear force is applied by sliding the two halves in opposite directions until

failure occurs in the soil sample. "The direct shear test is the simplest and most economical for a dry or saturated sandy soil" (Das, 2005).

In this research, two types of soil sediments were analyzed, a clay and a sand. Clays can be characterized as a cohesive soil. Cohesive soils obtain their shear strength from the electrostatic forces between their soil grains. Sands can be characterized as a cohesionless soil. Cohesionless soils obtain their shear strength solely from the friction between their soil grains (McCarthy, 1998).

A direct shear test can be run on saturated specimens of cohesionless and cohesive sediments. By allowing the pore water to drain through a porous stone in the bottom of the shear box, the excess pore water pressure created in the sample entirely dissipates if the rate of loading is slow enough (Das, 2005). Since water can easily move through the pore spaces in sand, which gives sand a high hydraulic conductivity, the excess pore water pressure, created when the sample is loaded, dissipates rapidly. Thus, the friction angle in a dry sample of sand will be the same as a saturated sample (Das, 2005).

However, the hydraulic conductivity of clay is much lower than it is for sand, meaning water cannot easily move through the pore spaces in the clay. For an accurate direct shear test, it takes 2 to 5 days for the excess pore water pressure to drain from a saturated clay sample while the rate of loading is applied very slowly (Das, 2005). However, in this research, the load is being applied very quickly to the clay, giving the excess pore water pressure no time to drain. Therefore, the excess pore water pressure must be taken into account.

The triaxial shear test is a more reliable method for determining shear strength. The soil sample is placed in a chamber where it is subjected to both a confining pressure and axial stress. Increasing axial stress is applied until failure occurs (Das, 2005). Although there are three types

of triaxial tests, consolidated-drained, consolidated-undrained, and unconsolidated-undrained, only one was applicable in this research. The unconsolidated-undrained test does not allow drainage from the soil sample while the confining pressure is being applied. The test is mostly used to measure the shear strength of saturated cohesive soils (Das, 2005).

In this research, deformation of the seafloor sediment is happening very quickly (under a second), which does not allow time for the water to drain from the sediment, making the unconsolidated-undrained test the best choice. For saturated cohesive soils, the results of an undrained test produce total stress Mohr's circles with a horizontal failure envelope, meaning an internal friction angle of zero. The failure envelope is horizontal because the same added axial stress is needed to cause failure regardless of the confining pressure. For saturated soils, when the confining pressure is increased, the total stress increase is equal to the pore water pressure increase (Das, 2005).

For cohesionless sediment (sand), a friction angle other than zero is obtained. By varying the confining pressure, different major and minor principal stresses at failure will result. These values can be used to draw Mohr's circles and obtain a failure envelope. The failure envelope will have some slope greater than zero, which is the angle of internal friction (Das, 2005).

**Theory of Dynamic Penetration**

An iterative procedure is used to calculate dynamic penetration because the resisting force terms in the problem are velocity dependent. During the procedure, the penetrator is stepped into the soil in equal finite depth increments or layers ($\Delta z$). Using the entry velocities and soil properties of each step, the resisting soil and hydrodynamic forces are calculated by using Equation 3 from Rocker (1985).

$$F_i = F_{di} + W_{bi} - Q_{ni} - F_{si} - F_{hi} \qquad (3)$$

Where:

$F_i$ = net downward force exerted by the penetrometer
$F_{di}$ = external driving force, if any
$W_{bi}$ = penetrator buoyant weight
$Q_{ni}$ = tip or nose bearing resistance
$F_{si}$ = side friction or adhesion
$F_{hi}$ = fluid drag force

The nose bearing resistance is found from calculated as

$$Q_{ni} = s_{ui(nose)} S_{ei} N_{ti} A_t \qquad (4)$$

Where:

$s_{ui(nose)}$ = soil undrained shear strength at a depth $D/2$ below $z$, averaged over $i$th increment of penetration
$S_{ei}$ = strain rate factor
$A_t$ = end area of penetrometer

Similarly, the side friction at each step is found from

$$F_{si} = \left[ \frac{s_{ui}(side)}{S_{ti}} \right] S_{ei} A_s \qquad (5)$$

Where:

$S_{ti}$ = soil sensitivity (obtained from soils testing)
$A_s$ = side area of the penetrometer
$S_{ui(side)}$ = soil undrained shear strength averaged over the length of the penetrator in contact with the soil

The energy lost by the penetrator in overcoming the resistive forces of the first layer is equal to the work performed on the soil by the penetrator, and this reduced kinetic energy is used to calculate penetrator velocity entering the next layer. The calculations are repeated for each successive layer until the kinetic energy and velocity of the penetrator reaches zero. The depth of zero velocity is the predicted penetration depth (Rocker, 1985). Figure 2 illustrates this approach where $z_i$ and $v_i$ are the penetrometer position and velocity at step $i$. The forces $F_{di}$ and $W_{bi}$ are driving the penetrator into the soil, while the other three forces, $Q_{ni}$, $F_{si}$, $F_{hi}$, are resisting penetration.

Using this theory and experimental results of penetration depth, one can work in reverse of the procedure described above to determine the strain rate factor referred to in Equation 1 for a given situation. The strain rate factor, $S_{ei}$, is a variable in determining both nose resistance, $Q_n$, and side friction, $F_s$. Therefore, nose resistance and side friction can be determined from Equations 4 and 5 once the penetration depth is known.

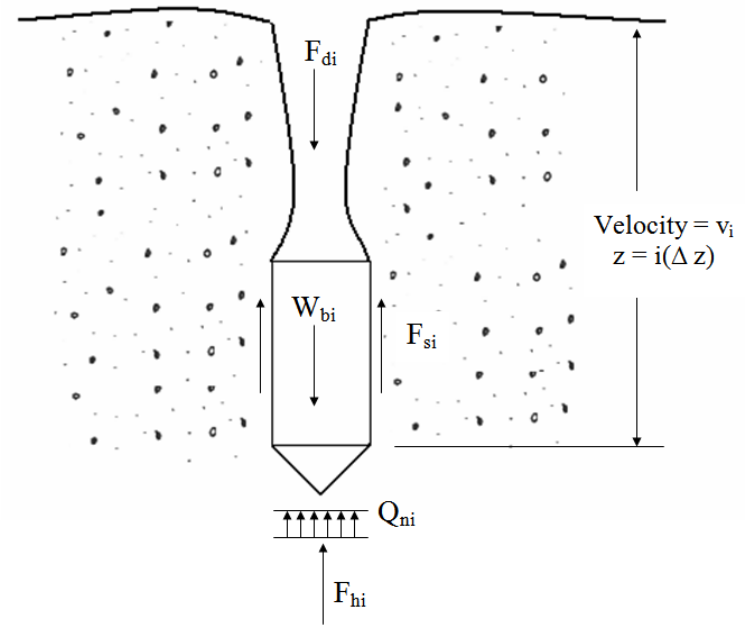


**Figure 2.** Forces acting on a penetrometer during contact with the seafloor (Rocker, 1985)

**Purpose of Project**

The objective of this project is to expand the applicability of existing algorithms for prediction of seabed penetration depth by (1) experimentally determining the effect of larger diameters on the empirical strain rate constants Se*, Ce, and Co; and (2) to use numerical modeling of the seabed penetration event to better understand the dependence of diameter on sediment strain rates.

Dynamic penetration is considered to occur when an object impacts the seafloor traveling at a velocity of three feet per second or greater, regardless if the object was being rapidly lowered or free-falling (Rocker, 1985). Improvements of the existing algorithms will be made for better prediction of the depth of penetration into the seafloor of objects larger than three inches in diameter. The new algorithms may be used to predict the depth to which an object will penetrate or the force required for a specified depth penetration. These algorithms could apply to objects such as gravity anchors, gravity corers and penetrometers, and propellant-embedded anchor plates. Application of this research therefore applies not only to the Navy, but also to oil extraction, pile driving, and underwater mines.

**Method of Investigation**

This research included both an experimental approach and numerical computer-aided analysis of the experimental approach. The experimental approach involved dropping penetrometers from the USNA Oceanography Research Vessel at three sites in the Chesapeake Bay. The drops were then modeled using LS-DYNA finite element analysis software. The research was conducted over a 9 month period from August 2007 to April 2008.

## *Numerical Analysis*

### LS-DYNA Background

A computational analysis of the seabed penetration problem was conducted using the LS-DYNA finite element analysis (FEA) code. LS-DYNA is a commercial version of the DYNA-3D Alternating Lagrangian-Eulerian (ALE) solver from Lawrence-Livermore National Laboratory (Hallquist, 2006). This code is particularly well-suited to modeling large displacement dynamic events and is used widely in the automotive and aerospace industries. A major advantage of LS-DYNA over other FEA packages is that several constitutive models for soil and fluid dynamics are included in the code, and additional soil models are available in the literature (Lewis, 2004). With these models, LS-DYNA is able to analyze both explosive-structure and soil-structure interaction problems (*LS-DYNA® Keyword*, 2007). LS-DYNA was used to model the experiments, and then the model predictions were compared with experimental results. The model time starts immediately before penetrometer impact and continues until the penetrometer stops. The model domain includes sufficient volume around the impact point so that the outer boundary remains undisturbed. Special care was taken in the development of the model to ensure that if model predictions showed reasonable agreement with experimental results, parametric study could be conducted using the model to further develop the empirical strain rate constants.

LS-DYNA uses explicit time integration as its main solution methodology (Hallquist, 2006). In this problem, the spatial discretization necessary for this process was achieved using a shell element for the penetrometer and a solid element for the soil. There are several different element formulations available in LS-DYNA and element choice relies heavily on the type of problem one is modeling. However, LS-DYNA is very capable of handling an extensive scope

of material behavior because it contains over one-hundred constitutive models and ten equations of state (Hallquist, 2006). The shell element for the penetrometer and solid element for the soil were found to be the best elements for this particular soil-structure interaction model. When the penetrometer was imported into LS-DYNA as a VDA file it was automatically read as a shell element by the program. Since the experimental penetrometer was hollow and all interactions occurred between the surface of the penetrometer and the soil, a shell element was acceptable for the penetrometer. Since the penetrometer was penetrating the soil model and interactions at the surface as well as the interior of the soil model were of concern, the soil was modeled as a solid element.

**Procedure**

The steps to use LS-DYNA to simulate a sensor impacting the ground include: (1) modeling and meshing the 3D geometry; (2) selecting the proper material model; (3) specifying the proper contact and control conditions; (4) assigning any initial conditions; (5) checking the model setup for errors or omissions; (6) running the solver to perform the actual computations; (7) post-processing the results and comparing with predicted behavior; and (8) adjusting the geometry, material model, and contact conditions as necessary to successfully simulate the impact. There are two ways to input data into LS-DYNA. A keyword file can be created and almost all model data can be input in block form using typed keyword cards. However, this is a very time consuming process. Full keyword cards of the four models created during this research can be found in Appendix A. The more efficient and intuitive way to input data, which was used to model this problem, is to use LS-Prepost, a pre- and post-processor utilizing OpenGL graphics which provides viewing and editing tools for all LS-DYNA keyword cards

(*Keyword*, 2007). An example of an input card in LS-Prepost can be seen in Figure 3. An explanation of the terms used in this input card can be found in the glossary. Each parameter in the input card can be changed manually to reflect the values of the object being modeled.

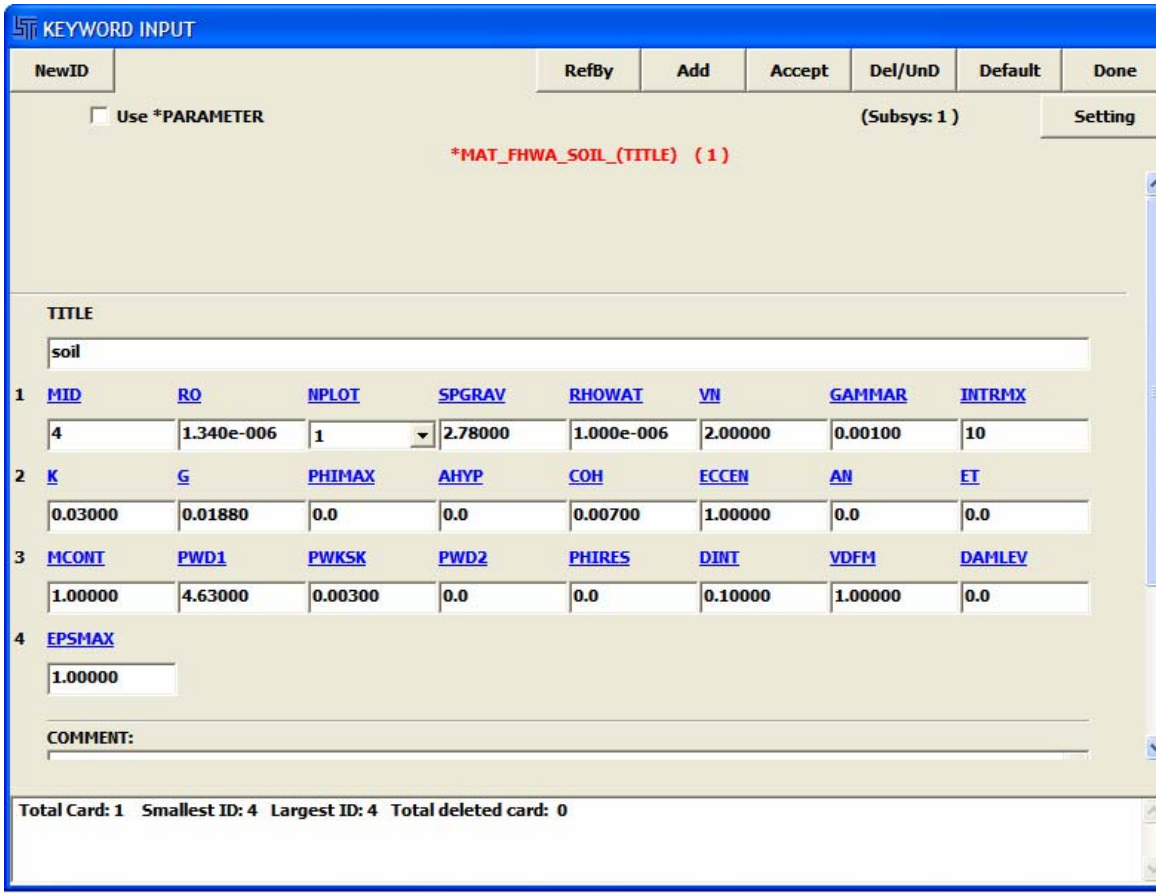


**Figure 3.** LS-Prepost input card specifying soil material parameters

For modeling the geometry of the penetrometer, SolidWorks, a commonly-used three-dimensional Computer Aided Design (CAD) software package, was used. It was used to model the penetrometer only because the simple geometry of a cylinder for the soil could be modeled in LS-DYNA. The penetrometer consisted of building a solid cylinder and connecting it to a solid cone for the penetrometer tip using the SolidWorks interface. It was decided the cone should not have a single point tip, since LS-DYNA does not handle singularities well in its calculations.

Instead, the cone tip of the penetrometer has a very small diameter circle as its front impact point. A model of the 3-inch penetrometer after being imported into LS-DYNA can be seen in Figure 4.

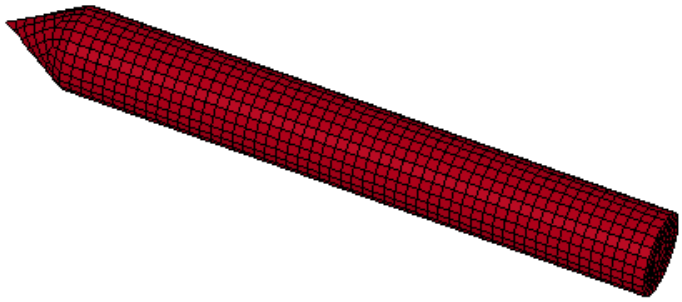

**Figure 4.** 3-inch cone penetrometer

The material models in LS-DYNA define the properties of all materials involved in the impact problem. LS-DYNA offers over 200 different model types. For the models, a basic penetrometer shape was inputted as a VDA file from SolidWorks and a cylinder with varying mesh was created to model the soil in LS-DYNA using the BlockM command. The soil's slave nodes which are capable of generating contact forces with the penetrometer's surface all exist in the central core region of the cylinder soil model. For this reason, the mesh outside the core region is considerably coarser and exists primarily to create a boundary condition that extends far enough away from the point of impact to not be affected. A model of the soil can be seen in Figure 5. Once the geometry for these shapes was inputted, selection of a proper material type was made and assigned to each. For the penetrometer, a basic material model 020-RIGID was used. This model will prevent the soil from penetrating the surface of the penetrometer. Parameters entered for this model included mass density, Young's modulus, and Poisson's ratio.

For the soil, material model 147-FHWA_SOIL was used. This model was chosen from among several soil models because it includes excess pore water effects. To define this material, over twenty parameters are necessary including, mass density, specific gravity, bulk modulus, and shear modulus.

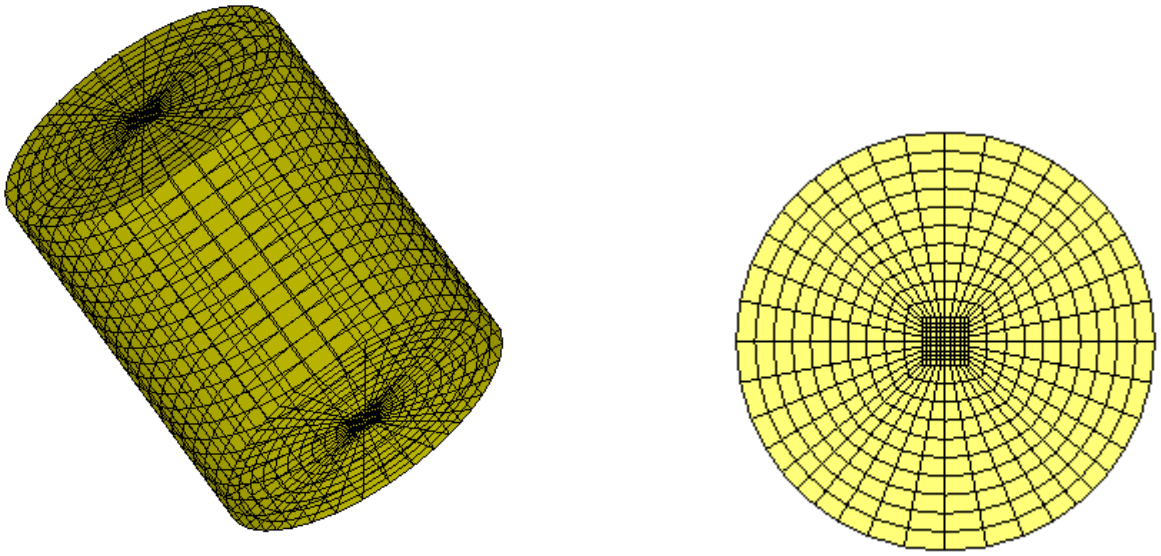

**Figure 5.** Side and top view of soil model with variable mesh

To successfully simulate impact, it is critical to properly specify the contact conditions between the object and the soil. For example, there are several options including single surface contact, one way surface to surface contact, eroding contact, and forming contact. To model the impact problem, the AUTOMATIC_ONE_WAY_SURFACE_TO_SURFACE model was used to allow penetration of the penetrometer into the soil, but not to allow penetration of the penetrometer surface. One-way contact allows for compression loads to be transferred between the slave nodes (soil) and the master segments (penetrometer). Tangential loads are also transmitted if relative sliding occurs when contact friction is active. A Coulomb friction formulation is used with an exponential interpolation function to transition from static to

dynamic friction. This transition requires that a decay coefficient be defined and that the static friction coefficient be larger than the dynamic friction coefficient (*LS-DYNA® Keyword*, 2007). The penetrometer was also assigned an initial velocity. Figure 6 is a final view of the penetrometer and soil model before analysis.

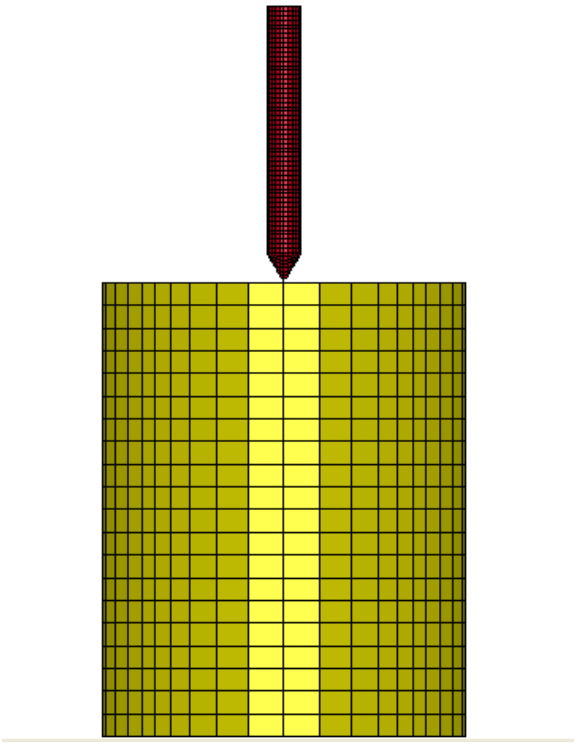

**Figure 6.** Model of soil and penetrometer

Once the model was checked for errors and any errors were corrected, the next step was to run the solver to perform the actual computations. This involves saving the model as a keyword file and then starting the LS-DYNA analysis in the program manager window. If the solver ran successfully and there were no errors, a d3plot file was created and saved by the software. This file can then be used to animate the impact problem or study the forces involved in the impact.

**Mesh Density Effect**

Since the model for the cone penetrometer was created using Solid Works and imported into LS-DYNA Prepost as a VDA file, the cone penetrometer could not be meshed until it was loaded in Prepost. Prepost automatically meshed the cone model with an acceptable mesh density for the program's capabilities. In LS Prepost, it is not possible to make the automated mesh density on an imported VDA file less dense. However, it is possible to decrease the mesh size (make the mesh more dense) using the element edit (ElEdit) interface. Using the element edit interface, an element's mesh can be split into different shapes, thus making the mesh finer.

For the experimental cone models in LS-DYNA, the automated mesh size was used. The automated mesh size for the cone is a 4-node quadrilateral shell element of 5mm by 5mm. Finer meshes created using the ElEdit interface were found to have little to no effect on the model results. Each time the mesh of the penetrometer was redefined, each mesh block was separated into equal fourths, thus increasing the density of the mesh by a power of four. Table 2 below summarizes the displacement results of the finer meshed models. A variation of maximum penetration of 6 mm in the cohesionless model is insignificant since the model is only at that penetration distance for a single second and then bounces back out. The experimenter is only concerned with the fact that the penetrometer should not penetrate more than 1.5 inches (38 mm) into the seabed.

**Table 2.** Displacement versus mesh density variation on cone

| Cone Model (3in) | Displacement (mm) |
|---|---|
| cohesion | 611.76 |
| cohesion 4x finer | 610.20 |
| cohesion 16x finer | 610.46 |
| cohesionless | 36.42 |
| cohesionless 4x finer | 29.63 |
| cohesionless 16x finer | 29.85 |
| cohesionless 64x finer | 30.36 |

The soil was modeled in LS-Prepost as a cylinder. The cylinder had a radius of 400 mm. However, a variable mesh was defined as shown in Figure 7. At the center of the cylinder is a central core which is a 90 mm square and 1000 mm long. The central core, where the contact occurs, consists of 9 mm squares, each of which is 50 mm long. All of the contact between the cone penetrometer and soil models is assumed to take place in this central core region of the soil model.

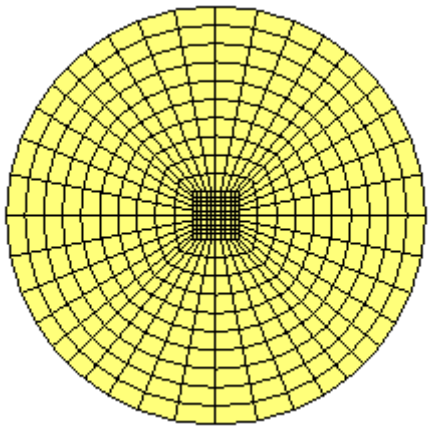

**Figure 7.** Model of soil.

Since the soil model was created as well as meshed in LS-Prepost using the BlockM interface, the creation of a range of mesh densities for the model was possible. The only limitation to how dense the central core region of the cylinder could be made was the computational power of the computer used to view, run, and analyze the model. The computer used in this experimentation was not able to analyze a file with a soil model with a central core region more than 1.4 times denser than the soil model in Figure 7. Regardless, during experimentation, it was found that a denser central core region did not affect the displacement results of the cone penetrometer. However, a less dense central core region did not provide enough contact points with the cone penetrometer's surface to provide accurate displacement

results. If the soil model was not dense enough to record contact with the cone's surface, the model produced a penetrometer that traveled completely through the 1000 mm long soil model without coming to rest. In conclusion, when modeling with LS-Prepost, mesh density should be increased until displacement results do not change. Table 3 summarizes the displacement results of the various mesh densities of the soil model.

**Table 3.** Displacement versus mesh density variation of soil

| Soil Model (using 3in cone model) | Displacement (mm) |
|---|---|
| cohesion | 611.76 |
| cohesion 1.4x finer | 611.76 |
| cohesion 5x less fine | >1000 |
| cohesion 2x less fine | >1000 |
| cohesion 1.43x less fine | >1000 |
| cohesion 1.11x less fine | >1000 |

**FHWA Soil Material Model 147**

Soil Material Model 147 was chosen for this research because it is an advanced soil model which includes strain softening, kinematic hardening, strain rate effects, element deletion, and most importantly, excess pore water effects, which was necessary since the soil being modeled in this research was saturated (Hallquist, 2006). The material model was developed by Brett Lewis for Federal Highway Administration in 2004 to analyze the dynamic soil-structure interaction of foundation soils and roadside safety structures during collisions by motor vehicles. Due to lack of material property data, the model was developed based on a single set of data available for cohesionless soils (Lewis, 2004). Yet, the soil modeled in this research has cohesion. However, the model was applicable since, according to the Manual for Material Model 147, the model can be applied to any soil type as long as only "one surface is exposed to the elements" (Lewis, 2004).

Material models for soils incline towards complexity, with determination of input parameters as the most difficult task (Lewis, 2004). The researcher believes this complexity often has led to arbitrary tweaking of models to obtain simulation results that correspond to physical data. When input parameters are tweaked without regard for their accepted values, the model can no longer be used in parametric study. For parametric study, all values must be able to be obtained through physical testing and/or calculation. If a model is tweaked, parametric study becomes impossible. The LS-DYNA Theory Manual contains equations which can be used to determine the input parameters. However, not all parameter and default values of the model could be validated with testing by the developers or evaluators (Lewis, 2004). Suggested values for the parameters are available in the Evaluation of LS-DYNA Soil Material Model by Reid and Coon (2004) and in the results of extensive sensitivity and trade studies performed by Wayne Lee (2006) in his dissertation on Numerical Modeling of Blast-induced Liquefaction. A discussion of each of the model's parameters (found in Table 4) and their values follows. Actual values used in the model can be found in Table 8 and Table 9 on page 42.

**Table 4.** FHWA Soil Material Model 147 Parameters

| | |
|---|---|
| Elastic and Soil Characteristics | **K** (bulk modulus or nonporous bulk modulus if pore-water effects are used, K)<br>**G** (shear modulus, G)<br>$\gamma_{sp}$ (specific gravity, Spgrav)<br>$m_c$ (moisture content, 0.0-1.00, Mcont)<br>$\rho$ (density of soil, RO) |
| Plasticity | $\varphi$ (friction angle, radians, Phimax)<br>**c** (cohesion, units of stress, Coh)<br>**ahyp** (coefficient for modified Drucker-Prager surface, units of stress, Ahyp)<br>**e** (eccentricity parameter for third invariant effects, Eccen) |
| Pore-Water Effects | $D_1$ (parameter for pore-water effects on bulk modulus, Pwd1)<br>$K_{sk}$ (skeleton bulk modulus pore-water parameter, PwKsk)<br>$D_2$ (parameter for pore-water effects on effective pressure, Pwd2) |
| Strain Hardening | $A_n$ (strain hardening, percent of phimax where nonlinear effects start, $A_n$)<br>$E_t$ (strain hardening, amount of nonlinear effects, $E_t$) |
| Strain Softening | $\xi_0$ (volumetric strain at initial damage threshold, Dint)<br>$G_f$ (void formation energy, Vdfm)<br>$\varphi_{res}$ (minimum internal friction angle used for residual strength, radians, Phires) |
| Strength Enhancement Caused by Strain-rate Effects | $\gamma$ (viscoplasticity parameter, strain-rate-enhanced strength, Gammar)<br>**n** (viscoplasticity parameter, strain-rate-enhanced strength, $V_n$) |
| Element Deletion | **Damlev:** Level of damage that will cause element deletion (0.0-1.0)<br>**Epsmax:** Maximum principal failure strain |
| Miscellaneous | **Nplot:** Element plotting variable to put into effective plastic strain variable<br>**Rhowat:** Density of water in model units, used to determine air void strain (saturation)<br>**Itermax:** Maximum number of iterations used in plasticity iterations |

*Bulk Modulus, K*

The bulk modulus is "an elastic constant that reflects the resistance of the material to an overall gain or loss of volume under conditions of hydrostatic stress." The evaluators recommended values of 23.00 to 36.80 MPa for silty sand and values of 46.00 to 115.00 MPa for sand and gravel (Reid and Coon, 2004). For this research, silty sand values were taken as the same values that would be found for saturated clay.

*Shear Modulus, G*

Shear modulus of elasticity "relates shear stress to shear strain." The evaluators recommended values of 13.80 to 22.08 MPa for silty sand and 27.60 to 69.00 MPa for sand and gravel (Reid and Coon, 2004).

*Specific Gravity, Spgrav*

Specific gravity is the ratio of the soil solids in the model to the density of water. The evaluators recommended a value for silts and clay of 2.78 and a value of 2.65 for sand and gravels (Reid and Coon, 2004).

*Moisture Content, Mcont*

Soil shear strength is considerably reduced as moisture content increases. The moisture content of saturated clay is 100 percent and the evaluators recommended a value of 3.4 percent for sand (Reid and Coon, 2004).

*Friction Angle, Phimax*

Phimax "represents the effect that increasing effective normal stress has on the shear strength of the soil." The evaluators recommended a baseline value of 63 degrees for cohesionless soils (Reid and Coon, 2004). Lee (2006), however, found that the value for the maximum allowable internal friction angle did not affect the results or the run time of the model significantly and recommended a baseline value of 35 degrees for cohesionless soils. An angle of zero degrees was used to model cohesive soil (clay) because an unconsolidated and undrained clay specimen has an undrained shear strength that is independent of pressure, thus, it has a horizontal line for its failure envelope (Das, 2005).

*Cohesion, Coh*

Cohesion, or shear strength, can be found by direct shear testing. The developer of material model 147 recommended a value of 6.2e-6 GPa for cohesionless soil (Reid and Coon, 2004). Lee (2006) found that results do not vary significantly due to the value of cohesion if the value is small. Lee also found that a high cohesion value will lead to excessive element distortion and a near-zero value will lead to excessive run time. Therefore, Lee recommended a cohesion value of 2 psi for a clay layer.

*Coefficient for Modified Drucker-Prager Surface, Ahyp*

A "reasonable approximation" of Ahyp can be found by treating Ahyp as a function of the angle of internal friction and cohesion, as seen in equation 6 (Reid and Coon, 2004).

$$Ahyp = \frac{c}{20}\cot(\phi) \qquad (6)$$

*Eccentricity Parameter for Third Invariant Effects, Eccen*

The value specified for Eccen generalizes the shape of the yield surface. A circular cone surface is formed when Eccen is set to 1.00. A triangular surface is formed when Eccen is set to 0.55. The developer of the model recommended a value of 0.70 for Eccen because it forms a smooth yield surface without over-smoothing the corners of the yield surface. However, the evaluators of the model "are unaware of any physical testing or theoretical means for determining recommended values for Eccen" (Reid and Coon, 2004).

*Parameter for Pore-water Effects on Bulk Modulus, Pwd1*

Pwd1 is "a constant relating the stiffness of the soil material before the air voids are collapsed." As the value of Pwd1 is increased, the stiffness of the response of the soil decreases (Reid and Coon, 2004). The developer recommended values for Pwd1 between 0.0 and 10.0 (Lewis, 2004). In fully saturated soil, Lee (2006) estimated the parameter to be 3.19E-05 per psi.

*Skeleton Bulk Modulus Pore-water Parameter, Pwksk*

The skeleton bulk modulus "determines the amount of effect that pore-water pressure has on the bulk modulus." To eliminate pore-water effects, this parameter can be set to zero. However, the evaluators "are unaware of any physical testing or theoretical means for determining specific recommended values" (Reid and Coon, 2004). Through trade study, Lee (2006) recommended a value between 5% and 20% of the corresponding value for bulk modulus, K, to achieve "maximum stability, reasonable run time, and reasonable amount of pore-water pressure build-up."

*Parameter for Pore-water Effects on Effective Pressure, Pwd2*

Pwd2 is one of the factors used to calculate a value for the pore-water pressure. As pore water pressure increases to excess, the shear strength of the soil is reduced. However, the evaluators "are unaware of any physical testing or theoretical means for determining specific recommended values" (Reid and Coon, 2004). In fully saturated soil, Lee (2006) showed that the parameter has no effect on pore water pressure and should therefore be input as zero.

*Strain Hardening, $A_n$ and $E_t$*

$E_t$ is the "amount of nonlinear strain hardening effects desired" and it "affects the rate at which nonlinear hardening occurs." $A_n$ is "the percentage of Phimax where nonlinear behavior begins." The evaluators "are unaware of any physical testing or theoretical means for determining the recommended values for $A_n$ and $E_t$" (Reid and Coon, 2004). Through trade studies, Lee (2006) found that "pore pressure results vary significantly as value of $E_t$ changes." The shortest run time occurred when $E_t$ equaled zero, meaning the friction angle did not increase with respect to strains. Different values for $A_n$ were found not to have a dramatic effect on pore pressure (Lee, 2006).

*Maximum Number of Iterations Used in Plasticity Iterations, Intrmx*

Intrmx "controls the number of iterations for the plasticity routine" (Reid and Coon, 2004). The developer recommended a value of 10 (Lewis, 2004). Through trade study, Lee (2006) recommended a value between 10 and 20. At a value of 20 or greater, Lee found that more iterations did not improve the accuracy of the model and increased the run time.

*Minimum Internal Friction Angle Used for Residual Strength, Phires*

Phires is "the angle, in radians, of the slope of the failure envelope" and it is material-dependent (Reid and Coon, 2004). The developer recommended a value between 0 and .001 radians for cohesionless soils (Lewis, 2004). Lee (2006) found that at an angle above 15 degrees results appear to stabilize and recommended a value of 30 degrees for cohesionless soils. However, Phires is a product of the tangent of Phimax. Therefore, in an undrained cohesive specimen (clay) the value of Phires is zero because Phimax is zero.

*Viscoplasticity Parameters, Strain-rate-enhanced Strength, Gammar and $V_n$*

According to the evaluators, if Gammar is set to 0.0 strain-rate-enhanced strength effects are eliminated, regardless of the value of $V_n$. The evaluators found that "additional work must be performed to determine the appropriate values for these strain-rate parameters" (Reid and Coon, 2004). Lee (2006) found that as Gammar decreases pore pressure decreases and run time increases. Lee also found that as $V_n$ decreases both pore pressure and run time increase. Lee performed trade studies and found "stable and consistent trends" for Gammar values between 1.0E-04 and 1.0E+03. Lee suggested that appropriate values are subjective depending on pore-pressure and run time magnitudes (Lee, 2006).

*Volumetric Strain at Initial Damage Threshold, Dint*

Dint is the "volumetric strain at peak pressure," which is the same as "the point where damage effects begin to occur." The evaluators "are unaware of any physical testing or theoretical means for determining the recommended values" (Reid and Coon, 2004). A trade study performed by Lee (2006) found that as Dint increased to 0.1, run time decreased. Other aspects of the model,

including stability, convergence, and results were not affected by several orders of magnitude change in Dint. Lee stated, "value is subjective based on personal preference when insufficient data are available to specify exact value."

*Void Formation Energy, Vdfm*

Mesh sensitivity in finite element models produces erroneous results. A softening parameter calculated using Vdfm is used to "reduce the effects of strain softening on mesh sensitivity." However, the evaluators "are unaware of any physical testing or theoretical means for determining the recommended [value]" (Reid and Coon, 2004). Trade studies by Lee (2006) found that when the Vdfm value equals zero "oscillatory and divergence behaviors are observed." Like Dint, Lee stated the value is "subjective when no data is available."

*Level of Damage that Will Cause Element Deletion, Damlev*

Damlev was created to delete elements during an analysis because as damage to a model increases there is a high likelihood that element distortion will increase. However, the evaluators "are unaware of any physical testing or theoretical means for determining the recommended [value]" (Reid and Coon, 2004). Lee (2006) recommended a value of zero (no deletion) because he found that when elements are deleted from a model a detrimental shock wave is produced.

*Maximum Principal Failure Strain, Epsmax*

Epsmax is the "maximum principal failure strain at which the element is deleted." The evaluators "are unaware of any physical testing or theoretical means for determining the

recommended values" (Reid and Coon, 2006). However, if Damlev equals zero, the value of Epsmax is ignored during analysis (Lee, 2006).

*Element Plotting Variable, Nplot*

Nplot offers several plotting options depending on which type of information concerning the soil the modeler would like plotted. Six options are given when modeling.

**Parametric Effects**

Certain parameters of Material Model 147 were varied to determine their effect on the overall output of the model. Each parameter was varied in increments of five percent, up to twenty-five percent, in both the negative and positive directions. The parameters that were evaluated were the bulk modulus, shear modulus, friction angle, cohesion, and the number of iterations, Itermax. For this parameter evaluation, a 3-inch model was used which had a penetrometer which had a low enough mass so that the penetrometer would come to complete rest in the soil. It was found that by varying the shear modulus, friction angle, and number of iterations the output of the three inch cohesive model was not affected as can be seen in Table 5.

**Table 5.** Effect of change in parameters G, Coh, Itermax on model displacement

| % Change | Shear Modulus, G | Model Displacement, mm | Cohesion, Coh | Model Displacement, mm | Number of Iterations, Itermax | Model Displacement, mm |
|---|---|---|---|---|---|---|
| -25 | 0.01035 | 611.95 | 0.00525 | 611.76 | | |
| -20 | 0.01104 | 612.21 | 0.00560 | 611.76 | 8 | 611.76 |
| -15 | 0.01173 | 611.95 | 0.00595 | 611.76 | | |
| -10 | 0.01242 | 611.83 | 0.00630 | 611.76 | 9 | 611.76 |
| -5 | 0.01311 | 611.95 | 0.00665 | 611.76 | | |
| 0 | 0.01380 | 611.76 | 0.00700 | 611.76 | 10 | 611.76 |
| 5 | 0.01449 | 611.56 | 0.00735 | 611.76 | | |
| 10 | 0.01518 | 611.71 | 0.00770 | 611.76 | 11 | 611.76 |
| 15 | 0.01587 | 611.69 | 0.00805 | 611.76 | | |
| 20 | 0.01656 | 611.62 | 0.00840 | 611.76 | 12 | 611.76 |
| 25 | 0.01725 | 611.57 | 0.00875 | 611.76 | | |

However, it was expected that by varying cohesion the model output would be affected. To apply the LS-DYNA models of this study to the depth of penetration of varying diameter penetrometers in varying sediment types, the cohesion parameter must be changeable based on the sediment type and different penetration depths should result. However, this result did not occur. Even when the cohesion parameter was varied by 2000 percent, there was no effect on the model's displacement. This result may have occurred because Material Model 147 was created for the National Cooperative Highway Research Program (NCHRP) 350 roadside safety hardware testing, but no material property data was available during the model's development. Instead, the model was "developed based on the one set of data available and the general behavior of cohesionless soils (Lewis, 2004). Since the cohesion parameter is zero or close to it in cohesionless soils, the cohesion parameter may not have been fully developed to handle cohesive soil values. If Material Model 147 is to be used in future research of cohesive soils, the cohesion parameter needs to be improved. However, APTEK Inc., the company which maintains Material Model 147, has no contract to further develop the material model (Murray, 2008).

The friction angle, Phimax, was found also to have no effect on the output of the 3-inch cohesionless model. The friction angle was varied in the cohesionless model instead of the cohesive model because the friction angle is zero in saturated cohesive soils. Also, as Phimax was varied it was necessary to vary the Ahyp parameter as well, since the two values are related by Equation 6. The results of the friction angle variation can be found in Table 6.

**Table 6.** Effect of change in Phimax on model displacement

| % Change | Friction Angle, Phimax | Ahyp | Model Displacement, mm |
|---|---|---|---|
| -25 | 0.825 | 2.864E-07 | 36.57 |
| -20 | 0.880 | 2.563E-07 | 36.52 |
| -15 | 0.935 | 2.288E-07 | 36.49 |
| -10 | 0.990 | 2.035E-07 | 36.47 |
| -5 | 1.045 | 1.799E-07 | 36.44 |
| 0 | 1.100 | 1.000E-07 | 36.42 |
| 5 | 1.155 | 1.369E-07 | 36.55 |
| 10 | 1.210 | 1.170E-07 | 36.41 |
| 15 | 1.265 | 9.787E-08 | 36.56 |
| 20 | 1.320 | 7.942E-08 | 36.56 |
| 25 | 1.375 | 6.148E-08 | 36.54 |

The changes in the cohesion and Phimax parameters were then compared to the reaction force output of the model to determine if a change in either parameter affected the model in any way. Again, the cohesion parameter was found to have no effect on the reaction force output of the model. Therefore, Material Model 147 should not be used to model problems involving cohesive sediment. However, the Phimax parameter did have an effect on the reaction force output of the model as can be seen in Figure 8 and Figure 9. As expected, increases in the value of Phimax caused the maximum reaction force to increase as well. Therefore, Material Model 147 can be used to model cohesionless sediments.

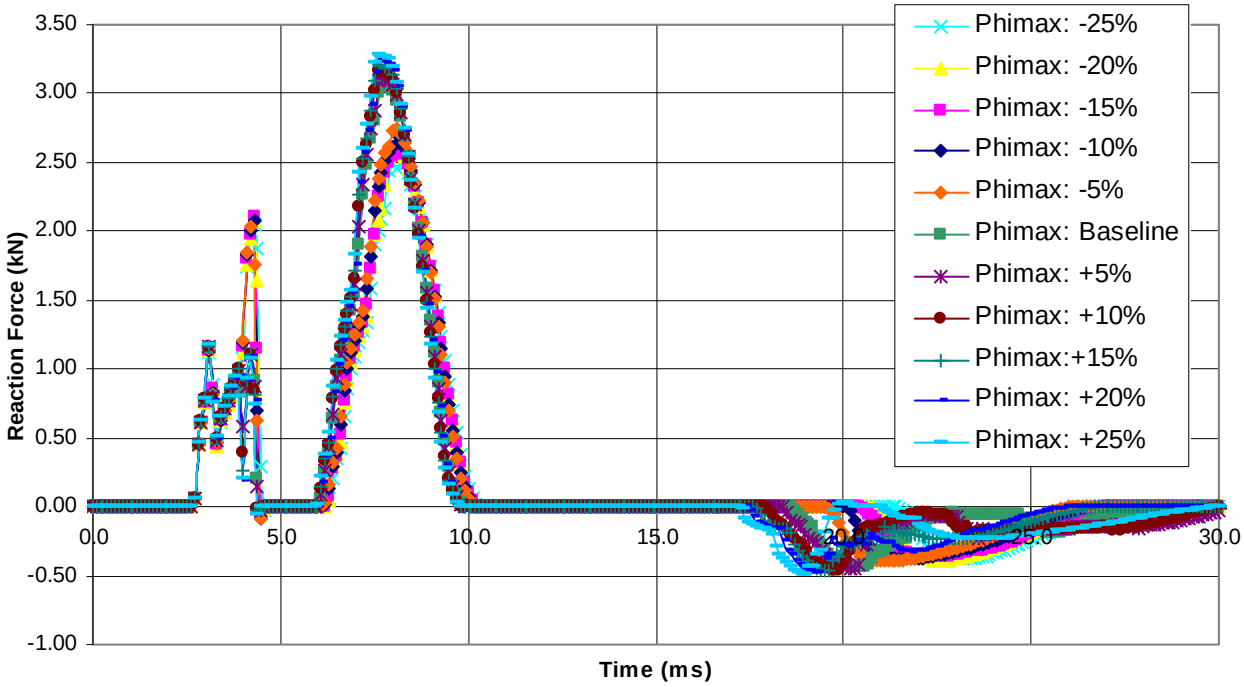


**Figure 8.** Reaction force vs. time for variations in Phimax

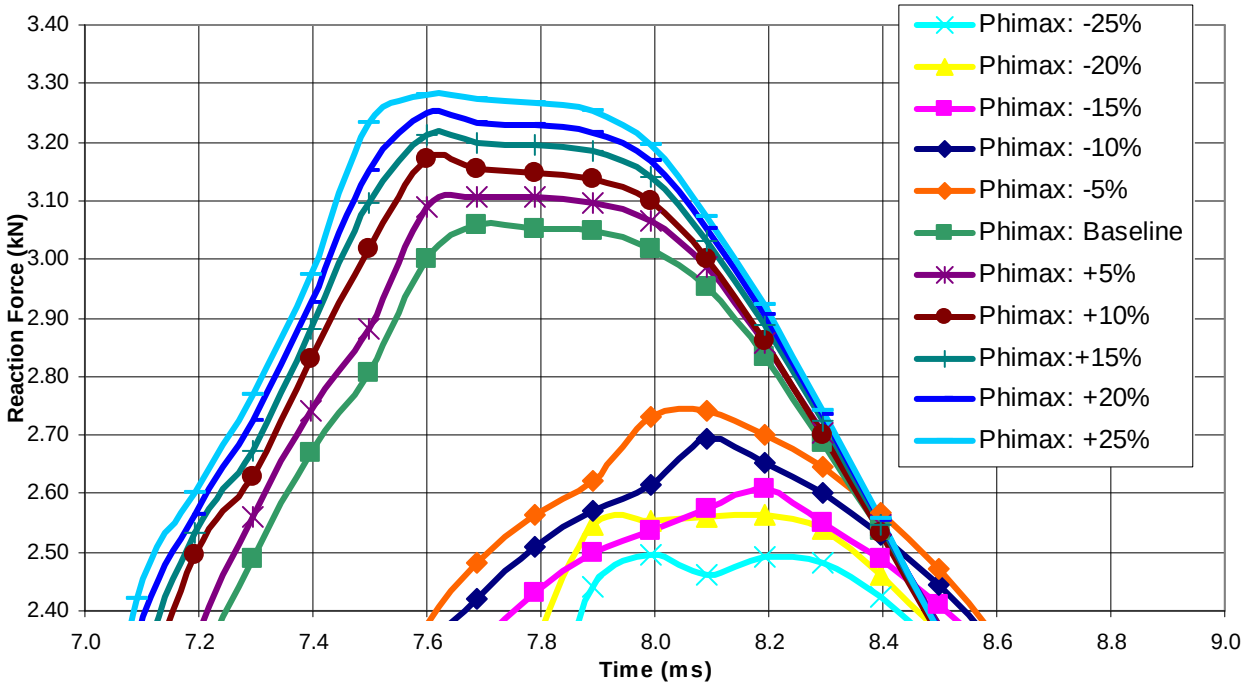


**Figure 9.** Reaction force vs. time for variations in Phimax from 7 ms to 9 ms

The only parameter that was found to have any effect on the displacement output of the 3-inch cohesive model was the bulk modulus, K. As the bulk modulus was decreased by fifteen percent and greater, the model's displacement exceeded the 1000 mm long soil model. The results of this experimentation, as shown in Table 7, illustrate that when using the model in future research special attention should be given to the determination of the value of the bulk modulus, so as not to produce excess penetration. If a value has to be estimated for the bulk modulus, it should be overestimated rather than underestimated.

**Table 7.** Effect of change in Bulk Modulus on model displacement

| % Change | Bulk Modulus, K | Model Displacement, mm |
|---|---|---|
| -25 | 0.01725 | >1000 |
| -20 | 0.01840 | >1000 |
| -15 | 0.01955 | >1000 |
| -10 | 0.02070 | 612.02 |
| -5 | 0.02185 | 611.63 |
| 0 | 0.02300 | 611.76 |
| 5 | 0.02415 | 611.73 |
| 10 | 0.02530 | 611.50 |
| 15 | 0.02645 | 611.54 |
| 20 | 0.02760 | 611.60 |
| 25 | 0.02875 | 611.52 |

**Results and Discussion**

A model to simulate the impact of a penetrometer into the seafloor was created. An example of a complete input deck can be found in Appendix A. When modeling in LS-DYNA it is very important to maintain consistent units. The units used for this research were: kg, mm, ms, KN, GPa, and KN-mm. After each new model, the keyword file was checked for errors and saved. The solver was then used to run an LS-DYNA analysis of the file. If the analysis ran successfully without any errors, a d3plot file was created. By analyzing the data in the d3plot file, penetration depth could be found.

The soil was first modeled as a cube with non-varying sized mesh. As mentioned before, the soil's slave nodes which are capable of generating contact forces with the penetrometer's surface all exist in the central core region of the soil model. For this reason, it was decided to make the mesh in the central region of the soil model coarser. To do this using LS-DYNA, the soil model had to be changed to a cylinder instead of a cube. It is not possible using the BlockM command to make a cube with varying mesh, but it is possible to make a cylinder with varying mesh. The radius of the cylinder was increased until no effects from penetration could be seen on the outer boundary of the cylinder. Originally, the soil model was not as long as the penetrometer because full depth penetration was not of concern. However, the length of the soil model had to be increased once the penetrometer was exiting the bottom of the soil model before it came to rest.

The contact type first used was AUTOMATIC_SINGLE_SURFACE. This contact type is one of the most widely used options in LS-DYNA and is very useful in crash analysis. However, in this contact option no master surface is defined (*LS-DYNA® Keyword*, 2007). As previously mentioned, eventually the contact type AUTOMATIC_ONE_WAY_SURFACE_TO_SURFACE was used to allow penetration of the penetrometer into the soil, but to prevent penetration of the penetrometer surface. One-way contact also allows for compression loads to be transferred between the slave nodes (soil) and the master segments (penetrometer) (*LS-DYNA® Keyword*, 2007).

For CONTROL options in LS-Prepost, one can specify the TIMESTEP. One of the parameter inputs for TIMESTEP is TSSFAC, the scale factor for the computed time step. Originally, TSSFAC was set to 0.9, the parameter's default value. After several models were

analyzed, it was decided to change TSSFAC from 0.9 to 0.5 to allow for more calculation time steps to take place. More calculation time steps should yield more accurate results.

One continual issue that was dealt with throughout the research was massing the penetrometer. The 3-inch penetrometer had a mass of 9.525 kg. In the material input, 020-RIGID, for the penetrometer there is a parameter for the density of the penetrometer material. Since the majority of the penetrometer, its body, was made of aluminum, the density of aluminum was originally used for the density of the rigid material. However, the penetrometer was modeled as a shell in LS-DYNA and for simplicity, was missing its fins. Therefore, LS-DYNA was probably not receiving an accurate value of the penetrometer's mass. However, it is possible to assign an element mass in LS-Prepost using ELEMENT_MASS_PART. With this option, a translational mass could be defined which was then distributed to the nodes of the element. Several models were attempted using this option, but the penetrometer was found to be greatly over massed because the translational mass was being added onto the density that already existed for the penetrometer and a density of zero could not be entered for the penetrometer material.

Trials were analyzed using a very small density, or almost zero density, but were unsuccessful. Another option was looking up exactly what value of mass for the penetrometer the program was using in its calculations. This option was found to be the best way to obtain an accurate mass for the penetrometer. After a model was run, the d3hsp output file could be analyzed to obtain the total mass of the penetrometer used in the program's calculations. The penetrometer's mass could be found under "mass properties of rigid body material." If the value of mass was too low, the density of the material for the penetrometer was increased until an accurate mass was obtained in the d3hsp output file. If the value of mass was too high, the

density of the material for the penetrometer was decreased until an accurate mass was obtained in the d3hsp output file.

During early modeling attempts, it was discovered that when the d3plot file was animated the penetrometer did not penetrate the soil. The LS-DYNA input deck for the simulation being modeled in this experiment has 19 input cards. An error in any of the 19 input cards could have been causing the penetrometer to not penetrate the soil. Since the material model for the soil (FHWA Soil Material Model 147) is the most complex, it was the first input card to be checked to see if it was causing the error. To check the material model of the soil, Material Model 147 was replaced with Material Model 5, a much simpler model used for modeling soil and foam. When the solver was run again, the penetrometer penetrated the soil. Thus, the error causing the penetrometer to not penetrate the soil existed in the input parameters to Material Model 147.

Over 50 different models were analyzed using varying inputs for Material Model 147 before the error was discovered. After the source of the error was discovered, at least 53 different input cards for Material Model 147 were analyzed, which each involved inputting the new parameters into LS-DYNA and running the finite element solver. The most common errors were non-penetration of the soil and penetrometers which had a slight decrease in their velocities, but then continued on through the model at that constant velocity (too much penetration).

Changes that were made to correct errors in the model included changing the soil parameters, especially the values where no physical testing or theoretical means exist for determining the parameter's value, and accurately modeling the mass of the penetrometer. The final inputs for Soil Material Model 147 for the cohesive and cohesionless soils used in the modeling of this research can be seen in Table 8 and Table 9 respectively. For definitions of the

variables in the tables refer back to their definitions in Table 4. Complete keyword input cards for all models can be found in Appendix A.

**Table 8.** Cohesive soil inputs

| Variable | MID | RO | Nplot | Spgrav | Rhowat | $V_n$ | Gammar | Itermax |
|---|---|---|---|---|---|---|---|---|
| Input | 4 | 1.87e-6 | 1 | 2.78 | 1.0e-6 | 2.0 | 0.001 | 10 |
| Default | None | None | 1 | None | 1.0 | 0.0 | 0.0 | 1 |
| Variable | K | G | Phimax | Ahyp | Coh | Eccen | $A_n$ | $E_t$ |
| Input | 0.065 | 0.106 | 0.0 | 0.0 | 0.007 | 1.0 | 0.0 | 0.0 |
| Default | None | None | None | None | None | None | None | None |
| Variable | Mcont | Pwd1 | PwKsk | Pwd2 | Phires | Dint | Vdfm | Damlev |
| Input | 1.0 | 4.63 | 0.003 | 0.0 | 0.0 | 0.1 | 1.0 | 0.0 |
| Default | None | None | None | None | 0.0 | None | None | None |
| Variable | Epsmax | | | | | | | |
| Input | 1.0 | | | | | | | |
| Default | None | | | | | | | |

**Table 9.** Cohesionless soil inputs

| Variable | MID | RO | Nplot | Spgrav | Rhowat | $V_n$ | Gammar | Itermax |
|---|---|---|---|---|---|---|---|---|
| Input | 4 | 2.082e-6 | 1 | 2.65 | 1.0e-6 | 2.0 | 0.001 | 10 |
| Default | None | None | 1 | None | 1.0 | 0.0 | 0.0 | 1 |
| Variable | K | G | Phimax | Ahyp | Coh | Eccen | $A_n$ | $E_t$ |
| Input | 0.115 | 0.069 | 0.61 | 4.44e-7 | 6.2e-6 | 1.0 | 0.0 | 0.0 |
| Default | None | None | None | None | None | None | None | None |
| Variable | Mcont | Pwd1 | PwKsk | Pwd2 | Phires | Dint | Vdfm | Damlev |
| Input | 0.0 | 0.0 | 0.0 | 0.0 | 0.001 | 0.1 | 1.0 | 0.0 |
| Default | None | None | None | None | 0.0 | None | None | None |
| Variable | Epsmax | | | | | | | |
| Input | 1.0 | | | | | | | |
| Default | None | | | | | | | |

The axis of travel for the penetrometer in all models was the y axis. Figure 10 shows the displacement results for the model created for the 3-inch penetrometer in cohesionless soil (sand). With this model, the penetrometer penetrates a maximum of 55.74 mm (2.19 in) into the soil. After thirteen milliseconds, the penetrometer does not come to rest, but bounces back out of

the soil, yielding a final penetration of zero millimeters. This behavior is expected because cohesionless soils act as elastic materials, therefore, when a soil object impacts an elastic material it bounces back. The fact that the model shows this behavior in the cohesionless model and not in the cohesive model proves the model is accurately analyzing the input parameters. Results were verified through experimentation on the YP, where no penetration was observed in cohesionless soil for the 3-inch penetrometer.

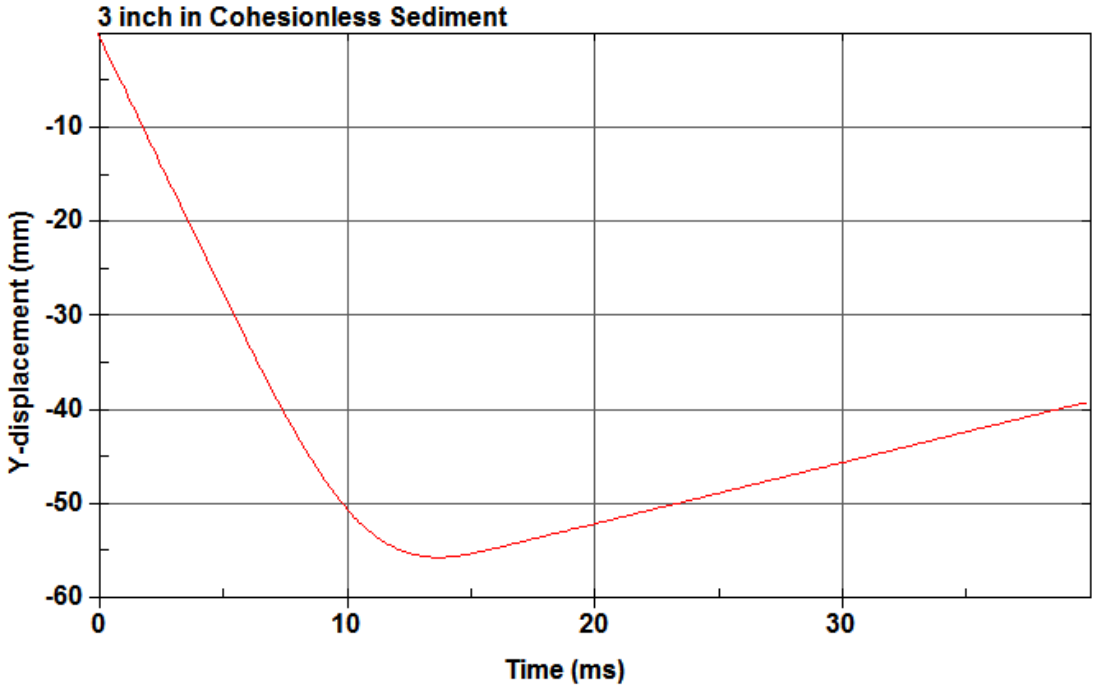


**Figure 10.** Penetration depth of 3-inch penetrometer in cohesionless soil for LS-DYNA model

For unknown reasons, penetration in cohesive sediment could not be accurately modeled in LS-DYNA. However, there are a few plausible reasons. According to the *Manual for LS-DYNA Soil Material Model 147,* Material Model 147 was developed "based on one set of data available and the general behavior of cohesionless soils," meaning it was not developed for cohesive soils (2004). Also, according to the *Evaluation of LS-DYNA Soil Material Model* 147, "the current implementation of the soil material model appears to be applicable for only small

displacement problems (on the order of 25 to 50 mm)" (2004). Through experimentation with the model, a third reason for the model's failure was observed. The model did not fail when the penetrometer's mass was low, 7.5 kg or less, as seen in Figure 11. It is possible Material Model 147 was not developed to handle impact from larger masses. After 50 mm of displacement, the soil material model has been observed to fail in tests performed by the model's evaluators, but model results in this research seem to suggest that even when the 3-inch model failed (the penetrometer did not come to rest), the model could still yield accurate displacement results for the 3-inch penetrometer in cohesive sediments. However, further experimental drops would need to be conducted on the YP to verify the model's displacement values as accurate.

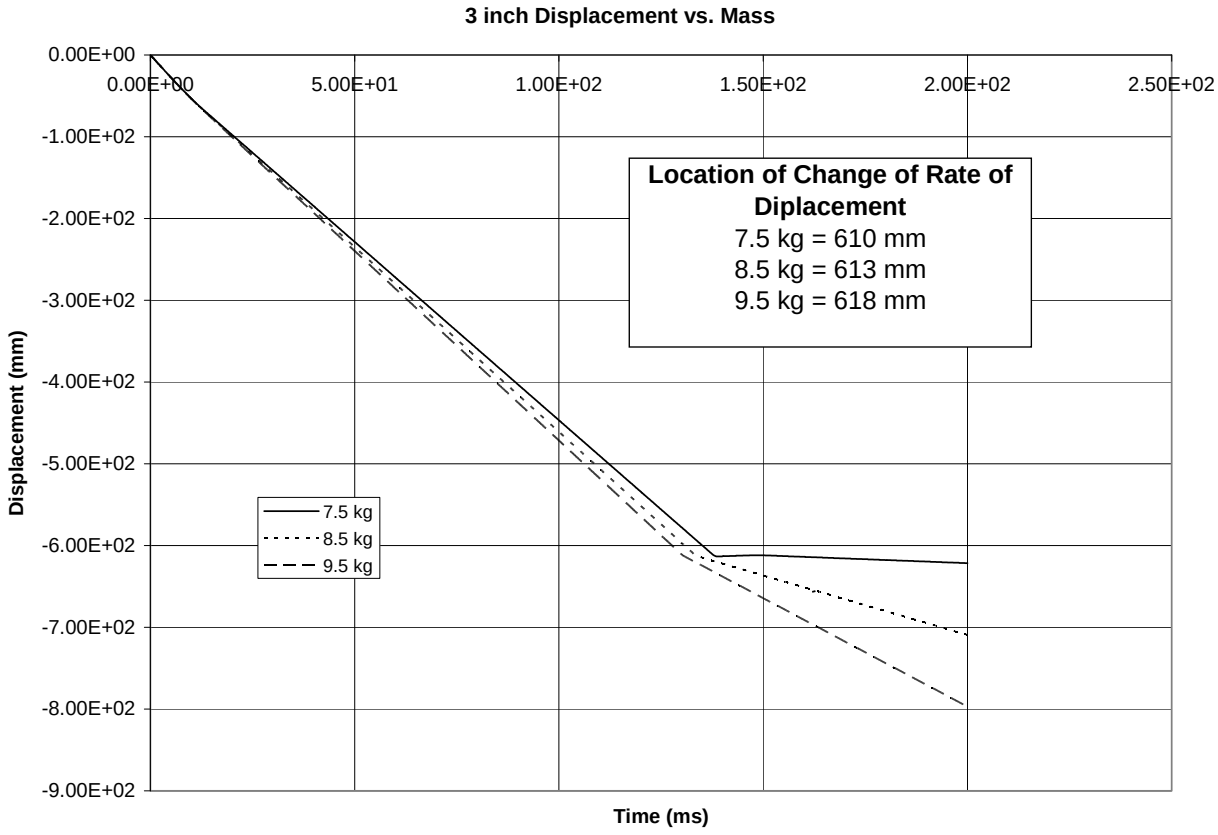


**Figure 11.** Displacement values based on mass for the 3-inch penetrometer in LS-DYNA

An accurate displacement value for the 3-inch penetrometer could be found by observing where the change in rate of displacement occurred, as seen in Figure 12. The location also corresponds with the maximum reaction force experienced by the 3-inch penetrometer, as seen in Figure 13. Figure 12 shows the displacement results for the model created for the 3-inch penetrometer in cohesive soil (clay). With this model, the penetrometer penetrates 618 mm (24.33 in) into the soil before the rate of change in displacement varies. Through the experimentation on the YP, an average of 23.64 inches of penetration is expected in cohesive soil for the 3-inch penetrometer. The percent error between the experimental value and the model's value for penetration for clay is only 2.92%. Both models for the 3-inch penetrometer were within the original goal of at least 15% accuracy between experimentation data and the computer-aided numerical analysis.

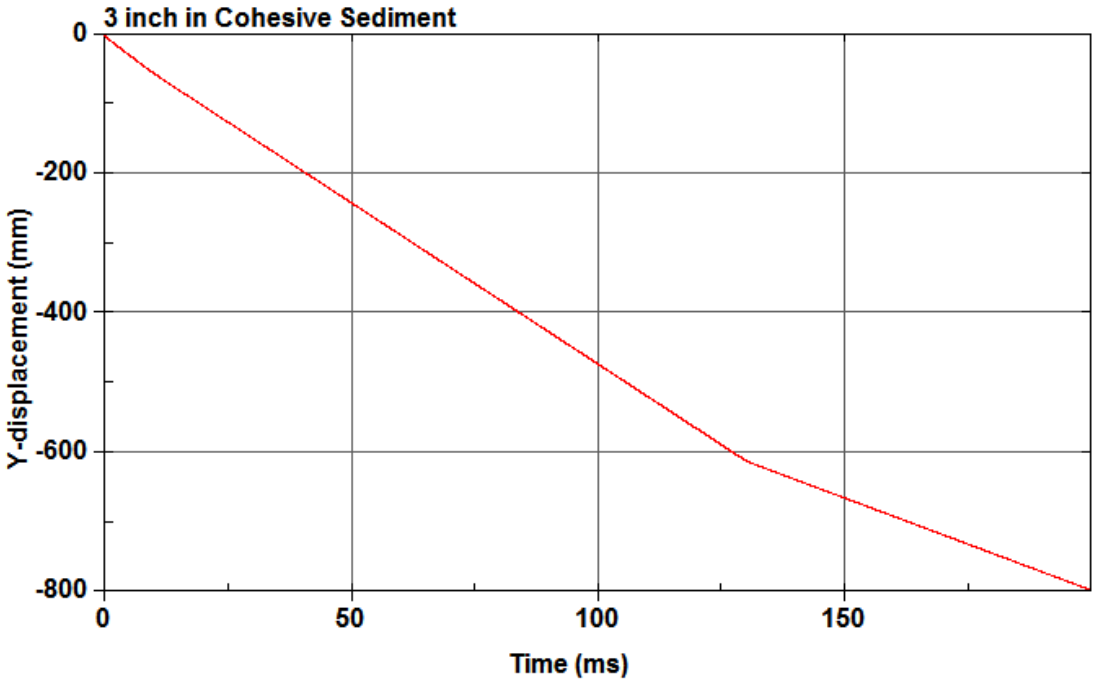


**Figure 12.** Penetration depth of 3-inch penetrometer in cohesive soil for LS-DYNA model

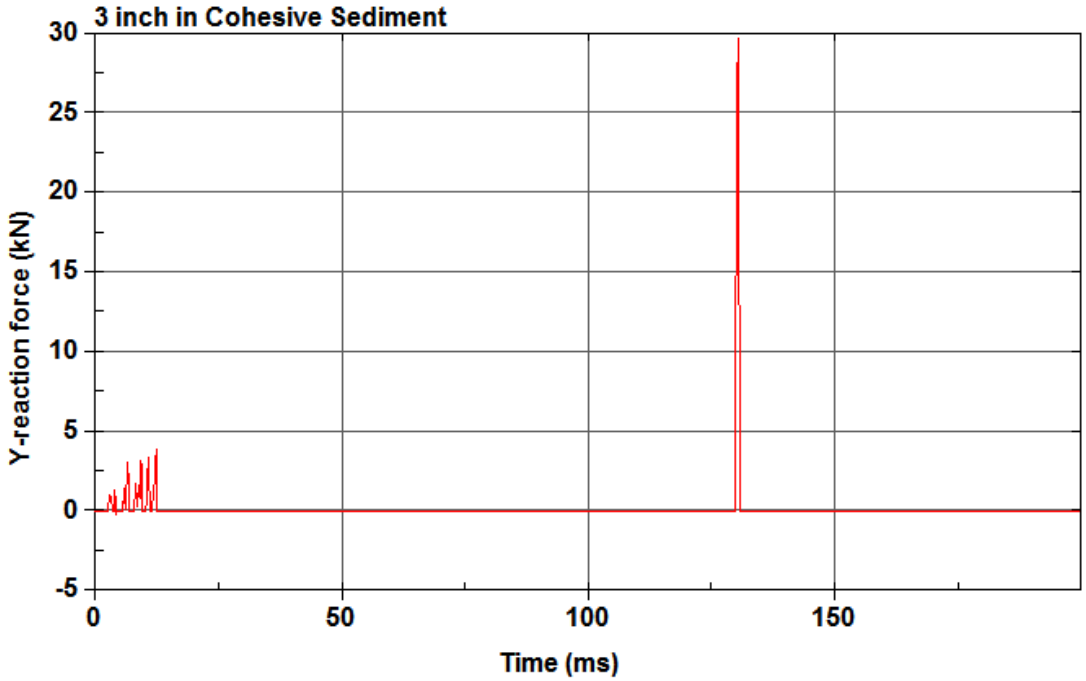


**Figure 13.** Reaction force for 3-inch penetrometer in cohesive soil for LS-DYNA model

Figure 14 shows the displacement results for the model created for the 9-inch penetrometer in cohesionless soil (sand). With this model, the penetrometer penetrates a maximum of 62.20 mm (2.45 in) into the soil. After eighteen milliseconds, the penetrometer does not come to rest, but bounces back out of the soil, yielding a final penetration of zero millimeters. The fact that the model shows higher maximum penetration in the 9-inch model versus the 3-inch model proves again that the model is accurately analyzing the input parameters. Results were verified through experimentation on the YP, where no penetration was observed in cohesionless soil for the 9-inch penetrometer.

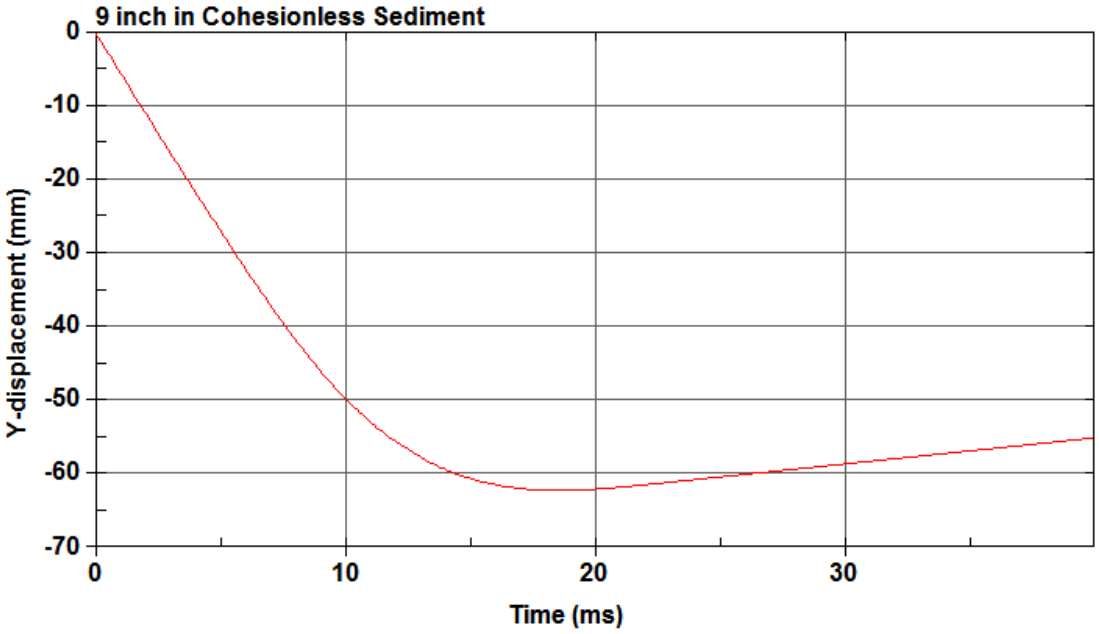


**Figure 14.** Penetration depth of 9-inch penetrometer in cohesionless soil for LS-DYNA model

An accurate model for the 9-inch penetrometer in cohesive soil could not be created. The most likely reason, being that an accurate displacement for the three inch in cohesive was able to be obtained, is that the larger diameter and increased weight of the 9-inch penetrometer caused much more displacement of the soil model in a shorter period of time which caused the model to fail. Unlike the 3-inch model, the penetrometer's displacement in the 9-inch model could not be found by observing where the change in rate of displacement occurred because no change in the rate of displacement occurred in the 9-inch cohesive model, as seen in Figure 15. There also was no reaction force present in the soil after the first thirty milliseconds like there was in the 3-inch cohesive model, as seen in Figure 16. Figure 15 shows the displacement results for the model created for the 9-inch penetrometer in cohesive soil (clay). With this model, the penetrometer penetrates over 1000 mm (39.37 in) into the soil with no variations in the rate of change in displacement. Through experimentation on the YP, an average of 30.36 inches of penetration was expected for the 9-inch penetrometer in cohesive soil. Both models for

cohesive sediment were unsuccessful at accurately modeling the penetrometer's impact, but the cohesionless models were both within the original goal of at least 15% accuracy between experimentation data and the computer-aided numerical analysis.

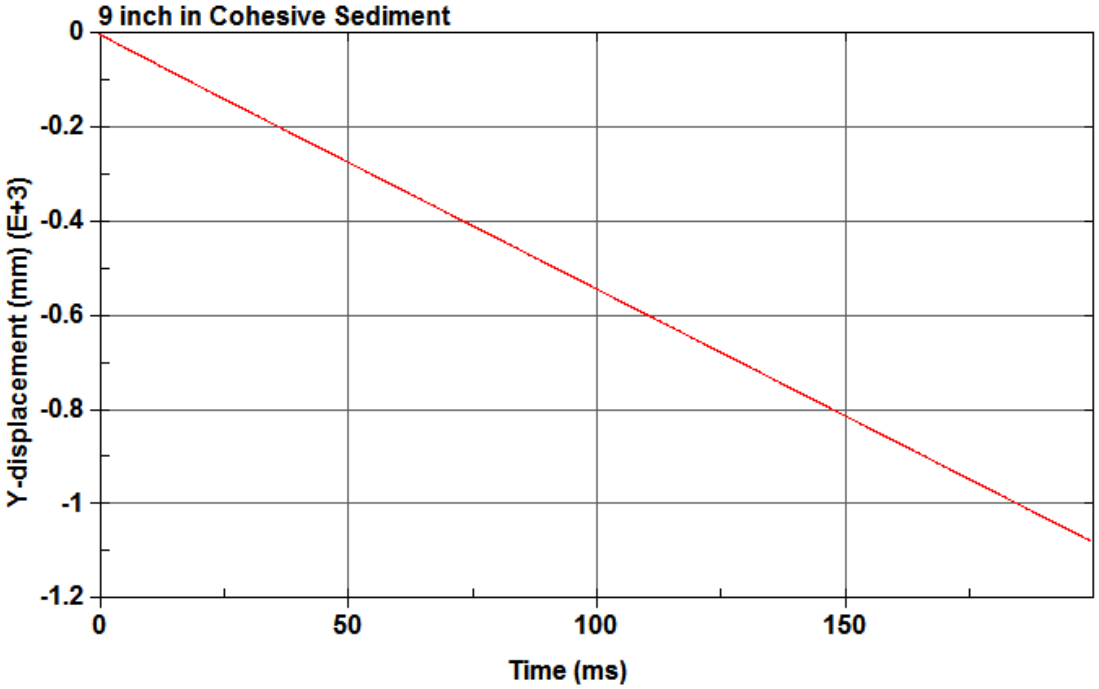


**Figure 15.** Penetration depth of 9-inch penetrometer in cohesive soil for LS-DYNA model

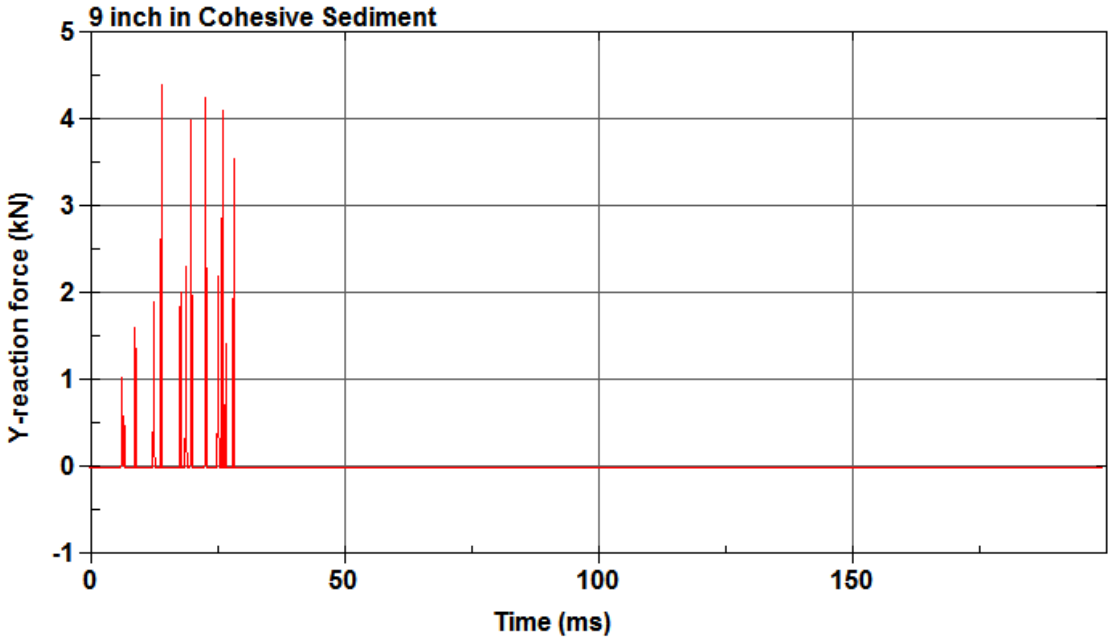


**Figure 16.** Reaction force for 9-inch penetrometer in cohesive soil for LS-DYNA model

***Experimental Approach***

Penetrometers with diameters ranging from 3-inches to 9-inches were constructed for another Navy test, and were made available by the government for this project. The tube and fins of the penetrometers were fabricated from 6061 aluminum, with a 316 stainless steel nose cone which has a 60 degree angle. Pictures of the penetrometers used in this experiment can be seen in Figure 17. It was unnecessary to attach fins to the 9-inch penetrometer because the objects large weight (146.1 lbs) acted as the penetrometer's sole stabilization.

**Figure 17.** 3 and 9-inch diameter experimental penetrometers

The original plan was to also include a 6-inch and 12-inch penetrometers, but the size and weight of the 12-inch would have made it very difficult to handle using the available equipment for this research. In the testing area, it was also difficult to obtain depths great enough to allow the 12-inch to penetrate the seabed. The 6-inch penetrometer was never fabricated.

Each penetrometer was fitted with an accelerometer and included a serial output. Using the USNA Oceanography Research Vessel (YP-686), these penetrometers were repeatedly

dropped off the stern of the YP and allowed to free fall to the seabed. A slackened lifting line and a wireless, external accelerometer remained attached to the penetrometer during each drop for data acquisition. Figure 18 shows the aft deck of the YP with the integral U-frame and the 3-inch penetrometer ready for deployment.

**Figure 18.** Stern deck view of Oceanography YP, showing U-frame and 3-inch penetrometer

The penetrometer was released from the U-frame by pulling a quick release, as seen in Figure 19. After the penetrometer came to rest, the YP winch pulled the lifting line taut and recovered the penetrometer. Figure 20 shows a recovered 3-inch penetrometer with mud up to the top of the fins after full penetration. Figure 22 shows a recovered 9-inch penetrometer with mud showing about 30 inches of penetration. The attached accelerometer started recording motion output before release and continually throughout the drop. The point where the penetrometer impacted the seabed was evident as a spike in the acceleration data. By integrating

the acceleration data twice, the distance the penetrometer traveled during its fall (and thus total penetration depth) was obtained.

**Figure 19.** Launch of 3-inch penetrometer


**Figure 21.** Recovery of 3-inch penetrometer

**Figure 22.** Recovery of 9-inch penetrometer

Experiments were conducted at three sites in the Chesapeake Bay with differing sediment parameters (sand and clay). Due to issues with water depth and where the YP was able to go, drops were made in only sand and clay. A core sample could not be taken of the sand because it was so hard that the corer was not able to penetrate and obtain a sample. Testing location was decided upon before departure, but often changed in transit. For example, one test site was unusable because it was covered in crab pots. The locations of the actual test sites used for experimentation can be found in Appendix B. Due to the variability in test sites, test site characterization (side scan sonar and core sample) was performed during penetrometer testing instead of beforehand as was planned. A picture of the corer used during experimentation to gather sediment samples can be seen in Figure 23.

**Figure 23.** Corer used to gather sediment samples during experimentation.

The average interval between drops was about 10 minutes, so each YP trip took about 2 hours. Since the test locations are all fairly close to the Naval Academy, transit time was less than 15 minutes each way. Four YP excursions were made. These four excursions resulted in a total of 36 drops of the penetrometers, 23 drops of the 3-inch and 13 drops of the 9-inch.

Each test drop produced a time-series of acceleration, which was integrated to determine terminal velocity and embedment depth. The results of each drop can be found in Appendix C. Since the accelerometer used in the experimentation was a three-axis accelerometer, accelerations were recorded in the x, y, and z directions. The axis of travel of the penetrometer for the experimental drops was the z axis. The x and y axes were parallel to the water's surface. Ideally, the penetrometer would travel completely vertical, perpendicular to the ground, recording accelerations in the x and y directions of zero. However, as can be seen in Figure 24

and Figure 25, this is not the case. Before release, the penetrometer is hanging vertical off the U-frame and is not moving. The x and y accelerations are zero and the z acceleration is -1 g, which accounts for gravity. The first changes in the x, y, and z accelerations are caused by a yank on the quick release mechanism attached to the penetrometer, causing the penetrometer to swing, thus giving the penetrometer acceleration in the x and y directions. At water impact, the z acceleration begins to decrease to a value less than -1 g due to fluid drag. The x and y accelerations continue to fluctuate throughout the penetrometers fall through the water due to deceleration and vibration. How much of the x and y acceleration is due to either deceleration or vibration is unknown since the angle at which the penetrometer is falling, if not vertical, is unknown. This problem could be solved by using an inertial navigation system, but an inertial navigation system was determined to be unnecessary in this study because of the assumption that the x and y accelerations were very small while the penetrometer was falling through the water. At impact, all three accelerations fluctuate again due to vibration, but once the penetrometer comes to rest the x and y accelerations return to zero and the z acceleration to -1 g.

Originally it was thought that an obvious spike in the acceleration data would help determine the length of time across which the acceleration data would be integrated to obtain embedment depth. For a hard bottom, such as sand, this is the case. There is an obvious spike in the acceleration data in Figure 24. However, with a soft bottom, such as clay, there is an obvious spike in the data, as seen in Figure 25, but it exists over the course of sixth tenths of a second, making it hard to distinguish where to integrate to. After this difficulty was discovered, each drop was timed from the point of launch of the accelerometer to the release of the penetrometer from the U-frame so as to better distinguish the time span for integration. After obtaining more

data, the drops were compared and it became easier to distinguish the time span for integration for each drop. Embedment depths for the clay drops can be found in Appendix C.

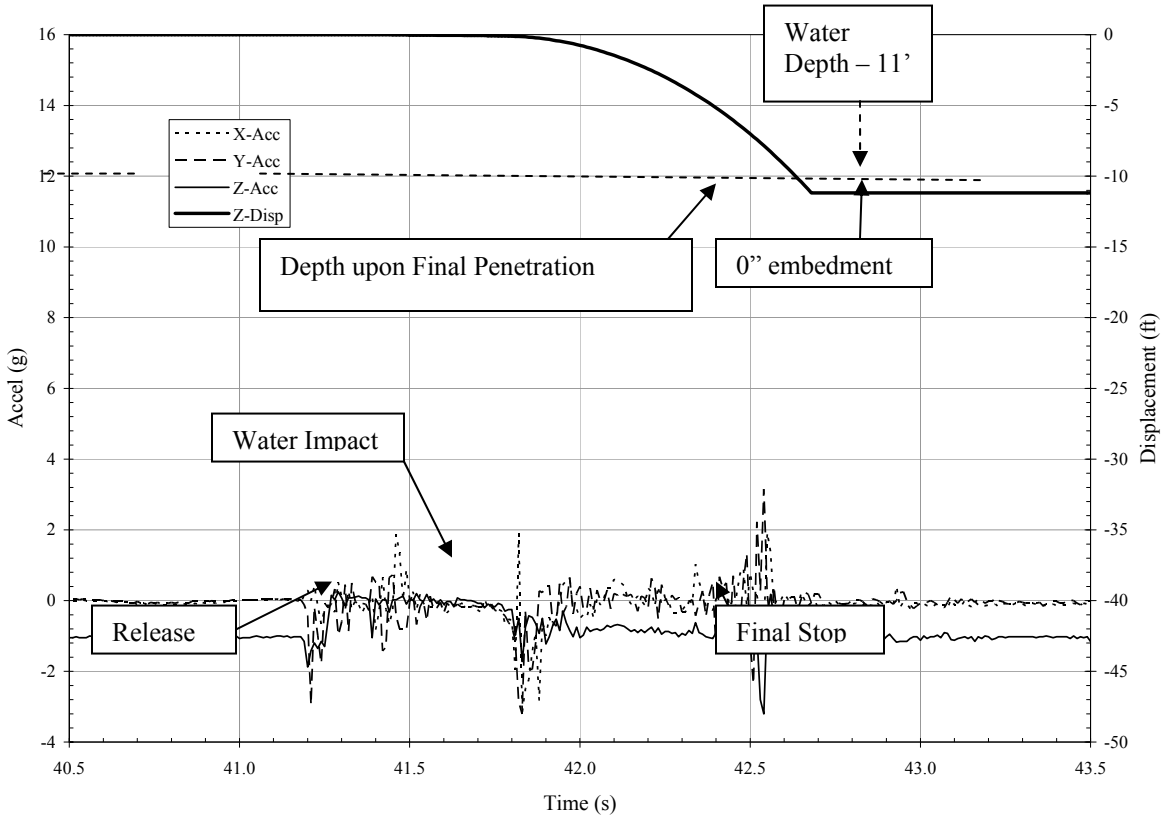


**Figure 24.** Typical drop test results for 3 and 9-inch penetrometer, sand bottom (11-ft water depth)

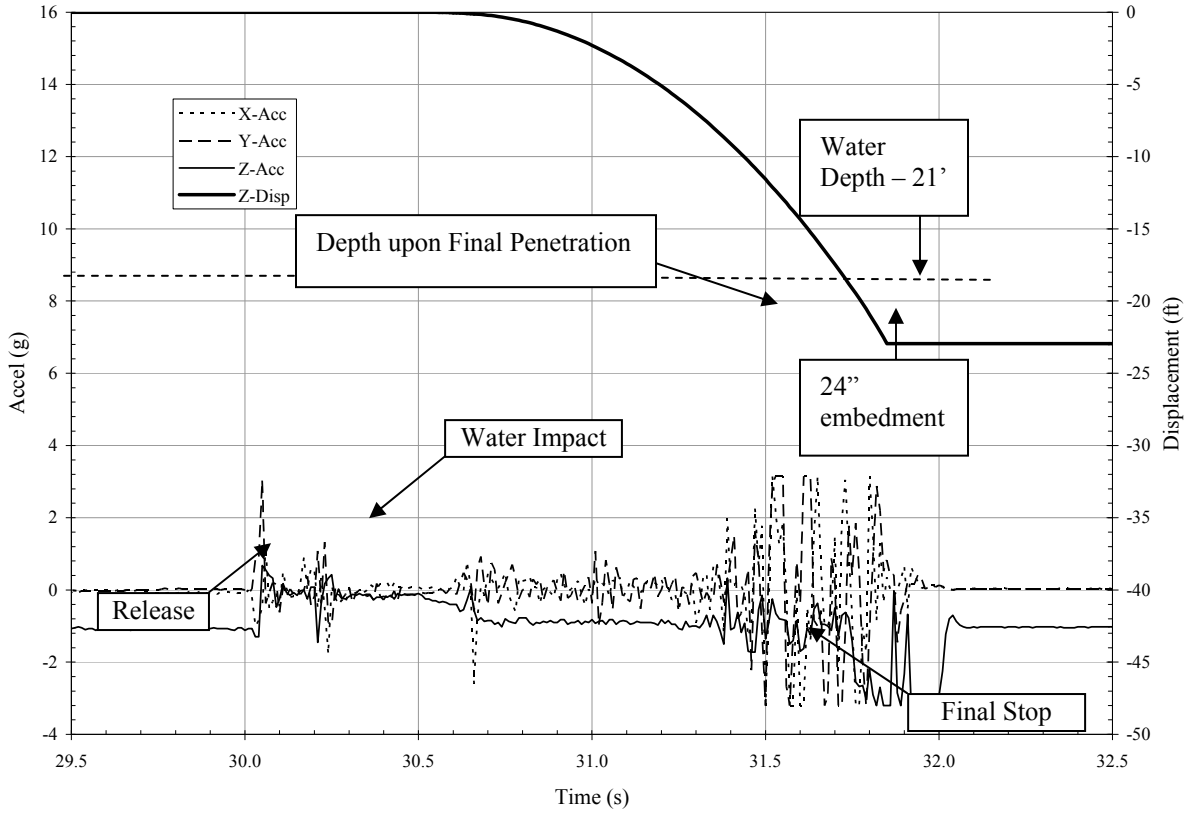


**Figure 25.** Typical drop test results 3-inch penetrometer, clay bottom (21-ft water depth)

Using the experimental data and equations 3, 4, and 5, new values were calculated for the strain rate constants shown in Table 1. The smallest experimental diameter (3-inch) is close to that by True (1976) in the founding research in this field and on which the Navy method is based. Since the other diameter tested was three times this baseline, and all other parameters (e.g. impact velocity, length-to-diameter ratio, nose angle, etc.) were held constant, we were able to discern how the strain rate constants were affected by diameter.

## Results and Discussion

For every location where drops were made, a core sample of the sediment was taken. As previously mentioned, the one exception is at the sand location where the corer was unable to

penetrate and obtain a sample. However, as long as the sediment type is known to be sand is not as important to obtain a sample of the sand because by definition, sand is cohesionless. Therefore, the shear strength of sand is zero. The water inside the core samples was not drained from the samples because it was important for this research to measure the undrained shear strength of the sample, so as to have an *in situ* value for the sediment's shear strength. The core samples were taken back to the lab and allowed to settle for at least two days before any measurements of their shear strengths were taken. This time allowed the disturbed sediments time to settle back into their original positions before they were removed from the sea floor. For drops made in clay, the shear strengths of all samples were measured using a vane shear test. The shear strength of all samples was measured at 1 KPa. However, the accuracy of these values is questionable because the available equipment was not ideal. A triaxial shear test could have been used to obtain more accurate values of shear strength, but the apparatus was not readily available.

For the drops made at site Bravo, the sand site, no penetration was expected with the 3-inch or 9-inch penetrometer. The water depth was 11 feet. Therefore, 11 feet of displacement was expected after integrating the data obtained from the accelerometer. As seen in Figure 24 and Appendix C, 11 feet of displacement was calculated. The penetrometers did not penetrate the seafloor.

For drops made at site Charlie, the clay site, penetration was known to have occurred with the 3-inch penetrometer because when the penetrometer was recovered it was covered in clay up to the top of its fins. The water depth was 21 feet. Therefore, over 21 feet of displacement was expected after integrating the data obtained from the accelerometer. As seen in Figure 25 and Appendix C and D, an average of 22.97 feet of displacement was calculated.

The penetrometer penetrated an average of 1.97 ft (23.64 in) into the seafloor, which is in agreement with the calculations for long, cylindrical penetrometers in the *Handbook for Marine Geotechnical Engineering*. These experimental penetration results verified that the strain rate constants in the handbook for the 3-inch penetrometer were correct.

For drops made with the 9-inch penetrometer at site Charlie, penetration was also known to have occurred because the penetrometer was recovered with clay covering over half of the penetrometer's body. As seen in Figure 26 and Appendix C and D, an average of 23.53 feet of displacement was calculated in the site's 21 foot water depth. The penetrometer penetrated an average of 2.53 ft (30.34 in) into the seafloor. The calculations in the handbook under-predicted the 9-inch penetrometer's penetration at 24.4 inches.

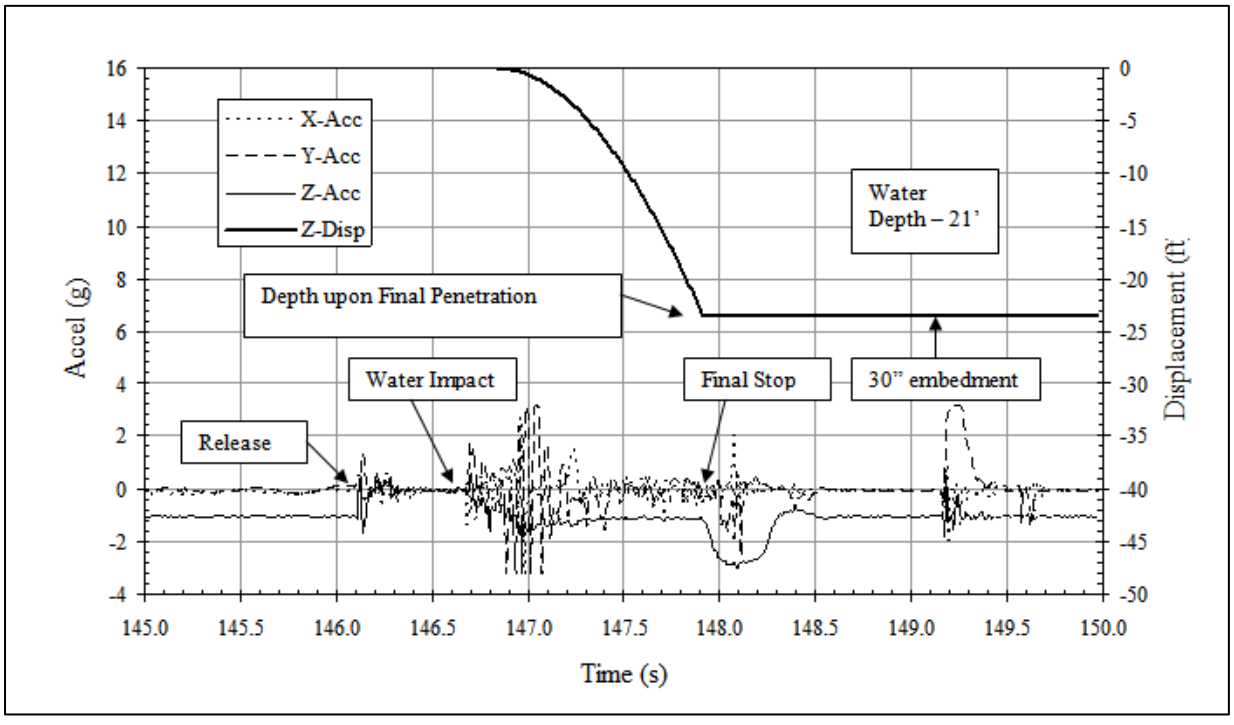


**Figure 26.** Typical drop test results 9-inch penetrometer, clay bottom (21-ft water depth)

**Strain Rate Constants**

New strain rate constants were calculated for larger diameter objects based on the experimental penetration depths of the 9-inch penetrometer. The original strain rate constants along with the new strain rate constants for problems with penetrators greater than 3-inches in diameter can be found in Table 10.

**Table 10.** Original and new values of strain rate constants.

| Condition for Use in Rapid Penetration Problems | Parameter Value | | |
|---|---|---|---|
| | $S_{\dot{e}}$* | $C_e$ | $C_o$ |
| Problems with long, cylindrical penetrators | 4 | 4 | 0.11 |
| All other object shapes where inadequate penetration is of concern | 3 | 10 | 0.25 |
| All other object shapes where excess penetration is of primary concern | 2 | 40 | 1 |
| **New Values of Strain Rate Constants** | | | |
| Problems with penetrators greater than 3 inches in diameter | 2 | 40 | 0.2 |

The new strain rate factors were calculated using the solver function in Excel. A view of the Excel file along with the macros and penetrometer specifications used for calculations can be found in Appendix E. Two different methods were used to calculate the strain rate factors. First, two of the strain rate factors were held constant while the other was allowed to vary for each drop's embedment depth. In the second method, all three strain rate factors were allowed to vary while solving for average embedment depth of the 3-inch and 9-inch penetrometer. This method

produced negative values for two of the three strain rate factors and produced values which were highly variant even with very slight changes in embedment for two of the three strain rate factors. The second method was chosen as the more accurate determination of the strain rate factors. The second method's strain rate factors for the average embedment depth of the 3-inch penetrometer agreed with the values in the *Handbook for Marine Geotechnical Engineering* verifying that the strain rate factors in the handbook for the 3-inch penetrometer were correct.

The calculated values for the strain rate constants $S_e^*$, $C_e$, and $C_o$ can be found in Figure 27, Figure 28, and Figure 29, respectively. The "3in" and "9in" data points represent the different values obtained for each embedment depth using method one. Several of the data points are repetitive. The "AVG" data point represents the values calculated for all three strain rate constants using method two. The "Excess" data point represents the value used in the *Handbook for Marine Geotechnical Engineering* to calculate penetration depth for "all other object shapes where excess penetration is of primary concern." The "Long, cylindrical" data point represents the value used in the handbook to calculate penetration depth for "problems with long, cylindrical penetrometers." The "Inadequate" data point represents the value used in the handbook to calculate penetration depth for "all other object shapes where inadequate penetration is of concern."

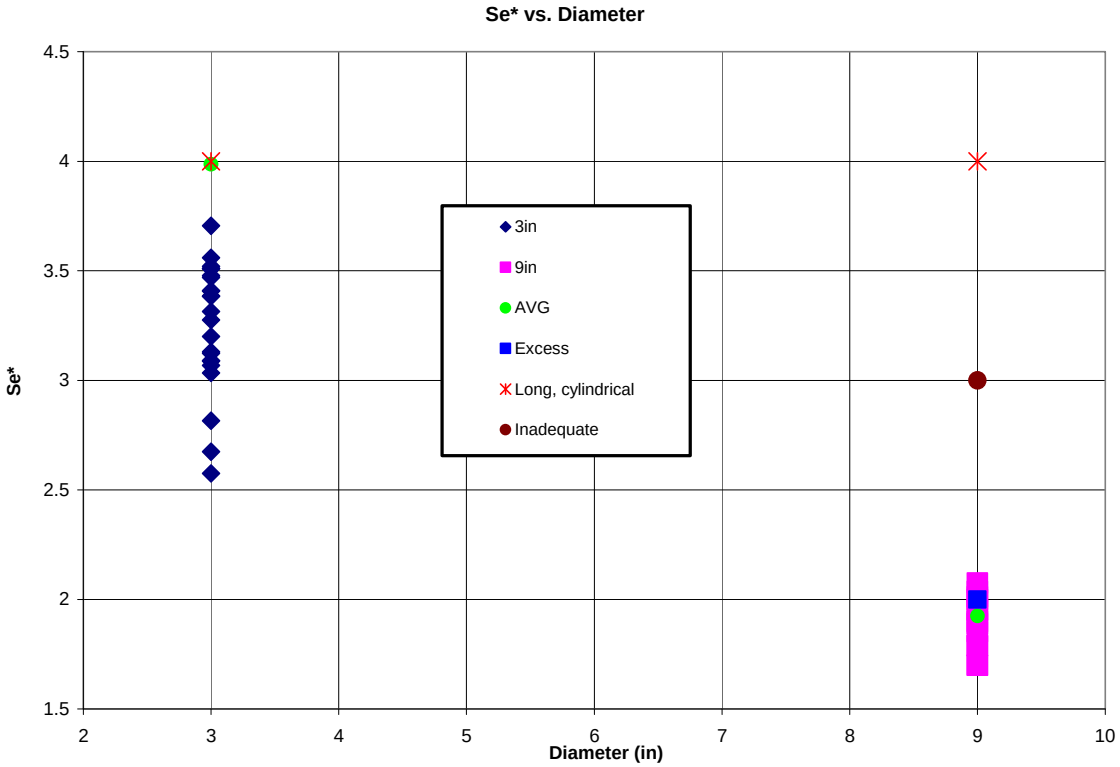


**Figure 27.** $S_e^*$ vs. Diameter for 3-inch and 9-inch penetrometer.

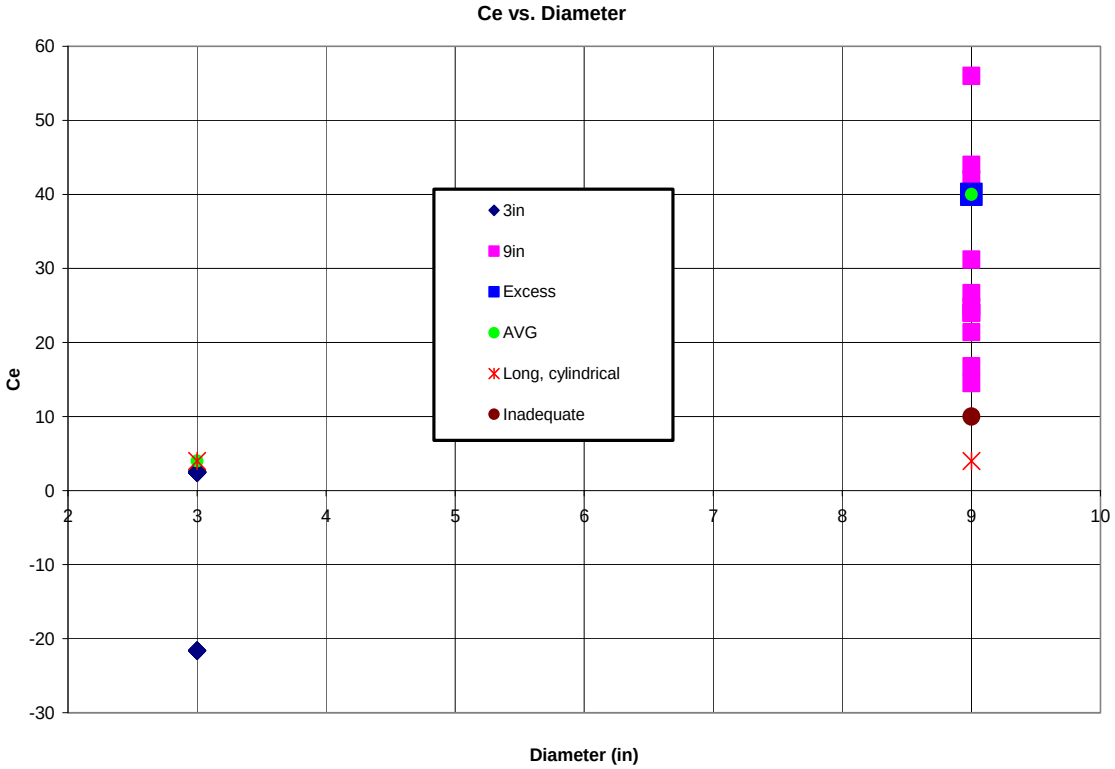


**Figure 28.** $C_e$ vs. Diameter for 3-inch and 9-inch penetrometer.

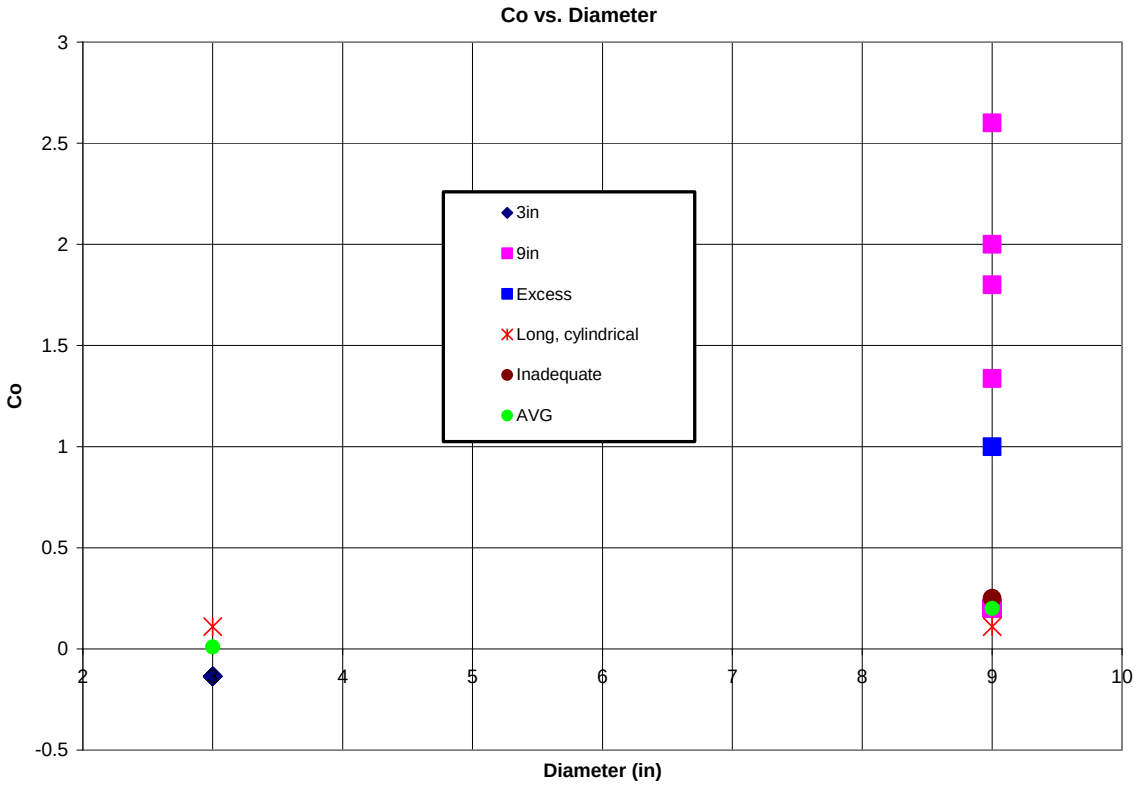


**Figure 29.** $C_o$ vs. Diameter for 3-inch and 9-inch penetrometer.

The overall effect of the new strain rate constants for objects larger than 3-inches in diameter was a decrease of the strain rate factor, $S_{ei}$. Based on this research, it could be agreed upon that as object diameter increases, the strain rate factor approaches zero. From the 3-inch to the 9-inch penetrometer, the strain rate constant $C_e$ increased from 4 to 40, the strain rate constant $C_o$ increased from 0.11 to 0.2, and the strain rate constant $S_e^*$ decreased from 4 to 2. The strain rate constants are related to the strain rate factor by Equation 1. Based on Equation 1, as $C_e$ and $C_o$ increase and $S_e^*$ decreases, the strain rate factor, $S_{ei}$, will decrease.

**Conclusion**

Many, if not all of the project's original goals were completed. A field investigation of the experimental drop sites was conducted to confirm bathymetry, soil properties, and rule out underwater obstructions. Then, the Naval Academy's Oceanography YP was used to collect soil samples, side-scan sonar data, and sub-bottom profiles of each of the three drop sites. Soil property tests were performed on the collected samples in the Naval Academy's Ocean Engineering Lab and the locations of the test sites were adjusted accordingly.

Excursions were made on the YP to collect data for the 3-inch and 9-inch penetrometers in both clay and sand. The acceleration data from the tests was integrated and penetration depth versus time was plotted for each drop. Experimental penetration results verified that the strain rate factors in the *Handbook for Marine Geotechnical Engineering* for the 3-inch penetrometer were correct.

In LS-DYNA, models for cohesive and cohesionless impact were modeled and analyzed using the finite element program. The predicted penetration depths by LS-DYNA were compared to experimental results and the validity of the modeling was evaluated. The model's predicted penetration depths agreed with experimental results in cohesionless soils. Therefore, a successful model of penetrometer impact in cohesionless soils which can be used for parametric study was created using LS-DYNA. However, it was discovered that LS-DYNA Material Model 147 should not be used to model cohesive soils and a successful model of cohesive soil impact could not be created. Material Model 147 is currently maintained by APTEK Inc. and they have no contract to further develop the material model (Murray, 2008).

Finally, new strain rate constants were calculated for larger diameter objects based on the experimental penetration depths of the 9-inch penetrometer. As object diameter increased, the

product of the strain rate constants, the strain rate factor, $S_{ei}$, decreased. Suggestions for future research of this topic include performing more experimentation with a wider array of larger diameter penetrometers. It is possible that research into the strain rate constants of objects between 3 and 9-inches may produce separate strain rate constants for each diameter. Also, attempts should be made to use other material models in LS-DYNA to model penetrometer impact in cohesive soil. Suggested models for future research include material models 5, 14, 78, and 79. All of these models have built-in soil elements. Also, a more accurate method to distinguish the time span for integration for each drop should be used. In this research, the time span for integration was decided upon by comparing each drop and keeping the time span for integration consistent. Underwater video footage of each drop would make it possible to have a more accurate idea of the time span for integration of each drop.

This research into sediment strain-rate dependence on penetrator diameter has improved the Navy's ability to predict embedment depth of objects placed-on or impacting the seabed by expanding the applicability of existing algorithms. The experimental portion of the study extends past published work by increasing object diameter, and the large-deformation finite element analysis provides more understanding of the dynamic soil-structure interaction problem.

## Glossary

Bearing Strength – maximum load that can be applied without producing shear failure in the soil

Bulk Modulus – measure of resistance to uniform compression

Calcareous Sand – sediment containing a high proportion of calcium carbonate

Coulomb Friction Formulation – used to determine the combination of shear and normal stress that will cause a fracture of the material

Hardpan – a distinct soil layer that is largely impervious to water, a dense layer of soil

Littoral Sediments – sediments from the coast of an ocean or sea, or the bank of a lake, river, or estuary

MID – material identification number, used in LS-DYNA to specify which object is assigned the properties in an input card

Mohr-Coulomb Criterion – a typical soil yield surface, describes response of material, such as soil, to shear and normal stress

Poisson's Ratio – ratio of transverse strain to axial strain

Shear Modulus – ratio of shear stress to shear strain

Vane Shear Test – a standard test used to measure in situ sediment strength

Young's Modulus – measure of the stiffness of a given material, ratio of the rate of change of stress versus strain

**References**

Aubeny, C.P. and Shi, H., (2006), "Interpretation of Impact Penetration Measurements in Soft Clays." *Journal of Geotechnical and Geoenvironmental Engineering*, June 2006, v132(6), 770-77.

Bowman, L., March, R., Orenberg, P., and True, D., (1995), "Evaluation of Dropped Versus Static Cone Penetrometers at a Calcerous Cohesive Site." *Proceedings of Oceans '95 Conference (IEEE) – October 1995*.

Das, Braja M., (2005), *Fundamentals of Geotechnical Engineering*, 2nd edition, Nelson-Thomson, Toronto, Ontario, Canada.

Foster, Winfred A. Jr., Johnson, Clarence E., Chiroux, Robert C. and Way, Tom R., (2004), "Finite Element Simulation of Cone Penetration." *Applied Mathematics and Computation*, v162(2), 735-49.

Hallquist, John O., (2006), *LS-DYNA® Theory Manual,* Livermore Software Technology Corporation, Livermore, CA.

Huang, W., Sheng, D., Sloan, S.W. and Yu, H.S., (2004), "Finite Element Analysis of Cone Penetration in Cohesionless Soil." *Computers and Geotechnics*, v31(7), 517-28.

Lee, Wayne Y., (2006), "Numerical modeling of blast-induced liquefaction." DAI, 67, no. 06B, 3305.

Lewis, Brett A., (2004), *Manual for LS-DYNA Soil Material Model 147*, Federal Highway Administration, FHWA-HRT-04-095, McLean, VA.

*LS-DYNA® Keyword User's Manual: Version 971*, (2007), Livermore Software Technology Corporation, Livermore, CA.

McCarthy, David F., (1998), *Essentials of Soil Mechanics and Foundations*, 5th edition, Prentice-Hall, Upper Saddle River, New Jersey.

Mulhearn, P.J., (2002), "Influences of Penetrometer Probe Tip Geometry on Bearing Strength Estimates for Mine Burial Prediction." Aeronautical and Maritime Research Laboratory, Victoria, Australia.

Murray, Yvonne. E-mail interview. 15 Feb. 2008.

Orenberg, Peter, (1996), "Use of a Dropped Penetrometer in Cohesionless Soil." *Offshore Technology Conference*, v1, 639-48.

Reid, J.D., Coon, B.A., Lewis, B.A., Sutherland, S.H., and Murray, Y.D., (2004), *Evaluation of LS-DYNA Soil Material Model 147*, Federal Highway Administration, FHWA-HRT-04-094, McLean, VA.

Rocker, Karl Jr., ed., (1985), *Handbook for Marine Geotechnical Engineering*, Naval Civil Engineering Laboratory, Port Hueneme, CA.

Tekeste, M.Z., Raper, R.L., Tollner, E.W., and Way, T.R., (2007), "Finite Element Analysis of Cone Penetration in Soil for Prediction of Hardpan Location." *Transactions of the ASABE*, v50(1), 23-31.

Thompson, D., (2002), "Groundtruth Results for Dynamic Penetrometers in Cohesive Soils." *Oceans Conference Record (IEEE)*, v4, 2117-23.

True, Daniel G., (1976), *Undrained Vertical Penetration into Ocean Bottom Soils*, Ph.D. Thesis, University of California, Berkeley, Berkeley, CA.

Voyiadjis, George Z. and Kim, Daekyu, (2001), "Finite element analysis of the piezocone test in cohesive soils using an elastoplastic-viscoplastic model and updated Langrangian formulaton." *International Journal of Plasticity*, v19, 253-80.

# Appendix A

## Keyword Files

```
*KEYWORD
*TITLE
3-inch Penetrometer in cohesive sediment
$
$ Units: kg, mm, ms, KN, GPa, KN-mm
$
*CONTROL_TERMINATION
$  endtim    endcyc     dtmin    endeng    endmas
   200.00
$
*CONTROL_TIMESTEP
$  dtinit    tssfac      isdo    tslimt     dt2ms      lctm     erode     ms1st
   0.10      0.500000
$  dt2msf    dt2mslc     imscl
   0.000     0           0
$
*DATABASE_GLSTAT
$  dt        binary
   0.10      1
*DATABASE_MATSUM
$  dt        binary
   0.10      1
*DATABASE_NODOUT
$  dt        binary
   0.10      3
*DATABASE_RBDOUT
$  dt    binary
   0.10      3
*DATABASE_RCFORC
$  dt    binary
   0.10      1
*DATABASE_BINARY_D3PLOT
$  dt      lcdt      beam      npltc
   1.00
$  ioopt
   0
*CONTACT_AUTOMATIC_ONE_WAY_SURFACE_TO_SURFACE_ID
$  cid
title         1contact set
$  ssid      msid      sstyp     mstyp sboxid    mboxid   spr      mpr
   4         1         3         3         0         0         1         1
$  fs        fd        dc        vc        vdc       penchk    bt        dt        0.00      0.00

   0.00      0.00      0.00      0         0.00      1.0E+20
```

```
$  sfs       sfm       sst       mst       sfst      sfmt      fsf       vsf
  1.00      1.00      0.00      0.00      1.00      1.00      1.00      1.00
$  soft      sofscl    lcidab    maxpar    sbopt     depth     bsort     frcfrq
  1         0.10      0         1.025     2.000000  2         25        1
*PART
$ title 3in penetrometer
$  pid       secid     mid       eosid     hgid      grav      adpopt    tmid
   1         1         1
*SECTION_SHELL_TITLE
penetrometer
$  secid     elform    shrf      nip       propt     qr/irid   icomp     setyp
   1         2         1.00      2         1         0         0         1
$  t1        t2        t3        t4        nloc      marea
1.000000  1.000000  1.000000  1.000000
*MAT_RIGID_TITLE
rigid material for penetrometer
$    mid         ro          e       pr          n     couple          m      alias
       1      6.654E-5    200.00  0.31      0.00    0.00        0.00
$     cmo       con1      con2
    0.000         0       0
$   lco or a1       a2        a3        v1        v2        v3
    0.000         0.000     0.000     0.000     0.000     0.000
*PART
$# title
soil
$    pid     secid       mid     eosid      hgid      grav    adpopt      tmid
     4         2         4
*SECTION_SOLID_TITLE
soil
$  secid    elform       aet
    2         1
*MAT_FHWA_SOIL_TITLE
soil
$   mid        ro      nplot    spgrav    rhowat        vn    gammar    intrmx
   4        1.874E-6    1      2.78      1.00E-6       2.00   0.001      10
$    k         g     phimax      ahyp       coh      eccen         an        et
   0.065     0.106     0.000     0.000     0.007      1.00
$   mcont      pwd1      pwksk     pwd2     phires      dint      vdfm     damlev
     1.0      4.63      0.003     0.000    0.000       0.10       1.00
$  epsmax
   1.000000
*INITIAL_VELOCITY_RIGID_BODY
$#     pid       vx        vy        vz        vxr       vyr       vzr
      1     0.000    -5.500000
```

```
*SET_SEGMENT_TITLE
soil
$#    sid      da1      da2      da3      da4
       1
$#     n1       n2       n3       n4       a1       a2       a3       a4
     6374     6385     6616     6605
     6539     6550     6781     6770
     3030     3031     2800     2799
     2810     2799     2800     2811
     3031     3032     2801     2800
     2811     2800     2801     2812

....
    10498     5351    10432     5406
     10548     5466    10432     5351


5406    10432     5340    10487
     5466    10537     5340    10432
*SET_SEGMENT_TITLE
penetrometer
$#    sid      da1      da2      da3      da4
            2
$#     n1       n2       n3       n4       a1       a2       a3       a4


    8        9      147      170
       1        2      171       21

     141       10       11      172
       2        3      173      171

.....
     1415     1414     1430     1429
     1416     1415     1429     1428


     1417     1416     1428     1427
     1418     1417     1427     1425
*ELEMENT_SOLID
$  eid     pid      n1      n2      n3      n4      n5      n6      n7      n8
  12467       4   13740   13971   13982   13751   13741   13972   13983   13752

  12468       4   13741   13972   13983   13752   13742   13973   13984   13753
```

```
......
    22465      4   16473   21439   16292   21489   21544   16347   21373   16407

  22466      4   21544   16347   21373   16407   16462   21428   16281   21478
*ELEMENT_SHELL

$#   eid     pid      n1      n2      n3      n4      n5      n6      n7      n8

    1       1       8       9      147     170

    2       1       1       2      171     21

    3       1      141     10     11      172

.............
    1465     1      1417    1416   1428    1427

    1466     1      1418    1417   1427    1425

*NODE
$#   nid     x             y             z             tc            rc

    1    4.66590          43e-015       65.99113464    -38.09999847

    2    4.0826662e-015    57.74224472    -33.33749771
    3    3.4994281e-015    49.49335098    -28.57499886

.............
  24678   149.16967773     -350.00003052   -29.83395195

  24679   151.50001526     -350.00006104   -9.4978013e-006
  24680   149.16967773     -350.00006104   29.83392143

*END
```

```
*KEYWORD
*TITLE
3-inch Penetrometer in cohesionless sediment
$
$ Units: kg, mm, ms, KN, GPa, KN-mm
$
*CONTROL_TERMINATION
$#  endtim    endcyc     dtmin    endeng    endmas

40.000000

*CONTROL_TIMESTEP

$#  dtinit    tssfac      isdo    tslimt     dt2ms      lctm     erode     ms1st

  1.000000  0.450000         0     0.000     0.000         0         1

$#  dt2msf   dt2mslc     imscl

0.010000

*DATABASE_GLSTAT

$#      dt    binary

0.100000         1

*DATABASE_MATSUM

$#      dt    binary

 0.100000         1

*DATABASE_NODOUT

$#      dt    binary

 0.100000         3

*DATABASE_RBDOUT

$#      dt    binary

 0.100000         3
```

```
*DATABASE_RCFORC
$#      dt    binary
 0.100000         1
*DATABASE_BINARY_D3PLOT
$#      dt      lcdt      beam     npltc
 1.000000
$#   ioopt
 0
*CONTACT_AUTOMATIC_ONE_WAY_SURFACE_TO_SURFACE_ID
$#     cid     title
   1contact set
$#    ssid      msid     sstyp     mstyp    sboxid    mboxid       spr       mpr
     4         1         3         3         0         0         1         1
$#      fs        fd        dc        vc       vdc    penchk        bt        dt
  0.000     0.000     0.000     0.000     0.000         0     0.0001.0000E+20
$#     sfs       sfm       sst       mst      sfst      sfmt       fsf       vsf
  1.000000  1.000000     0.000     0.000  1.000000  1.000000  1.000000  1.000000
$#    soft    sofscl    lcidab    maxpar     sbopt     depth     bsort    frcfrq
       1  0.100000         0  1.025000  2.000000         2        25         1
*PART
$# title
3in penetrometer
$#     pid     secid       mid     eosid      hgid      grav    adpopt      tmid
  1         1         1
```

```
*SECTION_SHELL_TITLE
penetrometer

$#   secid    elform      shrf       nip     propt   qr/irid     icomp     setyp

     1         2  1.000000         2         1         0         0         1

$#      t1        t2        t3        t4      nloc     marea

1.000000  1.000000  1.000000  1.000000

*MAT_RIGID_TITLE
rigid material for penetrometer

$#     mid        ro         e        pr         n    couple         m     alias

     1 6.6540E-5 200.00000  0.310000     0.000     0.000     0.000

$#     cmo      con1      con2

 0.000         0         0

$#lco or a1       a2        a3        v1        v2        v3

    0.000     0.000     0.000     0.000     0.000     0.000

*PART

$# title
soil
$#     pid     secid       mid     eosid      hgid      grav    adpopt      tmid

      4         2         4

*SECTION_SOLID_TITLE
soil

$#   secid    elform       aet

    2         1

*MAT_FHWA_SOIL_TITLE
soil
```

```
$#     mid        ro     nplot    spgrav    rhowat        vn    gammar    intrmx
       4 2.0820E-6         1  2.650000 1.0000E-6  2.000000  0.001000        10
$#       k         g    phimax      ahyp       coh     eccen        an        et
 0.115000  0.069000  0.610000 4.4350E-7 6.2000E-6  1.000000
$#   mcont      pwd1     pwksk      pwd2    phires      dint      vdfm    damlev
  0.000     0.000     0.000     0.000  0.001000  0.100000  1.000000
$#  epsmax
1.000000
*INITIAL_VELOCITY_RIGID_BODY
$#     pid        vx        vy        vz       vxr       vyr       vzr
       1     0.000 -5.500000
*SET_NODE_LIST_TITLE
NODESET(SPC) 1
$#     sid       da1       da2       da3       da4
1
$#    nid1      nid2      nid3      nid4      nid5      nid6      nid7      nid8
     1468      1469      1470      1471      1472      1473      1474      1475
    1476      1477      1478      1479      1489      1490      1500      1501
   1511      1512      1522      1523      1533      1534      1544      1545
  1555      1556      1566      1567      1577      1578      1579      1580
  1581      1582      1583      1584      1585      1586      1587      1588
  1589      1599      1699      1709      1710      1720      1820      1830
```

1831 1841 1941 1951 1952 1962 2062 2072

2073 2083 2183 2193 2194 2204 2304 2314

2315 2325 2425 2435 2436 2446 2546 2556

2557 2567 2667 2677 2678 2679 2680 2681

2682 2683 2684 2685 2686 2687 2688 2689

2699 2700 2710 2711 2721 2722 2732 2733

2743 2744 2754 2755 2765 2766 2776 2777

2787 2788 2789 2790 2791 2792 2793 2794

2795 2796 2797 2798

*SET_NODE_LIST_TITLE
NODESET(SPC)
2

$# sid da1 da2 da3 da4

2

$# nid1 nid2 nid3 nid4 nid5 nid6 nid7 nid8

1 2 3 4 5 6 7 8

9 10 11 12 13 14 15 16

17 18 19 20 21 22 23 24

25 26 27 28 29 30 31 32

33 34 35 36 37 38 39 40

.....

13700 13701 13702 13703 13704 13705 13706 13707

13708 13709 13710 13711 13712 13713 13714 13715

13716 13717 13718 13719 13720 13721 13722 13723

13724 13725 13726 13727 13728 13729 13730 13731

13732 13733 13734 13735 13736 13737 13738 13739

*SET_NODE_LIST_TITLE
NODESET(SPC) 3

$# sid da1 da2 da3 da4

3

$# nid1 nid2 nid3 nid4 nid5 nid6 nid7 nid8

2799 2800 2801 2802 2803 2804 2805 2806

2807 2808 2809 2810 2811 2812 2813 2814

2815 2816 2817 2818 2819 2820 2821 2822

2823 2824 2825 2826 2827 2828 2829 2830

.....
13695 13696 13697 13698 13699 13700 13701 13702

13703 13704 13705 13706 13707 13708 13709 13710

13711 13712 13713 13714 13715 13716 13717 13718

13719 13720 13721 13722 13723 13724 13725 13726

13727 13728 13729 13730 13731 13732 13733 13734

13735 13736 13737 13738 13739

*SET_NODE_LIST_TITLE
NODESET(SPC) 4

$# sid da1 da2 da3 da4

4

$# nid1 nid2 nid3 nid4 nid5 nid6 nid7 nid8

2799 2800 2801 2802 2803 2804 2805 2806

2807 2808 2809 2810 2811 2812 2813 2814

2815 2816 2817 2818 2819 2820 2821 2822

2823 2824 2825 2826 2827 2828 2829 2830

2831 2832 2833 2834 2835 2836 2837 2838

.....

13703 13704 13705 13706 13707 13708 13709 13710

13711 13712 13713 13714 13715 13716 13717 13718

13719 13720 13721 13722 13723 13724 13725 13726

13727 13728 13729 13730 13731 13732 13733 13734

13735 13736 13737 13738 13739

*SET_SEGMENT_TITLE
soil

$# sid da1 da2 da3 da4

1

$# n1 n2 n3 n4 a1 a2 a3 a4

6374 6385 6616 6605

6539 6550 6781 6770

3030 3031 2800 2799

2810 2799 2800 2811

3031 3032 2801 2800

.....

10498 5351 10432 5406

10548 5466 10432 5351

5406 10432 5340 10487

5466 10537 5340 10432

*SET_SEGMENT_TITLE
penetrometer

$# sid da1 da2 da3 da4

2

$# n1 n2 n3 n4 a1 a2 a3 a4

8 9 147 170

1 2 171 21

141 10 11 172

2 3 173 171

3 4 174 173

.....

1415 1414 1430 1429

1416 1415 1429 1428

1417 1416 1428 1427

1418 1417 1427 1425

*ELEMENT_SOLID

$# eid pid n1 n2 n3 n4 n5 n6 n7 n8

12467 4 13740 13971 13982 13751 13741 13972 13983 13752

12468 4 13741 13972 13983 13752 13742 13973 13984 13753

12469 4 13742 13973 13984 13753 13743 13974 13985 13754

12470 4 13743 13974 13985 13754 13744 13975 13986 13755

```
  12471       4   13744   13975   13986   13755   13745   13976   13987   13756

.....................................
 22463       4   16484   21450   16303   21500   21555   16358   21384   16418

 22464       4   21555   16358   21384   16418   16473   21439   16292   21489

 22465       4   16473   21439   16292   21489   21544   16347   21373   16407

 22466       4   21544   16347   21373   16407   16462   21428   16281   21478

*ELEMENT_SHELL

$#   eid     pid      n1      n2      n3      n4      n5      n6      n7      n8

      1       1       8       9     147     170

     2       1       1       2     171      21

     3       1     141      10      11     172

      4       1       2       3     173     171

    5       1       3       4     174     173

.............................
   1460       1    1412    1411    1433    1432
   1461       1    1413    1412    1432    1431

   1462       1    1414    1413    1431    1430
   1463       1    1415    1414    1430    1429

  1464       1    1416    1415    1429    1428
   1465       1    1417    1416    1428    1427

  1466       1    1418    1417    1427    1425

*NODE

$#   nid               x               y               z      tc      rc

   1  4.6659043e-015     65.99113464    -38.09999847
      2  4.0826662e-015     57.74224472    -33.33749771
```

```
     3  3.4994281e-015     49.49335098    -28.57499886
     4  2.9161902e-015     41.24446106    -23.81250000

     5  2.3329524e-015     32.99556732    -19.04999924
     6  1.7497139e-015     24.74667358    -14.28749752

     7  1.1664758e-015     16.49777985     -9.52499771
     8  5.8323756e-016      8.24888420     -4.76249552

.....
 24676    134.39915466   -350.00006104    -80.63949585

 24677    142.91722107   -350.00006104    -57.16689301

 24678    149.16967773   -350.00003052    -29.83395195

 24679    151.50001526   -350.00006104 -9.4978013e-006

 24680    149.16967773   -350.00006104     29.83392143

*END
```

```
*KEYWORD
*TITLE
9-inch Penetrometer in cohesive sediment
$
$ Units: kg, mm, ms, KN, GPa, KN-mm
$
*CONTROL_TERMINATION

$#  endtim    endcyc     dtmin    endeng    endmas

 200.00000

*CONTROL_TIMESTEP

$#  dtinit    tssfac      isdo    tslimt     dt2ms      lctm     erode     ms1st

  0.100000  0.500000

$#  dt2msf   dt2mslc     imscl

    0.000         0         0

*DATABASE_GLSTAT

$#      dt    binary

  0.100000         1

*DATABASE_MATSUM

$#      dt    binary

  0.100000         1

*DATABASE_NODOUT

$#      dt    binary

 0.100000         3

*DATABASE_RBDOUT

$#      dt    binary
```

```
 0.100000         3
*DATABASE_RCFORC
$#      dt    binary
 0.100000         1
*DATABASE_BINARY_D3PLOT
$#      dt      lcdt      beam     npltc
  1.000000
$#   ioopt
       0
*CONTACT_AUTOMATIC_ONE_WAY_SURFACE_TO_SURFACE_ID
$#     cid      title
2contact description
$#    ssid      msid     sstyp     mstyp    sboxid    mboxid       spr       mpr
       6         5         3         3         0         0         1
$#      fs        fd        dc        vc       vdc    penchk        bt        dt
    0.000     0.000     0.000     0.000     0.000         0     0.0001.0000E+20
$#     sfs       sfm       sst       mst      sfst      sfmt       fsf       vsf
  1.000000  1.000000     0.000     0.000  1.000000  1.000000  1.000000  1.000000
$#    soft    sofscl    lcidab    maxpar     sbopt     depth     bsort    frcfrq
       0  0.100000         0  1.025000  2.000000         2        25         1
*PART
$# title
9in penetrometer
$#     pid     secid       mid     eosid      hgid      grav    adpopt      tmid
    5         1         1
```

```
*SECTION_SHELL_TITLE
penetrometer

$#   secid    elform      shrf       nip     propt   qr/irid     icomp     setyp

  1         2  1.000000         2         1         0         0         1

$#      t1        t2        t3        t4      nloc     marea

1.000000  1.000000  1.000000  1.000000

*MAT_RIGID_TITLE

rigid material for penetrometer

$#     mid        ro         e        pr         n    couple         m     alias

      1 5.5130E-5 200.00000  0.310000     0.000     0.000     0.000

$#     cmo      con1      con2
    0.000         0         0

$#lco or a1       a2        a3        v1        v2        v3

   0.000     0.000     0.000     0.000     0.000     0.000

*PART

$# title

Solid1

$#     pid     secid       mid     eosid      hgid      grav    adpopt      tmid

    6         2         4

*SECTION_SOLID_TITLE
soil

$#   secid    elform       aet

    2         1
```

```
*MAT_FHWA_SOIL_TITLE
soil

$#     mid        ro     nplot    spgrav    rhowat        vn    gammar    intrmx

       4 1.8740E-6         1  2.780000 1.0000E-6  2.000000  0.001000        10

$#       k         g    phimax      ahyp       coh     eccen        an        et

0.065000  0.106000     0.000     0.000  0.007000  1.000000

$#   mcont      pwd1     pwksk      pwd2    phires      dint      vdfm    damlev

 1.000000  4.630000  0.003000     0.000     0.000  0.100000  1.000000

$#  epsmax
  1.000000

*INITIAL_VELOCITY_RIGID_BODY

$#     pid        vx        vy        vz       vxr       vyr       vzr

       5     0.000 -5.500000

*SET_NODE_LIST_TITLE
NODESET(SPC) 1

$#     sid       da1       da2       da3       da4

    1

$#    nid1      nid2      nid3      nid4      nid5      nid6      nid7      nid8

  1468      1469      1470      1471      1472      1473      1474      1475

 1476      1477      1478      1479      1489      1490      1500      1501

 1511      1512      1522      1523      1533      1534      1544      1545

   1555      1556      1566      1567      1577      1578      1579      1580

     1581      1582      1583      1584      1585      1586      1587      1588

      1589      1599      1699      1709      1710      1720      1820      1830
```

1831 1841 1941 1951 1952 1962 2062 2072

2073 2083 2183 2193 2194 2204 2304 2314

2315 2325 2425 2435 2436 2446 2546 2556

2557 2567 2667 2677 2678 2679 2680 2681

2682 2683 2684 2685 2686 2687 2688 2689

2699 2700 2710 2711 2721 2722 2732 2733

2743 2744 2754 2755 2765 2766 2776 2777

2787 2788 2789 2790 2791 2792 2793 2794

2795 2796 2797 2798

*SET_NODE_LIST_TITLE

NODESET(SPC) 2

$# sid da1 da2 da3 da4

2

$# nid1 nid2 nid3 nid4 nid5 nid6 nid7 nid8

1 2 3 4 5 6 7 8

9 10 11 12 13 14 15 16

17 18 19 20 21 22 23 24

25 26 27 28 29 30 31 32

.....

13708 13709 13710 13711 13712 13713 13714 13715

13716 13717 13718 13719 13720 13721 13722 13723

13724 13725 13726 13727 13728 13729 13730 13731

```
  13732     13733     13734     13735     13736     13737     13738     13739
*SET_NODE_LIST_TITLE
NODESET(SPC) 3
$#     sid       da1       da2       da3       da4
3
$#    nid1      nid2      nid3      nid4      nid5      nid6      nid7      nid8
    2799      2800      2801      2802      2803      2804      2805      2806
    2807      2808      2809      2810      2811      2812      2813      2814
    2815      2816      2817      2818      2819      2820      2821      2822
    2823      2824      2825      2826      2827      2828      2829      2830
    2831      2832      2833      2834      2835      2836      2837      2838
.........................
    13711     13712     13713     13714     13715     13716     13717     13718
   13719     13720     13721     13722     13723     13724     13725     13726
  13727     13728     13729     13730     13731     13732     13733     13734
 13735     13736     13737     13738     13739
*SET_NODE_LIST_TITLE
NODESET(SPC) 4
$#     sid       da1       da2       da3       da4
    4
$#    nid1      nid2      nid3      nid4      nid5      nid6      nid7      nid8
  2799      2800      2801      2802      2803      2804      2805      2806
 2807      2808      2809      2810      2811      2812      2813      2814
```

2815 2816 2817 2818 2819 2820 2821 2822

2823 2824 2825 2826 2827 2828 2829 2830

2831 2832 2833 2834 2835 2836 2837 2838

2839 2840 2841 2842 2843 2844 2845 2846

.....

13711 13712 13713 13714 13715 13716 13717 13718

13719 13720 13721 13722 13723 13724 13725 13726

13727 13728 13729 13730 13731 13732 13733 13734

13735 13736 13737 13738 13739

*SET_SEGMENT_TITLE
soil

$# sid da1 da2 da3 da4

1

$# n1 n2 n3 n4 a1 a2 a3 a4

6374 6385 6616 6605
6539 6550 6781 6770

3030 3031 2800 2799
2810 2799 2800 2811

3031 3032 2801 2800
2811 2800 2801 2812

3032 3033 2802 2801
2812 2801 2802 2813

3033 3034 2803 2802
2813 2802 2803 2814

.....

10509 5362 10443 5417
10559 5477 10443 5362

5417 10443 5351 10498
5477 10548 5351 10443

10498 5351 10432 5406
10548 5466 10432 5351

5406 10432 5340 10487
5466 10537 5340 10432

*SET_SEGMENT_TITLE
penetrometer

$# sid da1 da2 da3 da4

2

$# n1 n2 n3 n4 a1 a2 a3 a4

8 9 147 170

1 2 171 21

141 10 11 172

2 3 173 171

3 4 174 173

142 141 172 175

.....
1414 1413 1431 1430

1415 1414 1430 1429

1416 1415 1429 1428

1417 1416 1428 1427

1418 1417 1427 1425

*ELEMENT_SOLID

```
$#   eid     pid      n1      n2      n3      n4      n5      n6      n7      n8
  31166       6   33372   33713   33724   33383   33373   33714   33725   33384
  31167       6   33373   33714   33725   33384   33374   33715   33726   33385
  31168       6   33374   33715   33726   33385   33375   33716   33727   33386
  31169       6   33375   33716   33727   33386   33376   33717   33728   33387
.....................................
  46162       6   37381   44712   37145   44817   44872   37200   44646   37315
  46163       6   44872   37200   44646   37315   37370   44701   37134   44806
  46164       6   37370   44701   37134   44806   44861   37189   44635   37304
  46165       6   44861   37189   44635   37304   37359   44690   37123   44795
*ELEMENT_SHELL
$#   eid     pid      n1      n2      n3      n4      n5      n6      n7      n8
  22467       5   25047   25048   25065   25064
  22468       5   25046   25047   25064   25066
  22469       5   25045   25046   25066   25067
  22470       5   25044   25045   25067   25068
.................................
 31162       5   33322   33323   33250   33251
 31163       5   33249   33250   33323   33324
 31164       5   33248   33249   33324   33325
 31165       5   33247   33248   33325   33326
*NODE
$#   nid               x               y               z      tc      rc
```

1 4.6659043e-015 65.99113464 -38.09999847

2 4.0826662e-015 57.74224472 -33.33749771

3 3.4994281e-015 49.49335098 -28.57499886

4 2.9161902e-015 41.24446106 -23.81250000

.....

49519 308.13064575 -1000.0000000 61.62612152

49520 467.81451416 -950.00000000 -187.12582397

49521 263.19549561 -549.99993896 -210.55639648

49522 280.43591309 -549.99993896 -168.26155090

*END

```
*KEYWORD
*TITLE
9-inch Penetrometer in cohesionless sediment
$
$ Units: kg, mm, ms, KN, GPa, KN-mm
$
*CONTROL_TERMINATION

$#  endtim    endcyc     dtmin    endeng    endmas

 40.000000

*CONTROL_TIMESTEP

$#  dtinit    tssfac      isdo    tslimt     dt2ms      lctm     erode     ms1st

 1.000000  0.450000         0     0.000     0.000         0         1

$#  dt2msf   dt2mslc     imscl

0.010000

*DATABASE_GLSTAT

$#      dt    binary

 0.100000         1

*DATABASE_MATSUM

$#      dt    binary

 0.100000         1

*DATABASE_NODOUT

$#      dt    binary

  0.100000         3

*DATABASE_RBDOUT

$#      dt    binary
```

```
 0.100000         3
*DATABASE_RCFORC
$#      dt    binary
 0.100000         1
*DATABASE_BINARY_D3PLOT
$#      dt      lcdt      beam     npltc
 1.000000
$#   ioopt
       0
*CONTACT_AUTOMATIC_ONE_WAY_SURFACE_TO_SURFACE_ID
$#     cid  title
1contact set
$#    ssid      msid     sstyp     mstyp    sboxid    mboxid       spr       mpr
       7         5         3         3         0         0         1         1
$#      fs        fd        dc        vc       vdc    penchk        bt        dt
    0.000     0.000     0.000     0.000     0.000         0     0.0001.0000E+20
$#     sfs       sfm       sst       mst      sfst      sfmt       fsf       vsf
 1.000000  1.000000     0.000     0.000  1.000000  1.000000  1.000000  1.000000
$#    soft    sofscl    lcidab    maxpar     sbopt     depth     bsort    frcfrq
       1  0.100000         0  1.025000  2.000000         2        25         1
*PART
$# title
9in penetrometer
```

```
$#     pid     secid       mid     eosid      hgid      grav    adpopt      tmid

       5         1         1

*SECTION_SHELL_TITLE

penetrometer

$#   secid    elform      shrf       nip     propt   qr/irid     icomp     setyp

     1         2  1.000000         2         1         0         0         1
$#      t1        t2        t3        t4      nloc     marea

1.000000  1.000000  1.000000  1.000000

*MAT_RIGID_TITLE

rigid material for penetrometer

$#     mid        ro         e        pr         n    couple         m     alias

       1 5.5134E-5 200.00000  0.310000     0.000     0.000     0.000

$#     cmo      con1      con2
    0.000         0         0

$#lco or a1       a2        a3        v1        v2        v3

  0.000     0.000     0.000     0.000     0.000     0.000

*PART

$# title

9 in soil larger
$#     pid     secid       mid     eosid      hgid      grav    adpopt      tmid

       7         2         4

*SECTION_SOLID_TITLE
soil

$#   secid    elform       aet
```

```
      2       1
*MAT_FHWA_SOIL_TITLE
soil
$#    mid       ro    nplot   spgrav   rhowat       vn   gammar   intrmx
      4 2.0820E-6        1  2.650000 1.0000E-6  2.000000  0.001000       10
$#      k        g   phimax     ahyp      coh    eccen       an       et
0.115000  0.069000  0.610000 4.4350E-7 6.2000E-6  1.000000
$#  mcont     pwd1    pwksk     pwd2   phires     dint     vdfm   damlev
   0.000    0.000    0.000    0.000  0.001000  0.100000  1.000000
$#  epsmax
 1.000000
*INITIAL_VELOCITY_RIGID_BODY
$#    pid       vx       vy       vz      vxr      vyr      vzr
   5    0.000 -5.500000
*SET_NODE_LIST_TITLE
NODESET(SPC) 1
$#    sid      da1      da2      da3      da4
      1
$#   nid1     nid2     nid3     nid4     nid5     nid6     nid7     nid8
  1468     1469     1470     1471     1472     1473     1474     1475
    1476     1477     1478     1479     1489     1490     1500     1501
   1511     1512     1522     1523     1533     1534     1544     1545
    1555     1556     1566     1567     1577     1578     1579     1580
```

1581 1582 1583 1584 1585 1586 1587 1588

1589 1599 1699 1709 1710 1720 1820 1830

1831 1841 1941 1951 1952 1962 2062 2072

2073 2083 2183 2193 2194 2204 2304 2314

2315 2325 2425 2435 2436 2446 2546 2556

2557 2567 2667 2677 2678 2679 2680 2681

2682 2683 2684 2685 2686 2687 2688 2689

2699 2700 2710 2711 2721 2722 2732 2733

2743 2744 2754 2755 2765 2766 2776 2777

2787 2788 2789 2790 2791 2792 2793 2794

2795 2796 2797 2798

*SET_NODE_LIST_TITLE
NODESET(SPC) 2

$# sid da1 da2 da3 da4

2

$# nid1 nid2 nid3 nid4 nid5 nid6 nid7 nid8

1 2 3 4 5 6 7 8

9 10 11 12 13 14 15 16

17 18 19 20 21 22 23 24

25 26 27 28 29 30 31 32

.....

13711 13712 13713 13714 13715 13716 13717 13718

13719 13720 13721 13722 13723 13724 13725 13726

13727 13728 13729 13730 13731 13732 13733 13734

13735 13736 13737 13738 13739

*SET_NODE_LIST_TITLE
NODESET(SPC) 4

$# sid da1 da2 da3 da4
4

$# nid1 nid2 nid3 nid4 nid5 nid6 nid7 nid8

2799 2800 2801 2802 2803 2804 2805 2806

2807 2808 2809 2810 2811 2812 2813 2814

2815 2816 2817 2818 2819 2820 2821 2822

2823 2824 2825 2826 2827 2828 2829 2830

.....
13711 13712 13713 13714 13715 13716 13717 13718

13719 13720 13721 13722 13723 13724 13725 13726

13727 13728 13729 13730 13731 13732 13733 13734

13735 13736 13737 13738 13739

*SET_SEGMENT_TITLE

soil

$# sid da1 da2 da3 da4

1

$# n1 n2 n3 n4 a1 a2 a3 a4

6374 6385 6616 6605

6539 6550 6781 6770

3030 3031 2800 2799

```
    2810      2799      2800      2811

.................................
   10509      5362     10443      5417
    10559      5477     10443      5362

    5417     10443      5351     10498
     5477     10548      5351     10443

   10498      5351     10432      5406
    10548      5466     10432      5351

    5406     10432      5340     10487
     5466     10537      5340     10432

*SET_SEGMENT_TITLE
penetrometer

$#     sid       da1       da2       da3       da4
         2

$#      n1        n2        n3        n4        a1        a2        a3        a4

       8         9       147       170

         1         2       171        21

       141        10        11       172

         2         3       173       171

         3         4       174       173

.................................
    1412      1411      1433      1432
     1413      1412      1432      1431

     1414      1413      1431      1430
     1415      1414      1430      1429

     1416      1415      1429      1428
     1417      1416      1428      1427
```

```
   1418     1417     1427     1425
*ELEMENT_SOLID
$#   eid     pid      n1      n2      n3      n4      n5      n6      n7      n8
 46166       7   49523   49864   49875   49534   49524   49865   49876   49535
  46167      7   49524   49865   49876   49535   49525   49866   49877   49536
  46168      7   49525   49866   49877   49536   49526   49867   49878   49537
  46169      7   49526   49867   49878   49537   49527   49868   49879   49538
.............................
 61162       7   57029   60863   53296   61052   57028   53351   60797   61041
  61163      7   57028   53351   60797   61041   57027   60852   53285   61030
  61164      7   57027   60852   53285   61030   57026   53340   60786   61019
 61165       7   57026   53340   60786   61019   57025   60841   53274   61008
*ELEMENT_SHELL
$#   eid     pid      n1      n2      n3      n4      n5      n6      n7      n8
  22467      5   25047   25048   25065   25064
 22468       5   25046   25047   25064   25066
 22469       5   25045   25046   25066   25067
 22470       5   25044   25045   25067   25068
.................................
31162       5   33322   33323   33250   33251
31163       5   33249   33250   33323   33324
31164       5   33248   33249   33324   33325
 31165      5   33247   33248   33325   33326
```

*NODE

$#  nid  x  y  z  tc  rc

1 4.6659043e-015 65.99113464 -38.09999847

2 4.0826662e-015 57.74224472 -33.33749771

3 3.4994281e-015 49.49335098 -28.57499886

4 2.9161902e-015 41.24446106 -23.81250000

.....

66204 487.07330322 -1866.6665039 -12.07333469
66205 476.89093018 -1866.6665039 83.78777313

66206 453.63470459 -1866.6665039 171.31225586
66207 422.82650757 -1866.6665039 245.96894836

66208 389.76220703 -1866.6665039 307.46334839
66209 464.50061035 -2000.0000000 -196.66627502

66210 382.85171509 -1933.3332520 -382.85171509
66211 409.85565186 -1933.3332520 -332.38616943

*END

# Appendix B

## Test Site Locations

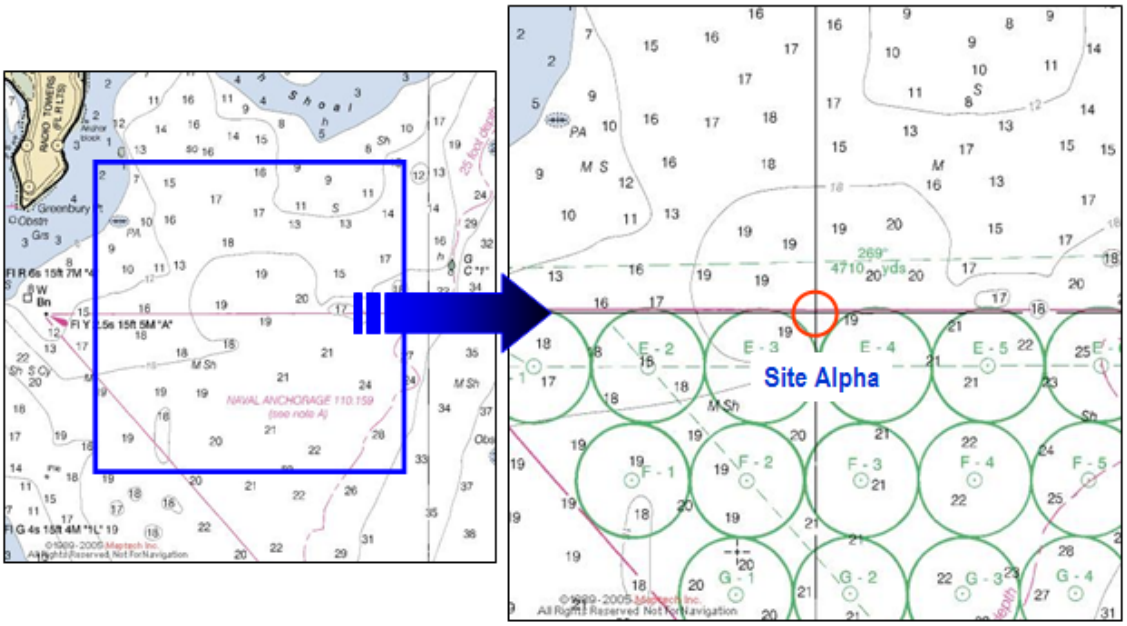


1 Oct 07, Site Alpha (38°58’N 76°26’W), Clay

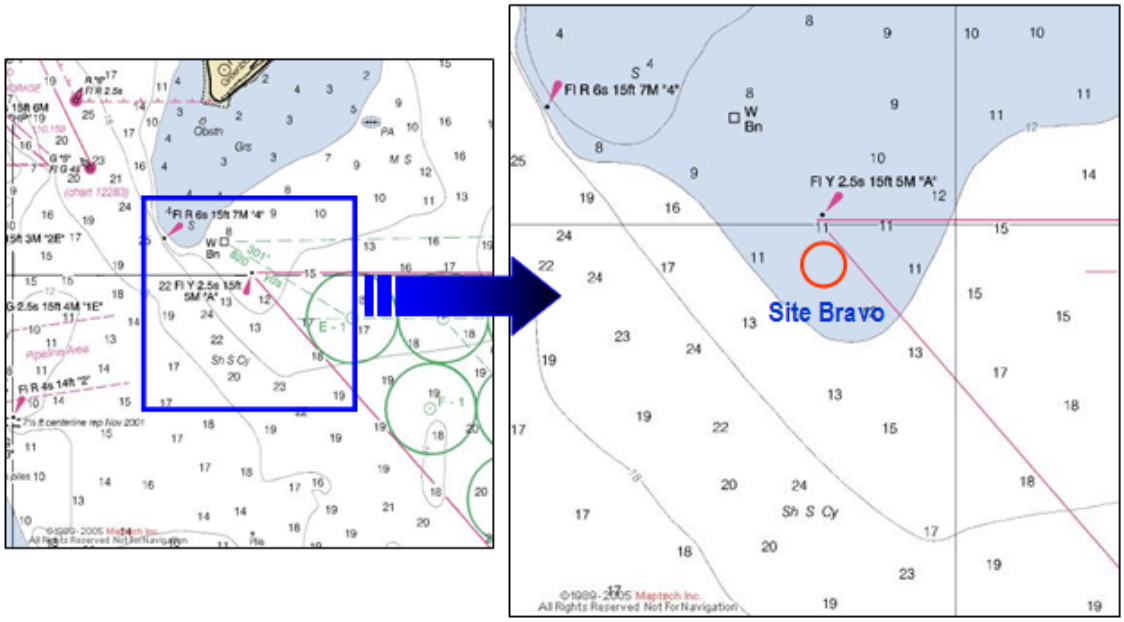


15 Oct 07 and 19 Feb 08, Site Bravo (38°57.95’N 76°27.15’W), Sand

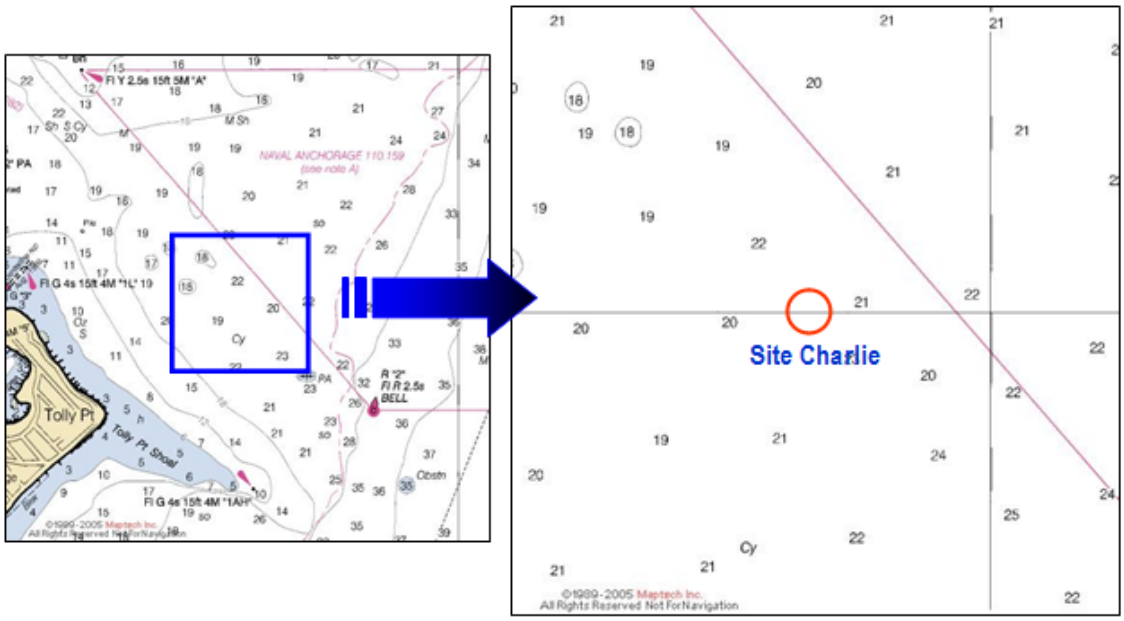


15 Oct 07, 19 Feb 08, and 31 Mar, Site Charlie (38°57.0’N 76°26.2’W), Clay

# Appendix C

## Accelerometer Results

Oct 1 – Site Alpha – 21 ft water depth
Clay Drops - 3 inch…108

Oct 15 – Sit Charlie – 21 ft water depth
Clay Drops - 3 inch…115
Site Bravo – 11 ft water depth
Sand Drops - 3 inch…120

Feb 19 – Site Charlie - 21 ft water depth
Clay drops - 9 inch…123
Site Bravo - 10 ft water depth
Sand Drops – 9 inch…125

Mar 31 – Site Charlie – 21 ft water depth
Clay Drops - 9 inch …126

Drop 1

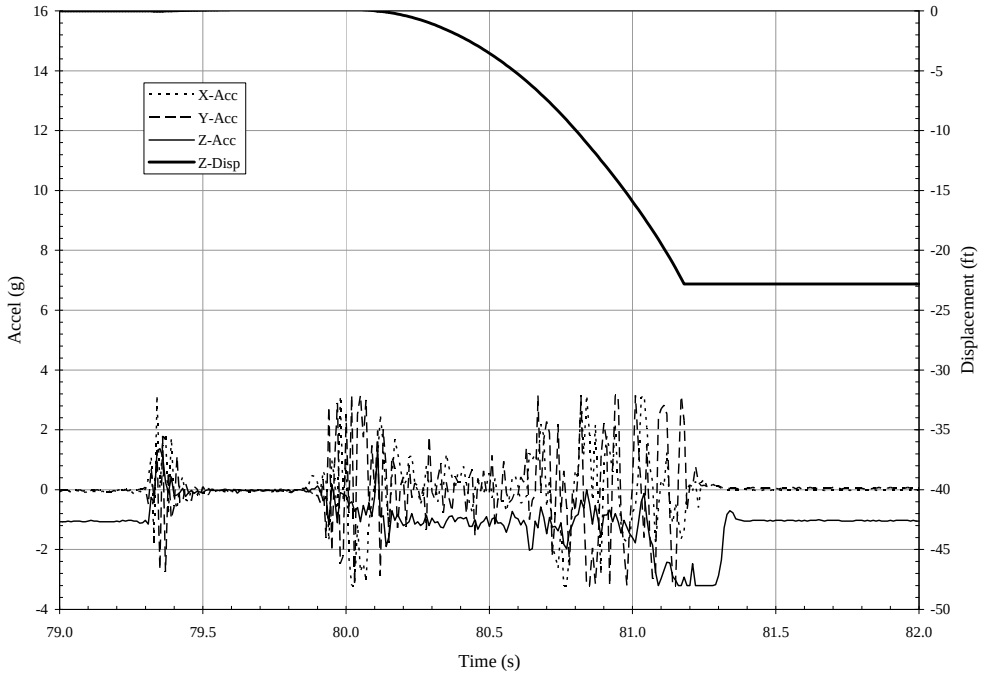
X-Acc
Y-Acc
Z-Acc
Z-Disp
Accel (g)
Displacement (ft)
Time (s)
16
14
12
10
8
6
4
2
0
-4
0
-5
-10
-15
-20
-25
-30
-35
-40
-45
-50
79.0
79.5
80.0
80.5
81.0
81.5
82.0

Drop 2

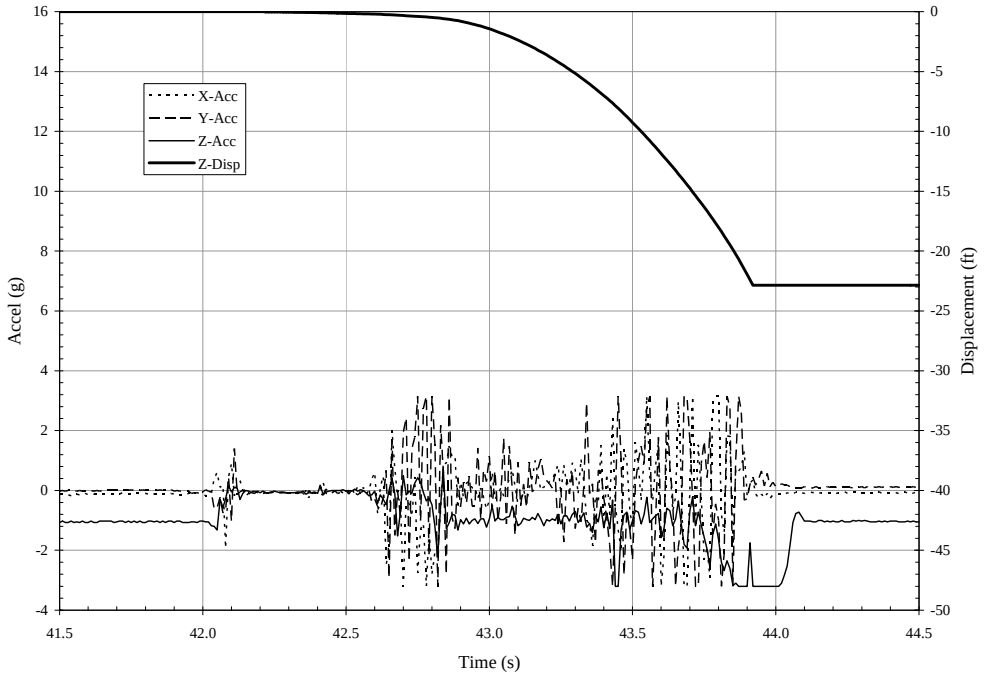
X-Acc
Y-Acc
Z-Acc
Z-Disp
Accel (g)
Displacement (ft)
Time (s)
16
14
12
10
8
6
4
2
0
-4
0
-5
-10
-15
-20
-25
-30
-35
-40
-45
-50
41.5
42.0
42.5
43.0
43.5
44.0
44.5

Drop 3

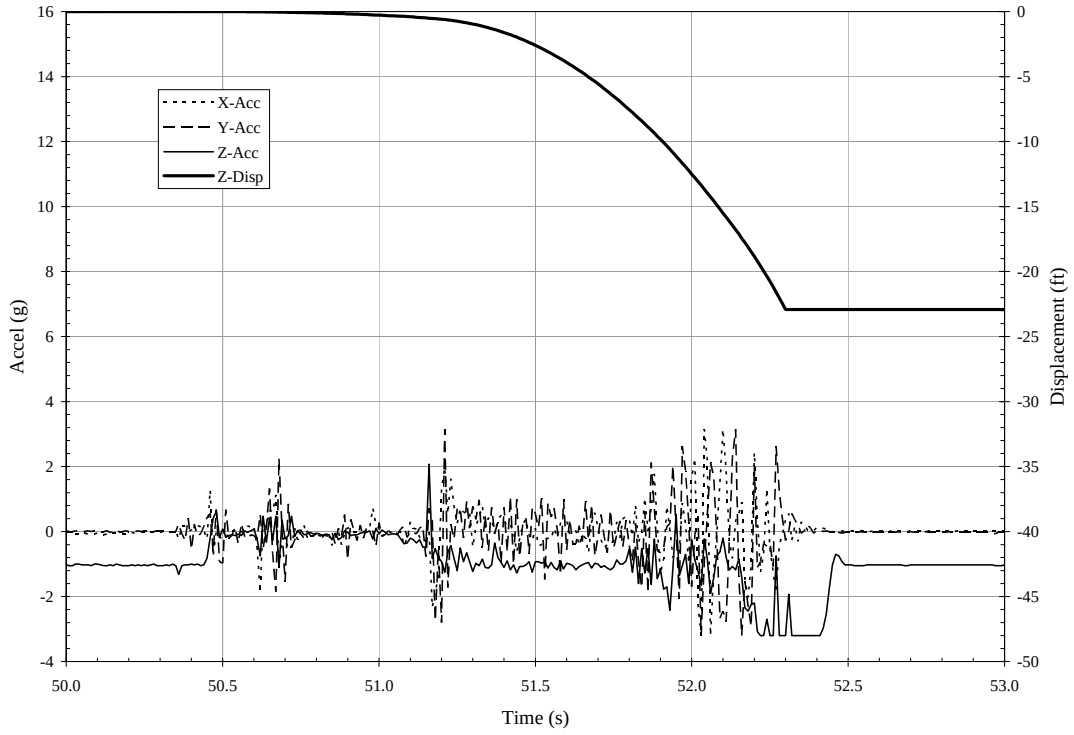
X-Acc
Y-Acc
Z-Acc
Z-Disp
Accel (g)
Displacement (ft)
Time (s)
16
14
12
10
8
6
4
2
0
-2
-4
0
-5
-10
-15
-20
-25
-30
-35
-40
-45
-50
50.0
50.5
51.0
51.5
52.0
52.5
53.0

Drop 4

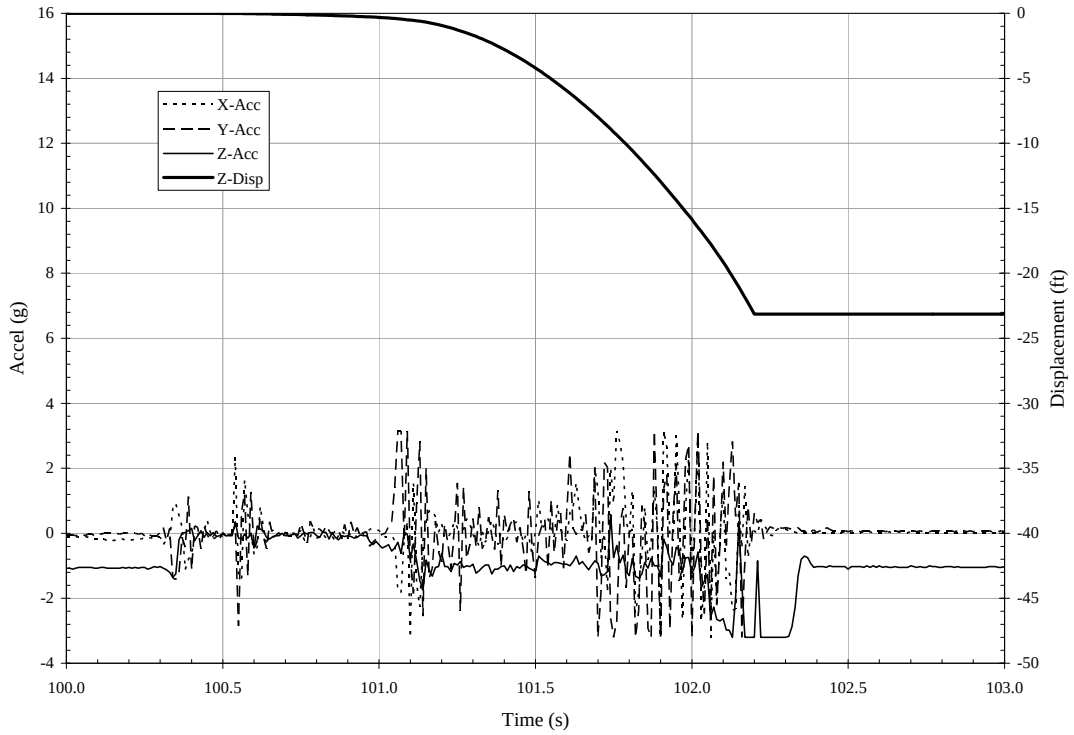
X-Acc
Y-Acc
Z-Acc
Z-Disp
Accel (g)
Displacement (ft)
Time (s)
16
14
12
10
8
6
4
2
0
-2
-4
0
-5
-10
-15
-20
-25
-30
-35
-40
-45
-50
100.0
100.5
101.0
101.5
102.0
102.5
103.0

Drop 5

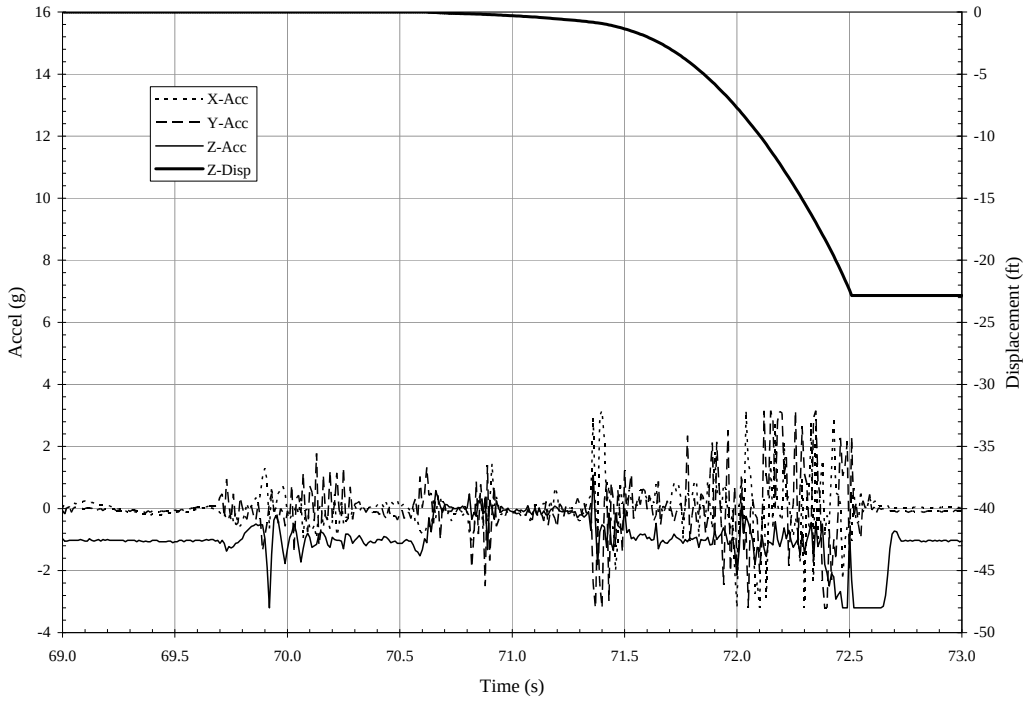
X-Acc
Y-Acc
Z-Acc
Z-Disp
Accel (g)
Displacement (ft)
Time (s)
16
14
12
10
8
6
4
2
0
-2
-4
0
-5
-10
-15
-20
-25
-30
-35
-40
-45
-50
69.0
69.5
70.0
70.5
71.0
71.5
72.0
72.5
73.0

Drop 6

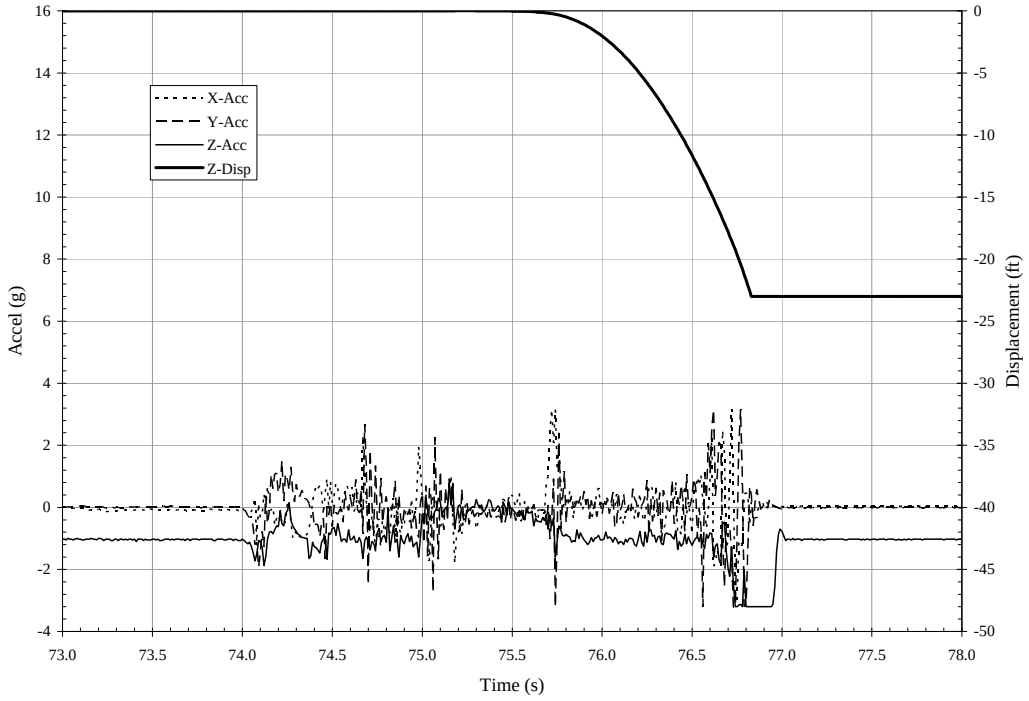
X-Acc
Y-Acc
Z-Acc
Z-Disp
Accel (g)
Displacement (ft)
Time (s)
16
14
12
10
8
6
4
2
0
-2
-4
0
-5
-10
-15
-20
-25
-30
-35
-40
-45
-50
73.0
73.5
74.0
74.5
75.0
75.5
76.0
76.5
77.0
77.5
78.0

Drop 7

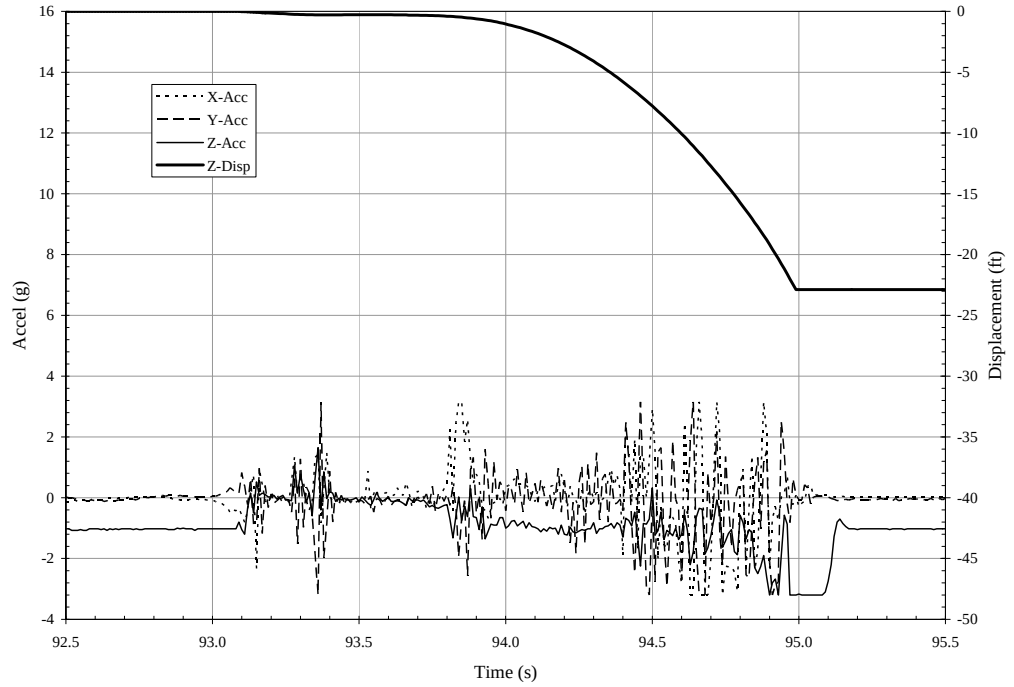
X-Acc
Y-Acc
Z-Acc
Z-Disp
Accel (g)
Displacement (ft)
Time (s)
16
14
12
10
8
6
4
2
0
-2
-4
0
-5
-10
-15
-20
-25
-30
-35
-40
-45
-50
92.5
93.0
93.5
94.0
94.5
95.0
95.5

Drop 8

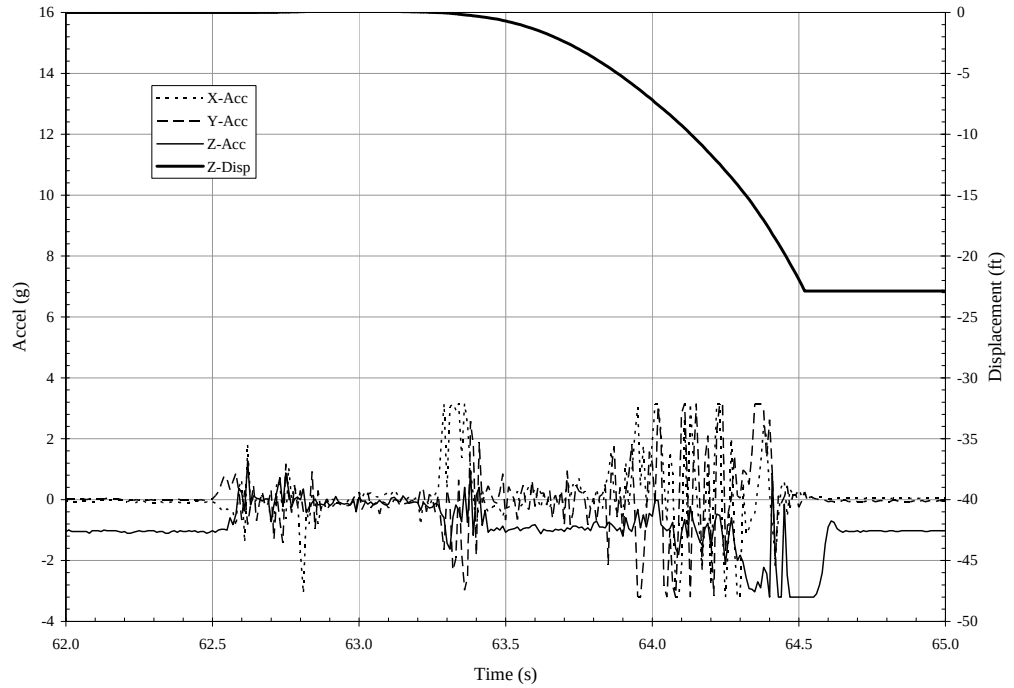
X-Acc
Y-Acc
Z-Acc
Z-Disp
Accel (g)
Displacement (ft)
Time (s)
16
14
12
10
8
6
4
2
0
-2
-4
0
-5
-10
-15
-20
-25
-30
-35
-40
-45
-50
62.0
62.5
63.0
63.5
64.0
64.5
65.0

Drop 9

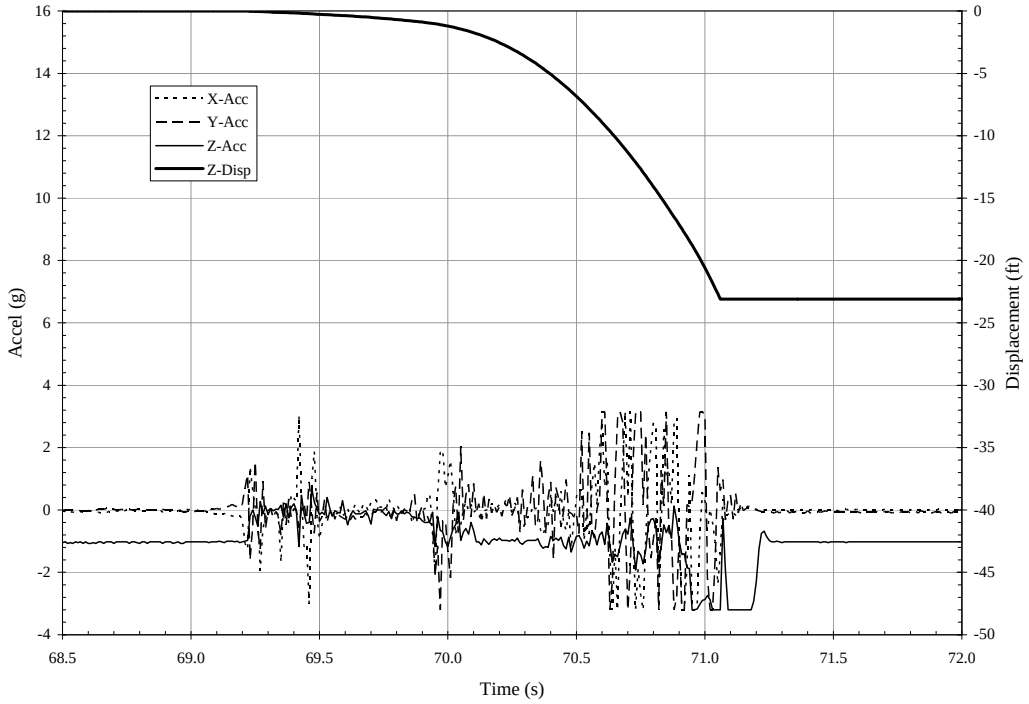


Drop 10

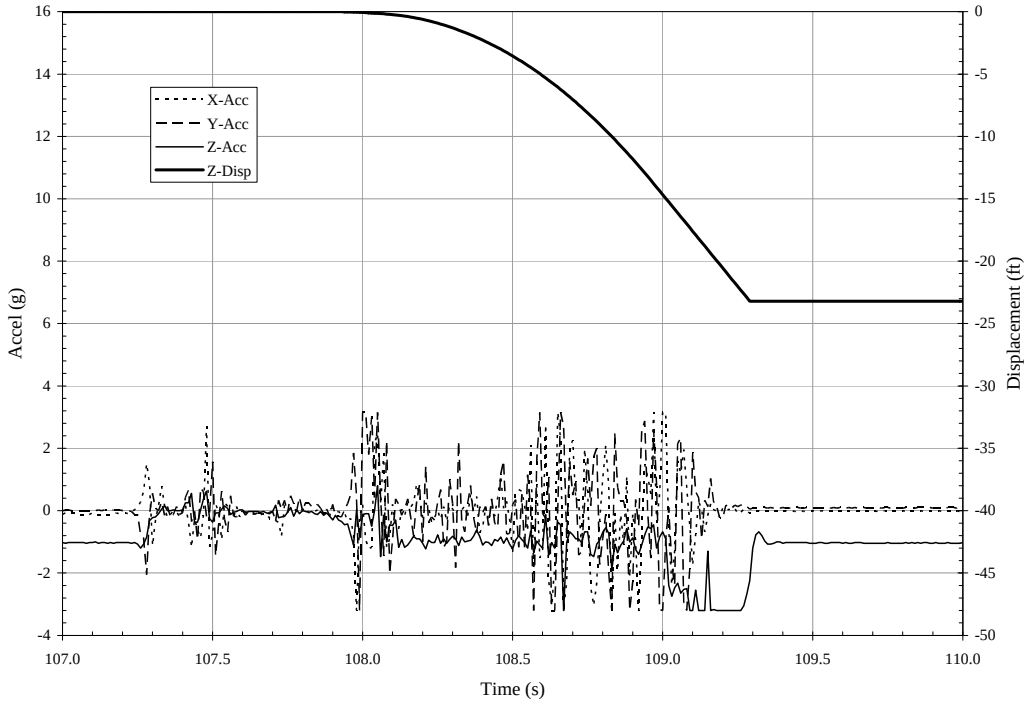

Drop 11

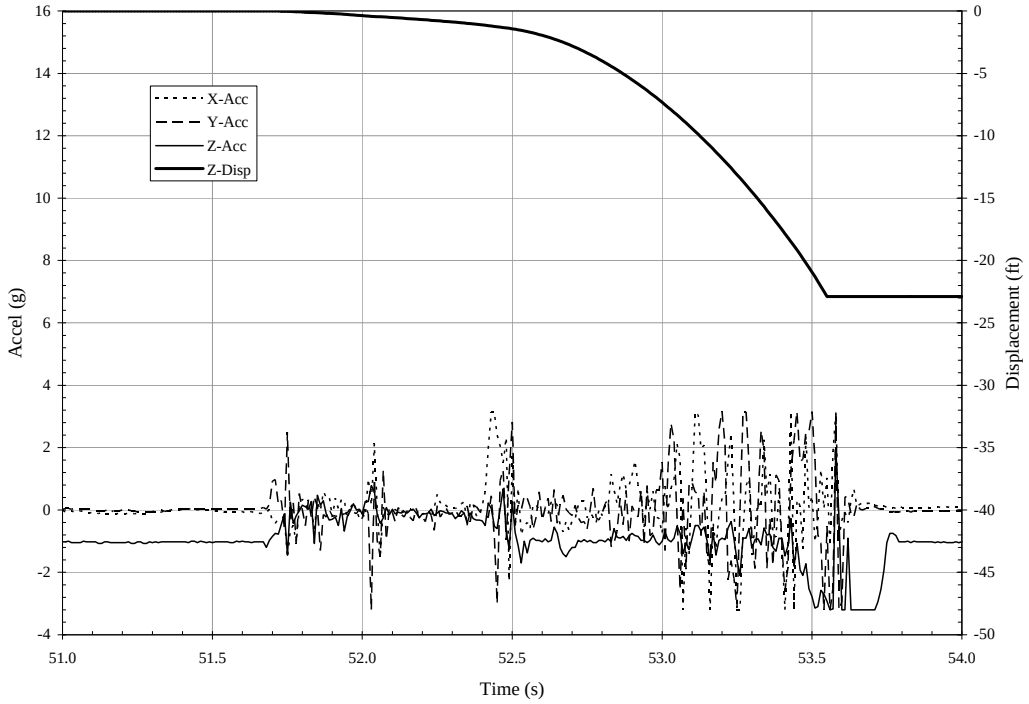


Drop 12

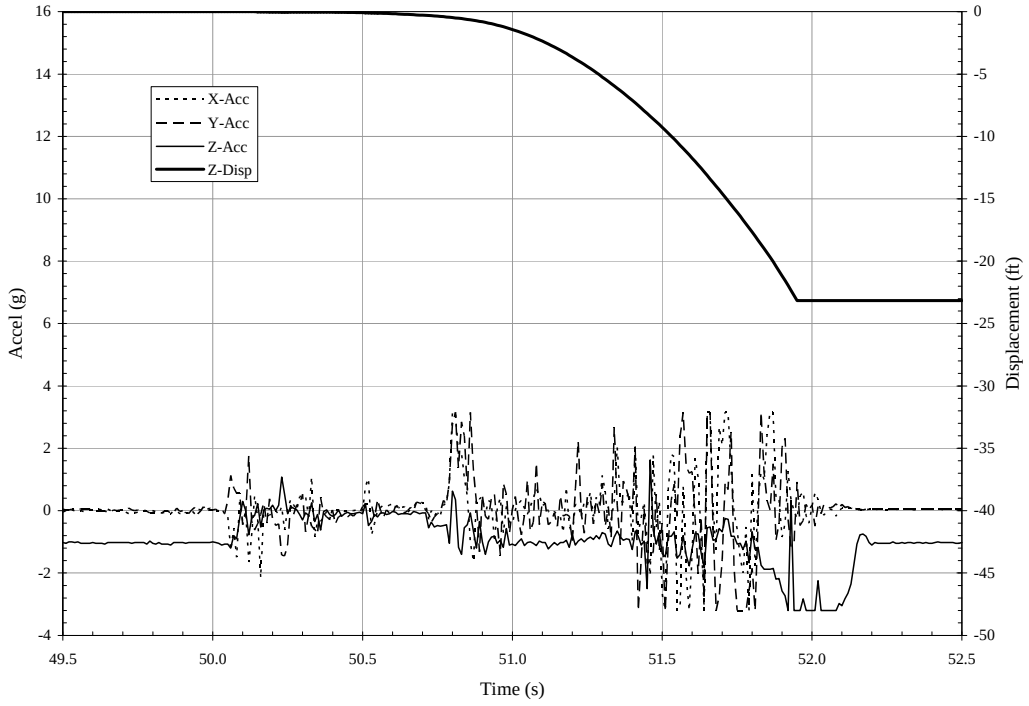

Drop 13

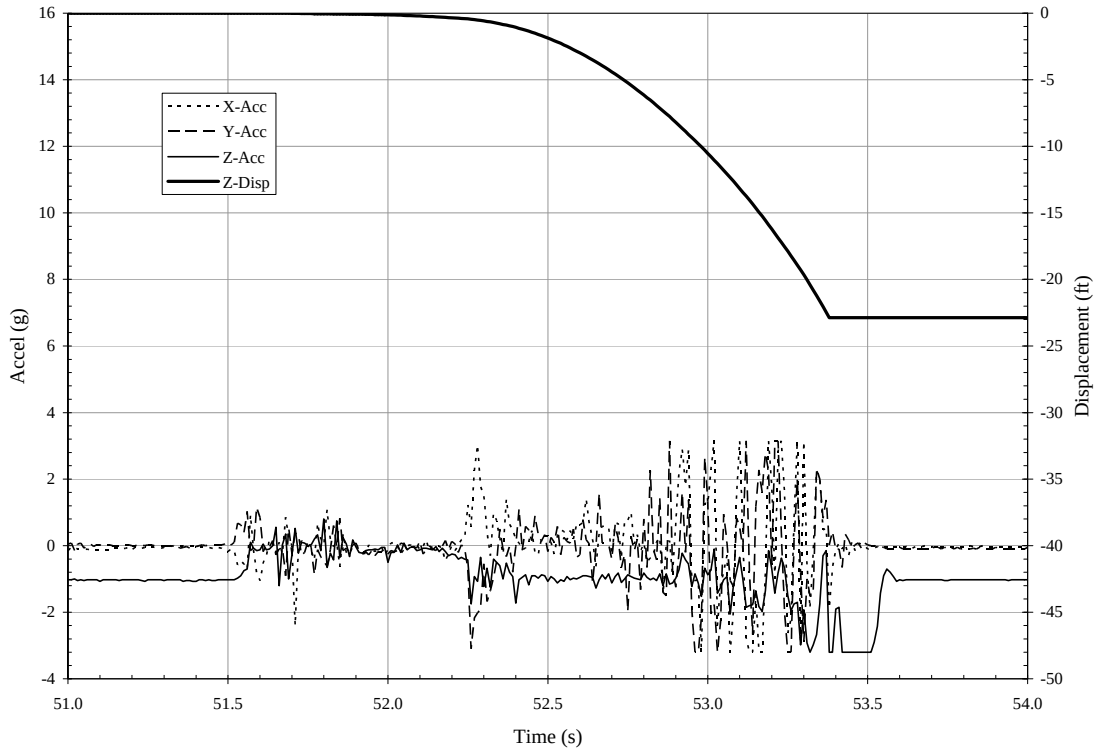
X-Acc
Y-Acc
Z-Acc
Z-Disp
Accel (g)
Displacement (ft)
Time (s)
16
14
12
10
8
6
4
2
0
-2
-4
0
-5
-10
-15
-20
-25
-30
-35
-40
-45
-50
51.0
51.5
52.0
52.5
53.0
53.5
54.0

Drop 1

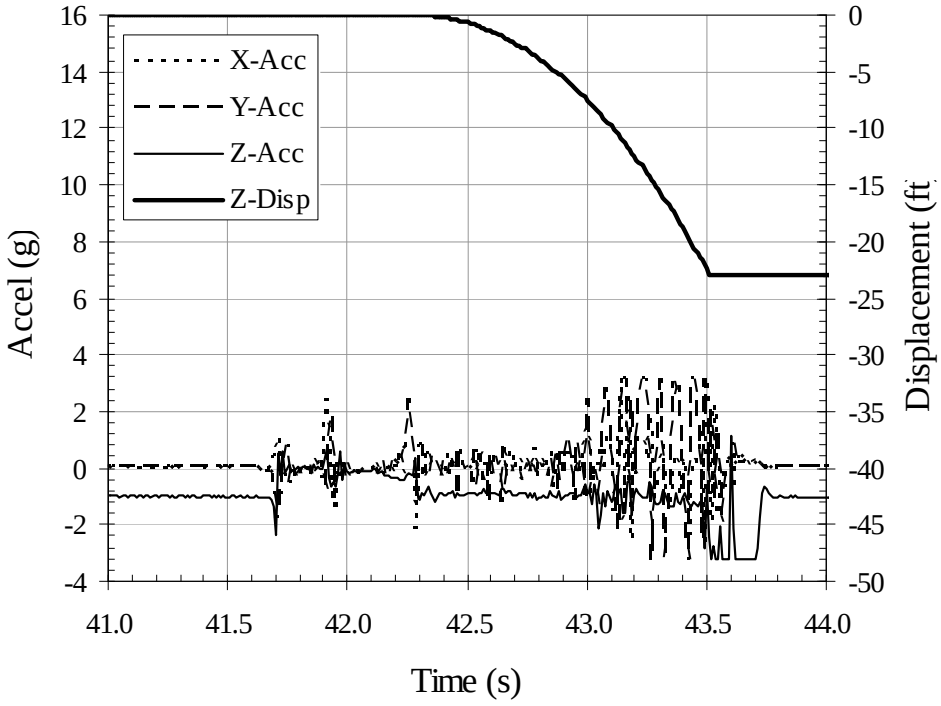
X-Acc
Y-Acc
Z-Acc
Z-Disp
Accel (g)
Displacement (ft
Time (s)
16
14
12
10
8
6
4
2
0
-2
-4
0
-5
-10
-15
-20
-25
-30
-35
-40
-45
-50
41.0
41.5
42.0
42.5
43.0
43.5
44.0

Drop 2

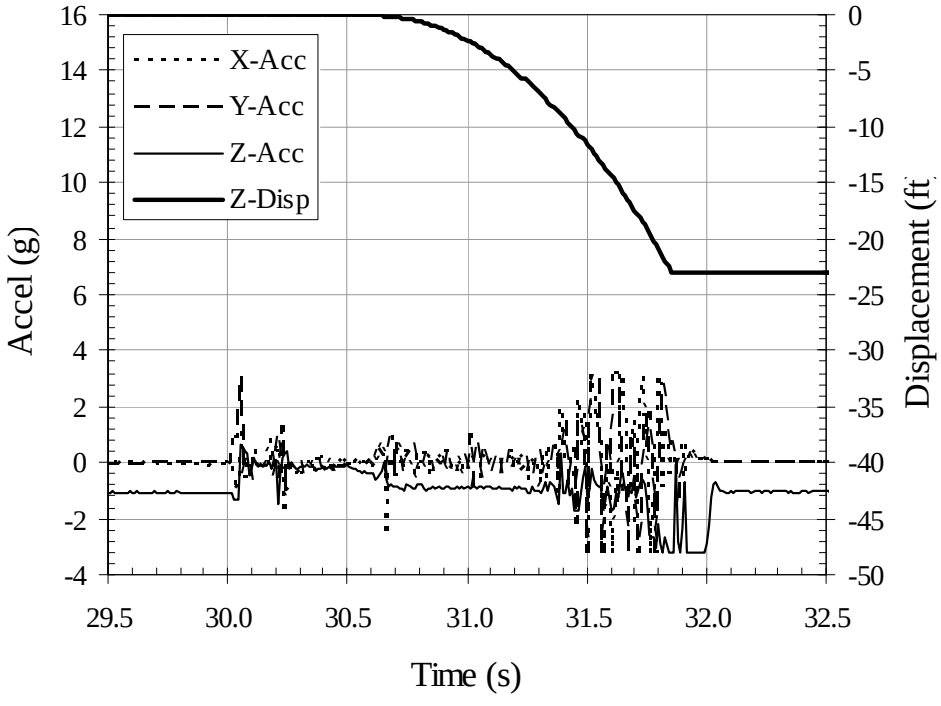
X-Acc
Y-Acc
Z-Acc
Z-Disp
Accel (g)
Displacement (ft
Time (s)
16
14
12
10
8
6
4
2
0
-2
-4
0
-5
-10
-15
-20
-25
-30
-35
-40
-45
-50
29.5
30.0
30.5
31.0
31.5
32.0
32.5

Drop 3

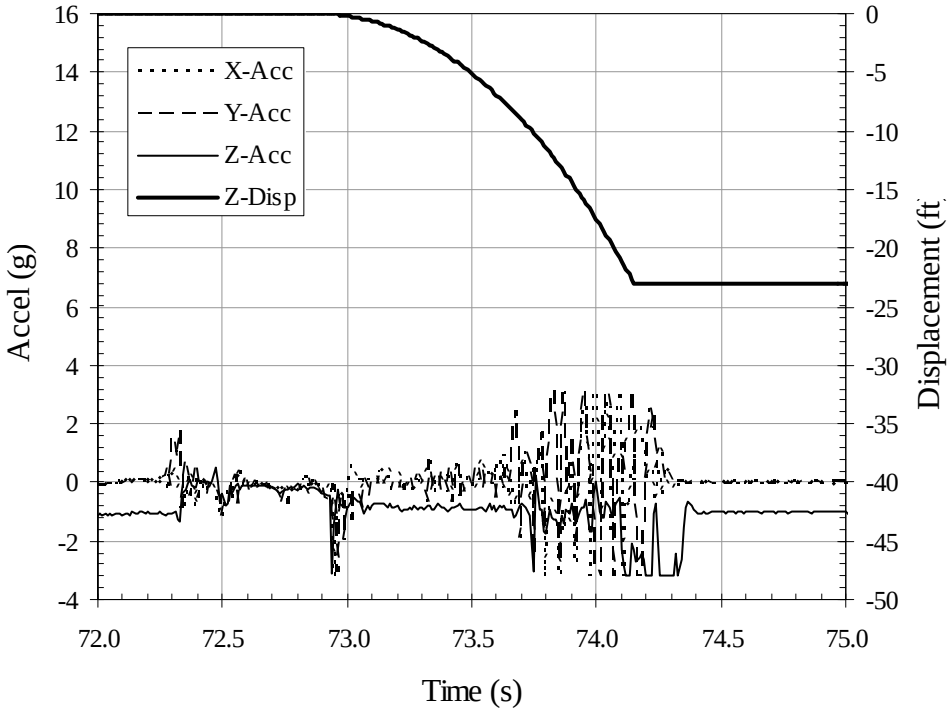
X-Acc
Y-Acc
Z-Acc
Z-Disp
Accel (g)
Displacement (ft)
Time (s)
16
14
12
10
8
6
4
2
0
-2
-4
0
-5
-10
-15
-20
-25
-30
-35
-40
-45
-50
72.0
72.5
73.0
73.5
74.0
74.5
75.0

Drop 4

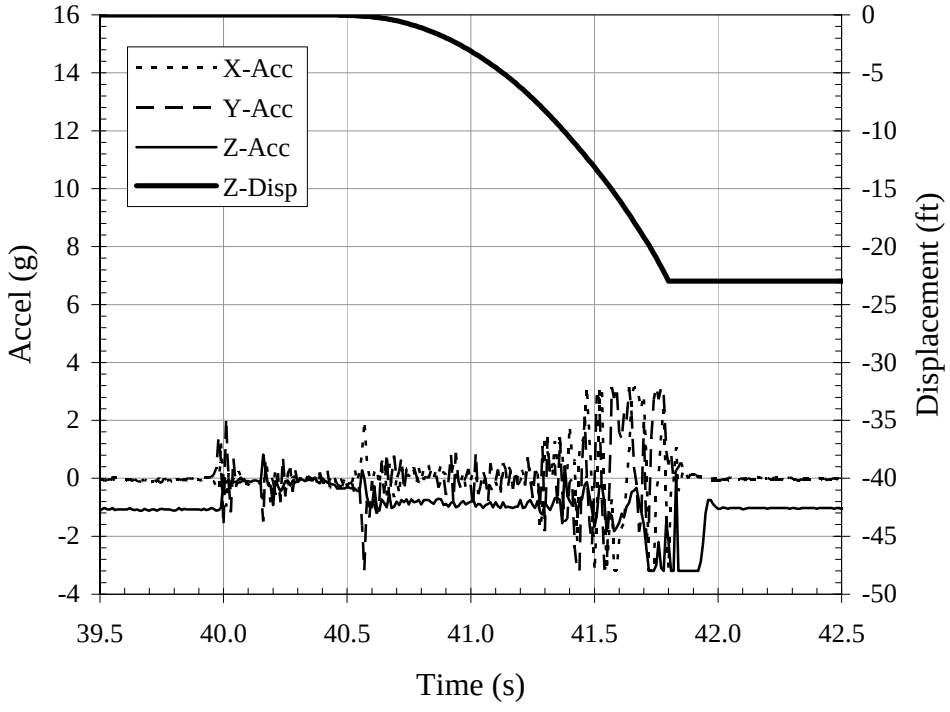
X-Acc
Y-Acc
Z-Acc
Z-Disp
Accel (g)
Displacement (ft)
Time (s)
16
14
12
10
8
6
4
2
0
-2
-4
0
-5
-10
-15
-20
-25
-30
-35
-40
-45
-50
39.5
40.0
40.5
41.0
41.5
42.0
42.5

Drop 5

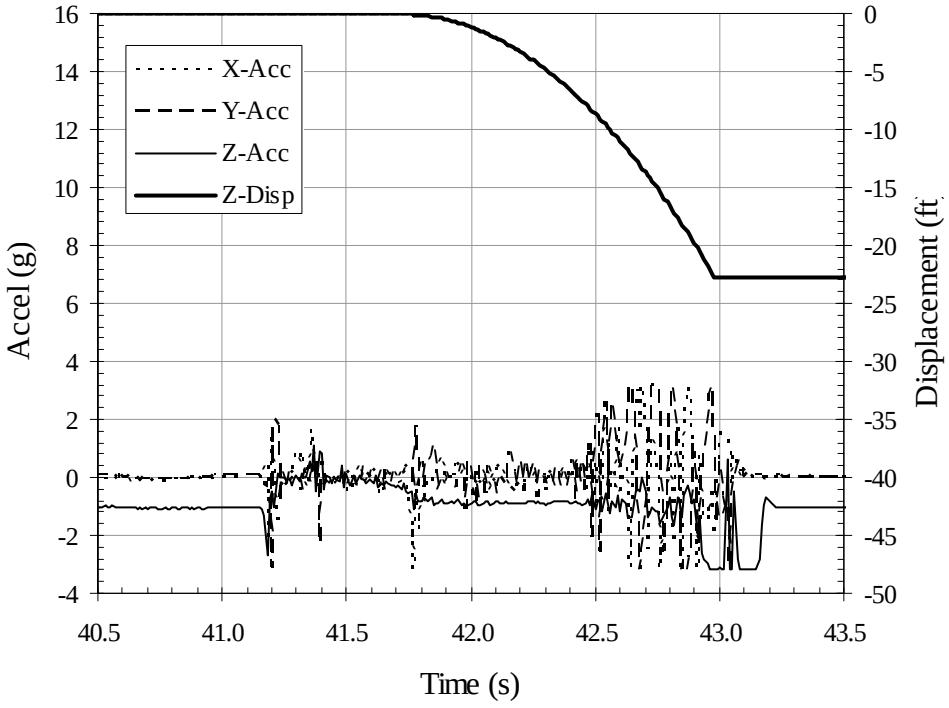
X-Acc
Y-Acc
Z-Acc
Z-Disp
Accel (g)
Displacement (ft)
Time (s)
16
14
12
10
8
6
4
2
0
-2
-4
0
-5
-10
-15
-20
-25
-30
-35
-40
-45
-50
40.5
41.0
41.5
42.0
42.5
43.0
43.5

Drop 6

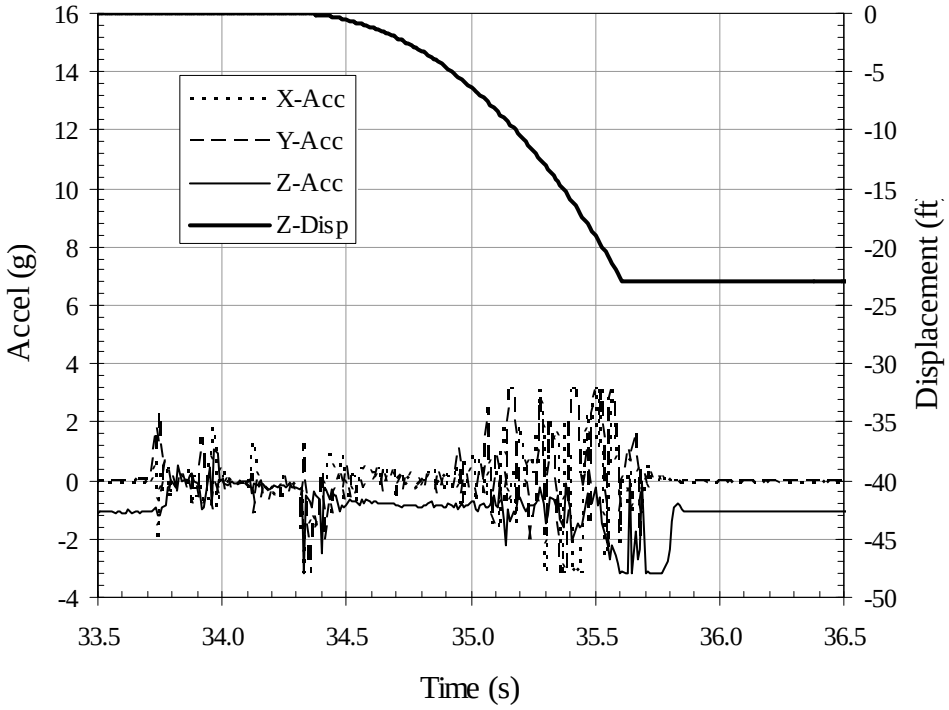
X-Acc
Y-Acc
Z-Acc
Z-Disp
Accel (g)
Displacement (ft)
Time (s)
16
14
12
10
8
6
4
2
0
-2
-4
0
-5
-10
-15
-20
-25
-30
-35
-40
-45
-50
33.5
34.0
34.5
35.0
35.5
36.0
36.5

Drop 7

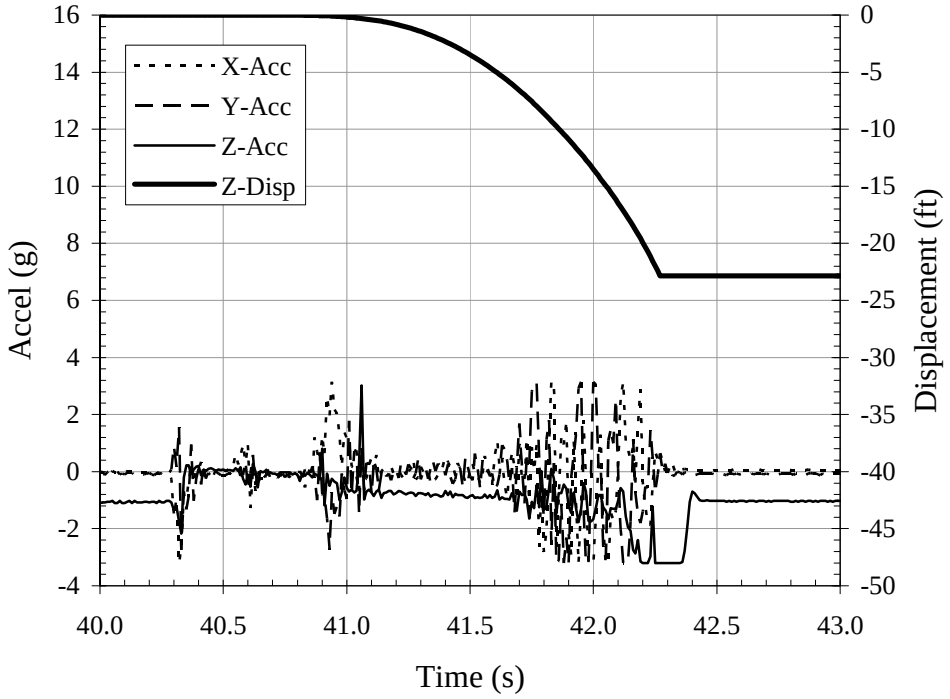
X-Acc
Y-Acc
Z-Acc
Z-Disp
Accel (g)
Displacement (ft)
Time (s)
16
14
12
10
8
6
4
2
0
-2
-4
0
-5
-10
-15
-20
-25
-30
-35
-40
-45
-50
40.0
40.5
41.0
41.5
42.0
42.5
43.0

Drop 8

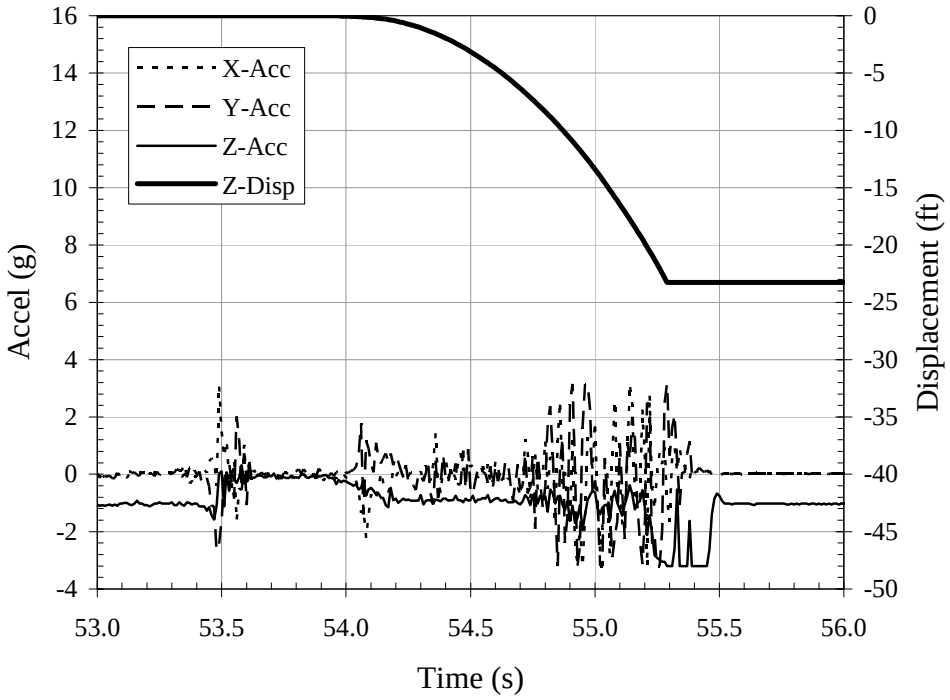
X-Acc
Y-Acc
Z-Acc
Z-Disp
Accel (g)
Displacement (ft)
Time (s)
16
14
12
10
8
6
4
2
0
-2
-4
0
-5
-10
-15
-20
-25
-30
-35
-40
-45
-50
53.0
53.5
54.0
54.5
55.0
55.5
56.0

Drop 9

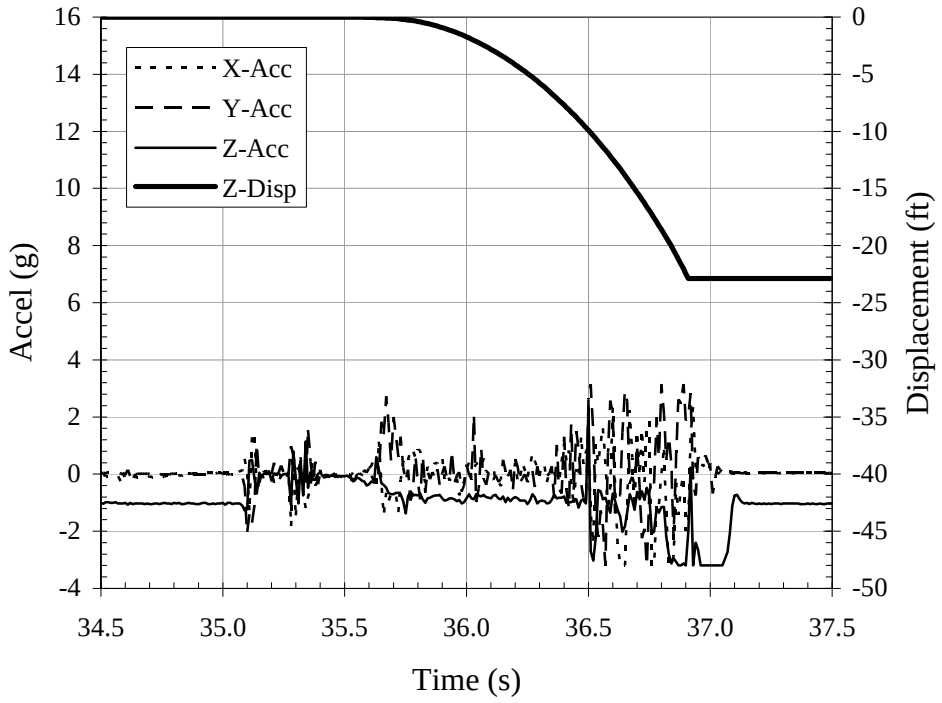


Drop 10

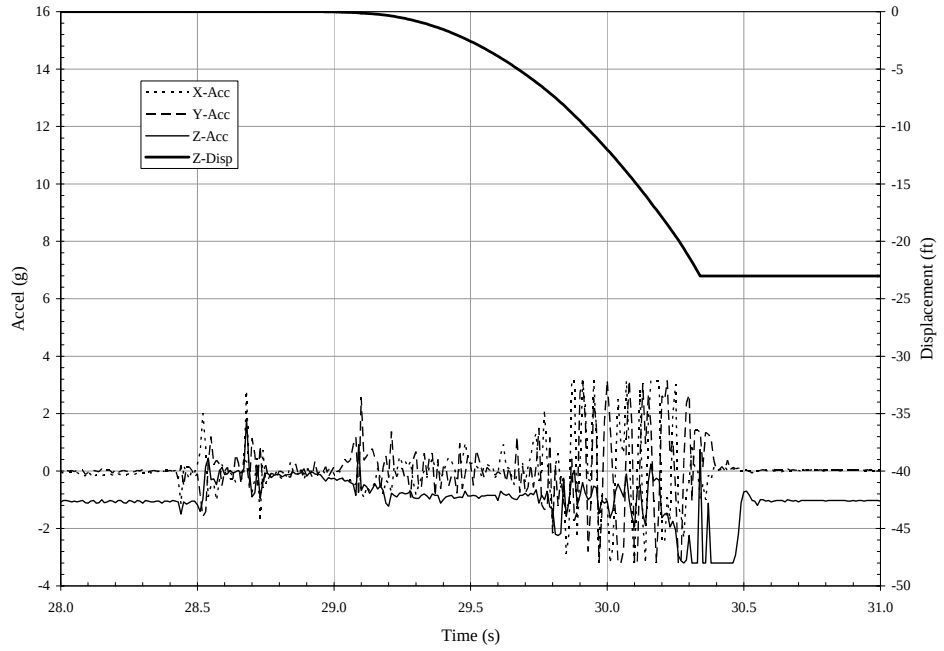

Drop 1

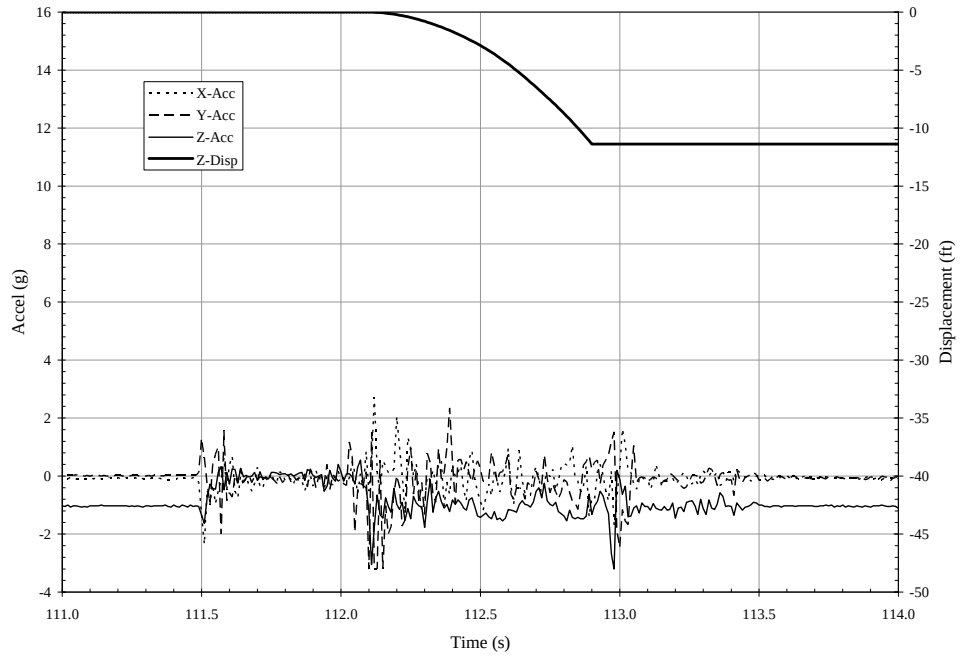
X-Acc
Y-Acc
Z-Acc
Z-Disp
Accel (g)
Displacement (ft)
Time (s)
16
14
12
10
8
6
4
2
0
-2
-4
0
-5
-10
-15
-20
-25
-30
-35
-40
-45
-50
111.0
111.5
112.0
112.5
113.0
113.5
114.0

Drop 2

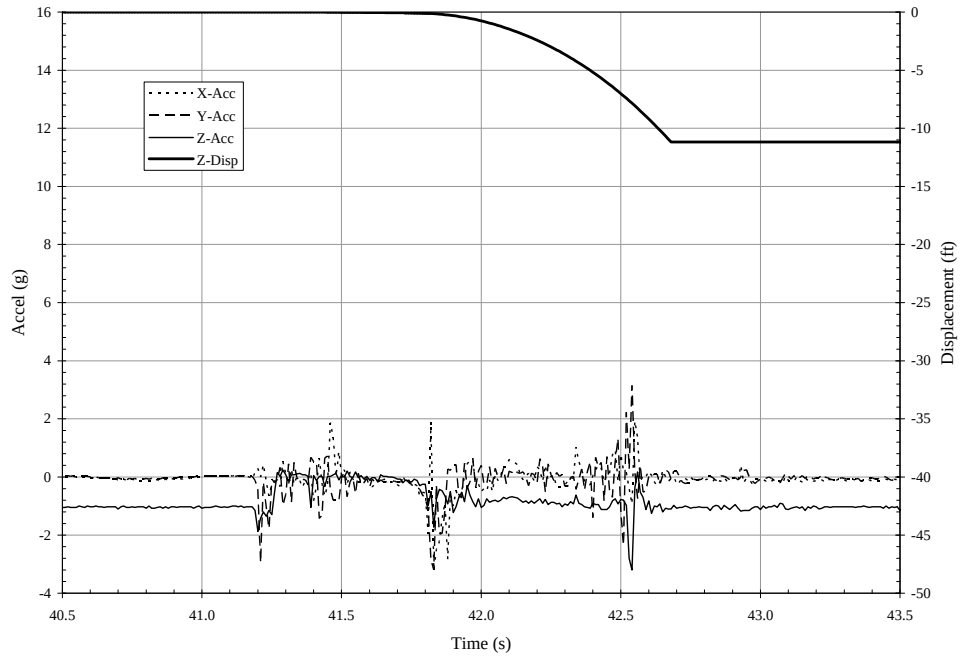
X-Acc
Y-Acc
Z-Acc
Z-Disp
Accel (g)
Displacement (ft)
Time (s)
16
14
12
10
8
6
4
2
0
-2
-4
0
-5
-10
-15
-20
-25
-30
-35
-40
-45
-50
40.5
41.0
41.5
42.0
42.5
43.0
43.5

Drop 3

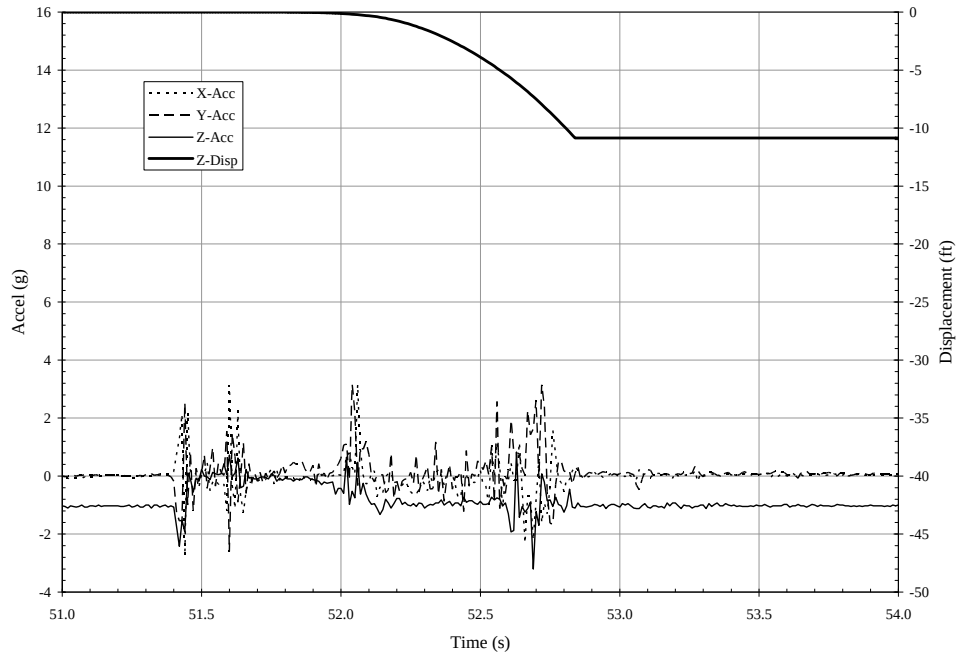
X-Acc
Y-Acc
Z-Acc
Z-Disp
Accel (g)
Displacement (ft)
Time (s)
16
14
12
10
8
6
4
2
0
-2
-4
0
-5
-10
-15
-20
-25
-30
-35
-40
-45
-50
51.0
51.5
52.0
52.5
53.0
53.5
54.0

Drop 4

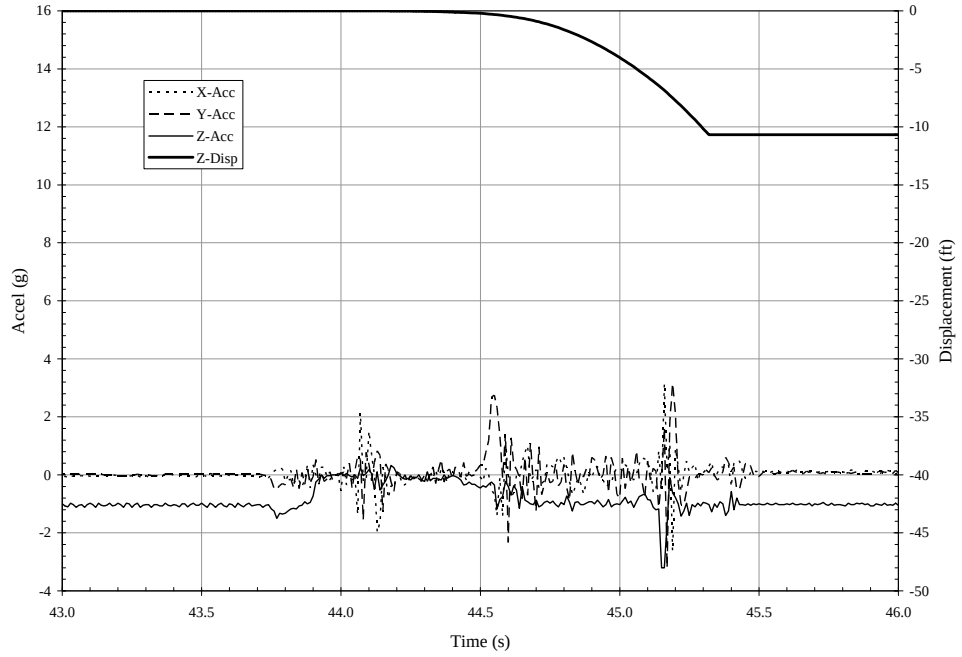
X-Acc
Y-Acc
Z-Acc
Z-Disp
Accel (g)
Displacement (ft)
Time (s)
16
14
12
10
8
6
4
2
0
-2
-4
0
-5
-10
-15
-20
-25
-30
-35
-40
-45
-50
43.0
43.5
44.0
44.5
45.0
45.5
46.0

Drop 5

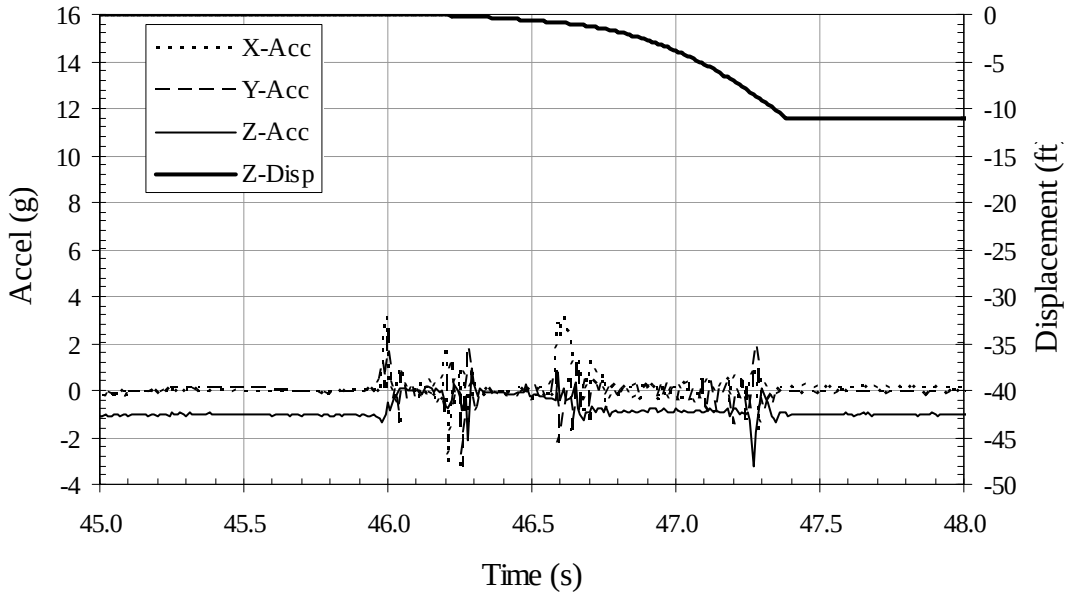
X-Acc
Y-Acc
Z-Acc
Z-Disp
Accel (g)
Displacement (ft)
Time (s)
16
14
12
10
8
6
4
2
0
-2
-4
0
-5
-10
-15
-20
-25
-30
-35
-40
-45
-50
45.0
45.5
46.0
46.5
47.0
47.5
48.0

Drop 1

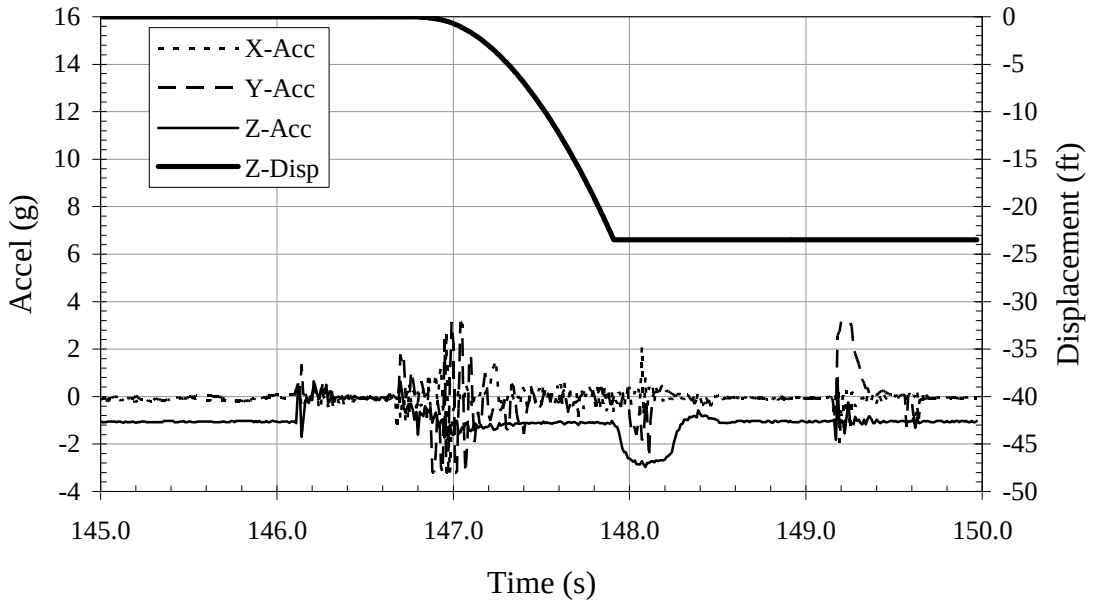
X-Acc
Y-Acc
Z-Acc
Z-Disp
Accel (g)
Displacement (ft)
Time (s)
16
14
12
10
8
6
4
2
0
-2
-4
0
-5
-10
-15
-20
-25
-30
-35
-40
-45
-50
145.0
146.0
147.0
148.0
149.0
150.0

Drop 2

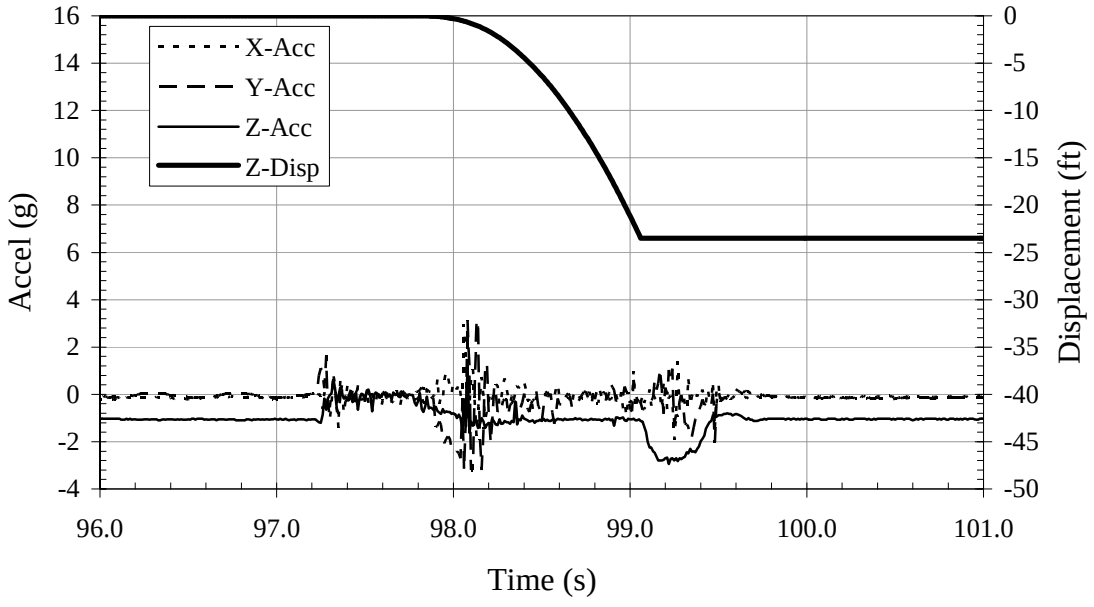
X-Acc
Y-Acc
Z-Acc
Z-Disp
Accel (g)
Displacement (ft)
Time (s)
16
14
12
10
8
6
4
2
0
-2
-4
0
-5
-10
-15
-20
-25
-30
-35
-40
-45
-50
96.0
97.0
98.0
99.0
100.0
101.0

Drop 3

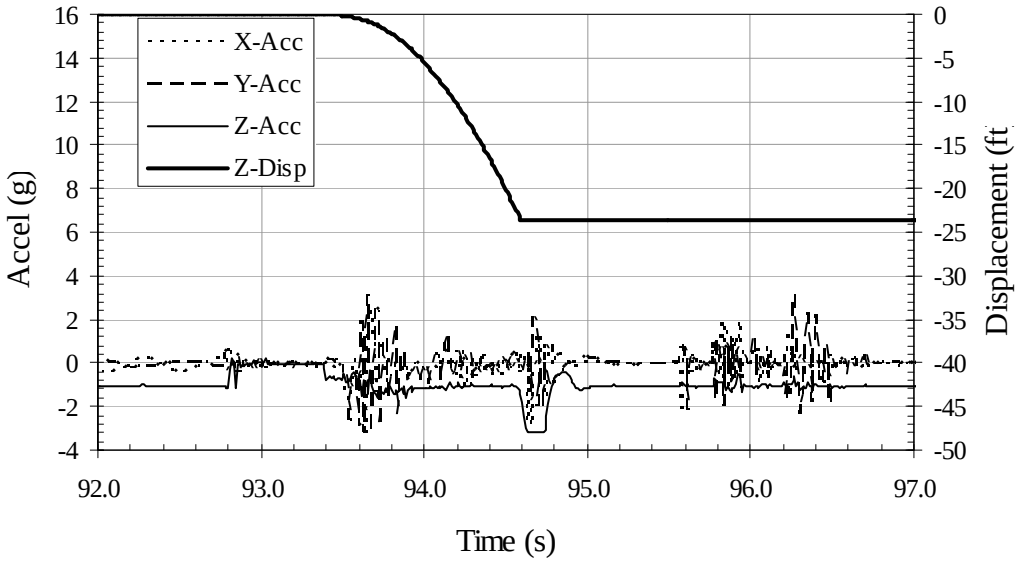
X-Acc
Y-Acc
Z-Acc
Z-Disp
Accel (g)
Displacement (ft
Time (s)
16
14
12
10
8
6
4
2
0
-2
-4
0
-5
-10
-15
-20
-25
-30
-35
-40
-45
-50
92.0
93.0
94.0
95.0
96.0
97.0

Drop 1

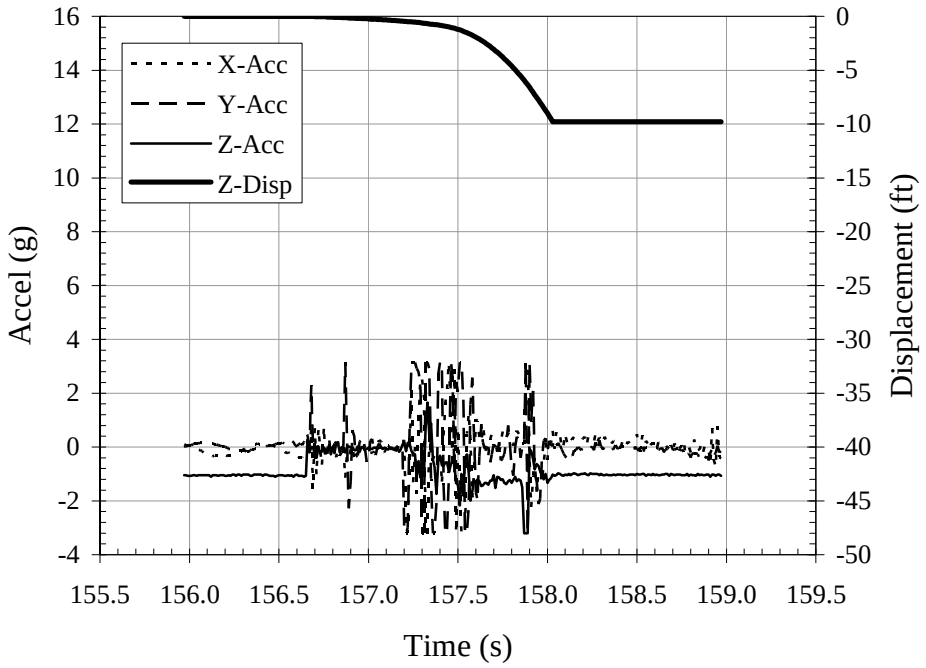
X-Acc
Y-Acc
Z-Acc
Z-Disp
Accel (g)
Displacement (ft)
Time (s)
16
14
12
10
8
6
4
2
0
-2
-4
0
-5
-10
-15
-20
-25
-30
-35
-40
-45
-50
155.5
156.0
156.5
157.0
157.5
158.0
158.5
159.0
159.5

Drop 2

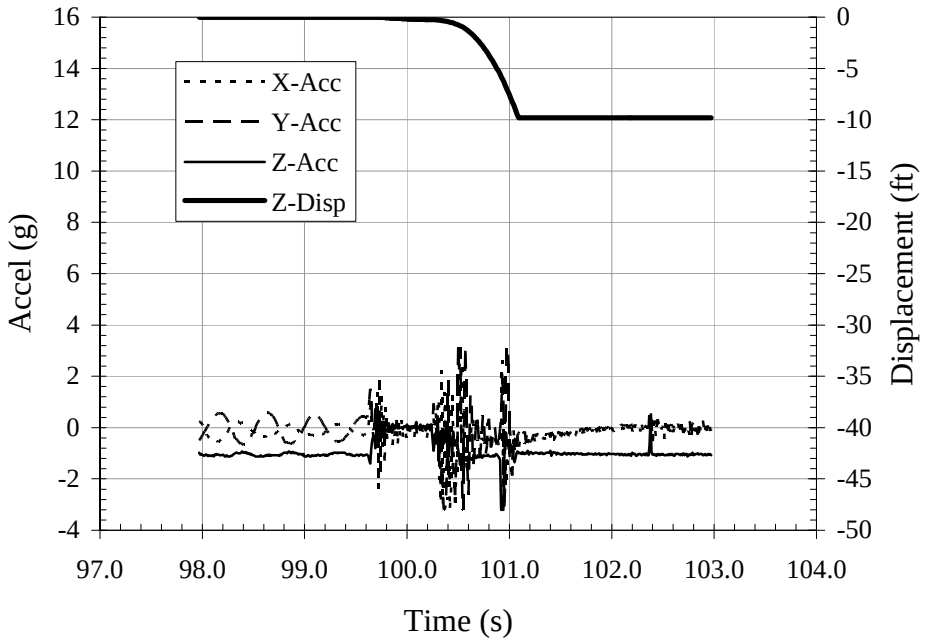
X-Acc
Y-Acc
Z-Acc
Z-Disp
Accel (g)
Displacement (ft)
Time (s)
16
14
12
10
8
6
4
2
0
-2
-4
0
-5
-10
-15
-20
-25
-30
-35
-40
-45
-50
97.0
98.0
99.0
100.0
101.0
102.0
103.0
104.0

Drop 1

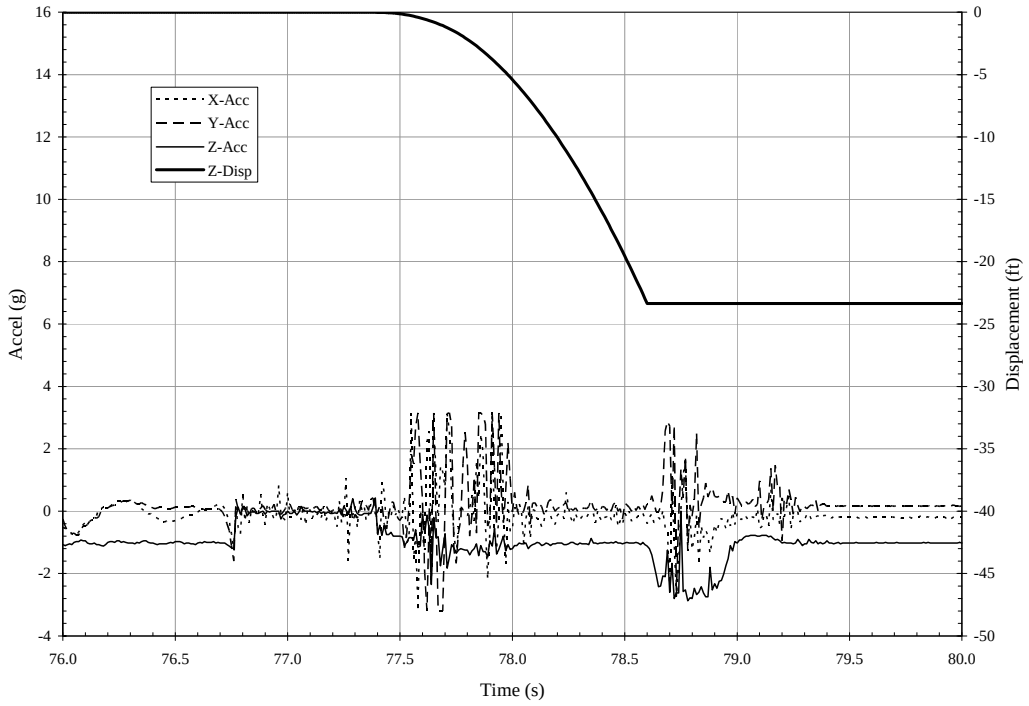
X-Acc
Y-Acc
Z-Acc
Z-Disp
Accel (g)
Displacement (ft)
Time (s)
16
14
12
10
8
6
4
2
0
-4
0
-5
-10
-15
-20
-25
-30
-35
-40
-45
-50
76.0
76.5
77.0
77.5
78.0
78.5
79.0
79.5
80.0

Drop 2

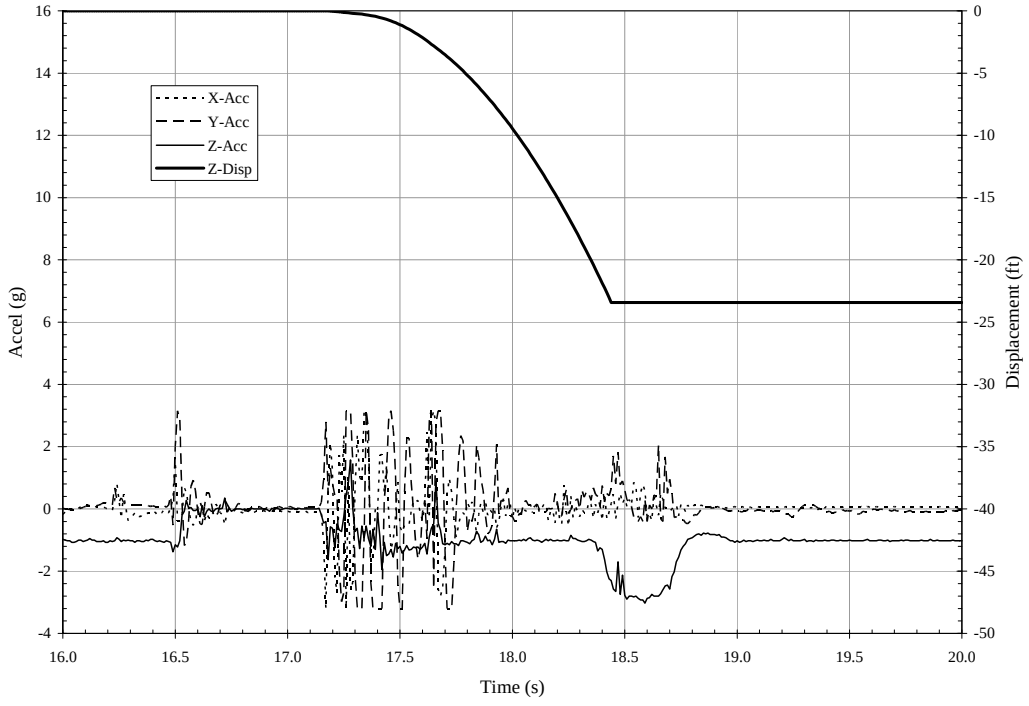
X-Acc
Y-Acc
Z-Acc
Z-Disp
Accel (g)
Displacement (ft)
Time (s)
16
14
12
10
8
6
4
2
0
-4
0
-5
-10
-15
-20
-25
-30
-35
-40
-45
-50
16.0
16.5
17.0
17.5
18.0
18.5
19.0
19.5
20.0

Drop 3

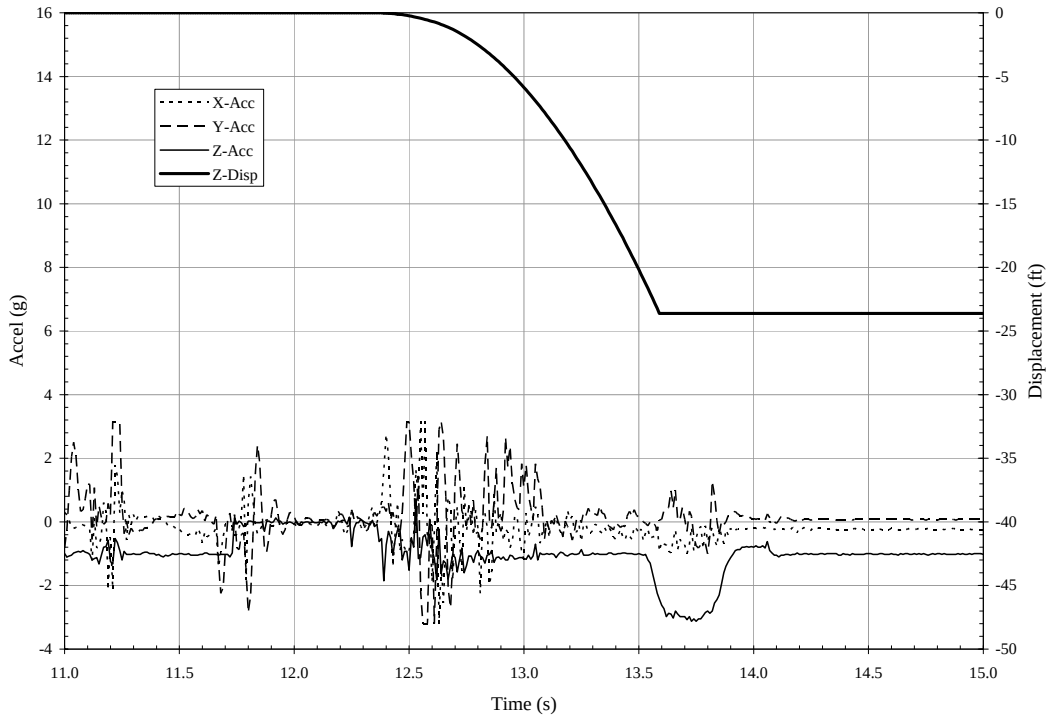
X-Acc
Y-Acc
Z-Acc
Z-Disp
Accel (g)
Displacement (ft)
Time (s)
16
14
12
10
8
6
4
2
0
-4
0
-5
-10
-15
-20
-25
-30
-35
-40
-45
-50
11.0
11.5
12.0
12.5
13.0
13.5
14.0
14.5
15.0

Drop 4

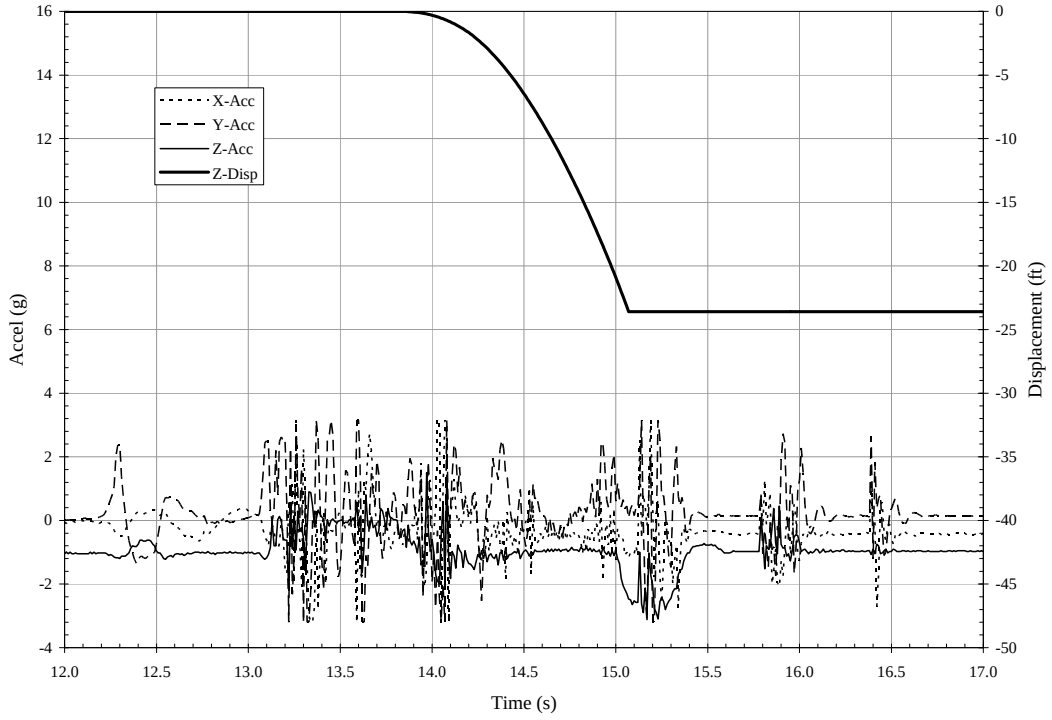
X-Acc
Y-Acc
Z-Acc
Z-Disp
Accel (g)
Displacement (ft)
Time (s)
16
14
12
10
8
6
4
2
0
-4
0
-5
-10
-15
-20
-25
-30
-35
-40
-45
-50
12.0
12.5
13.0
13.5
14.0
14.5
15.0
15.5
16.0
16.5
17.0

Drop 5

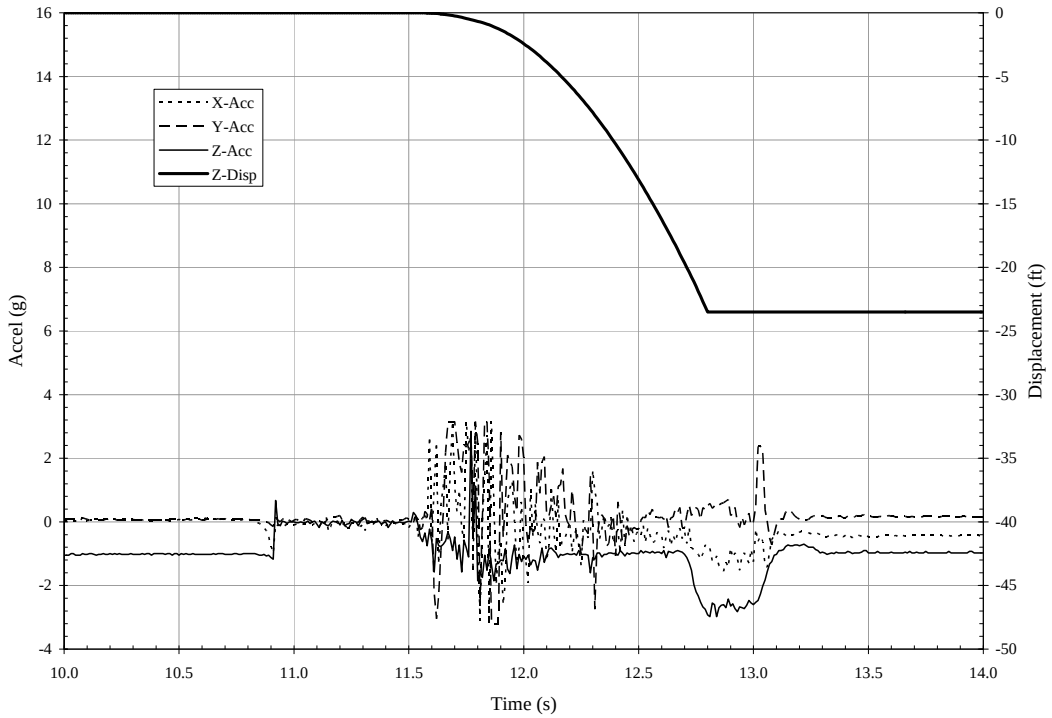
X-Acc
Y-Acc
Z-Acc
Z-Disp
Accel (g)
Displacement (ft)
Time (s)
16
14
12
10
8
6
4
2
0
-2
-4
0
-5
-10
-15
-20
-25
-30
-35
-40
-45
-50
10.0
10.5
11.0
11.5
12.0
12.5
13.0
13.5
14.0

Drop 6

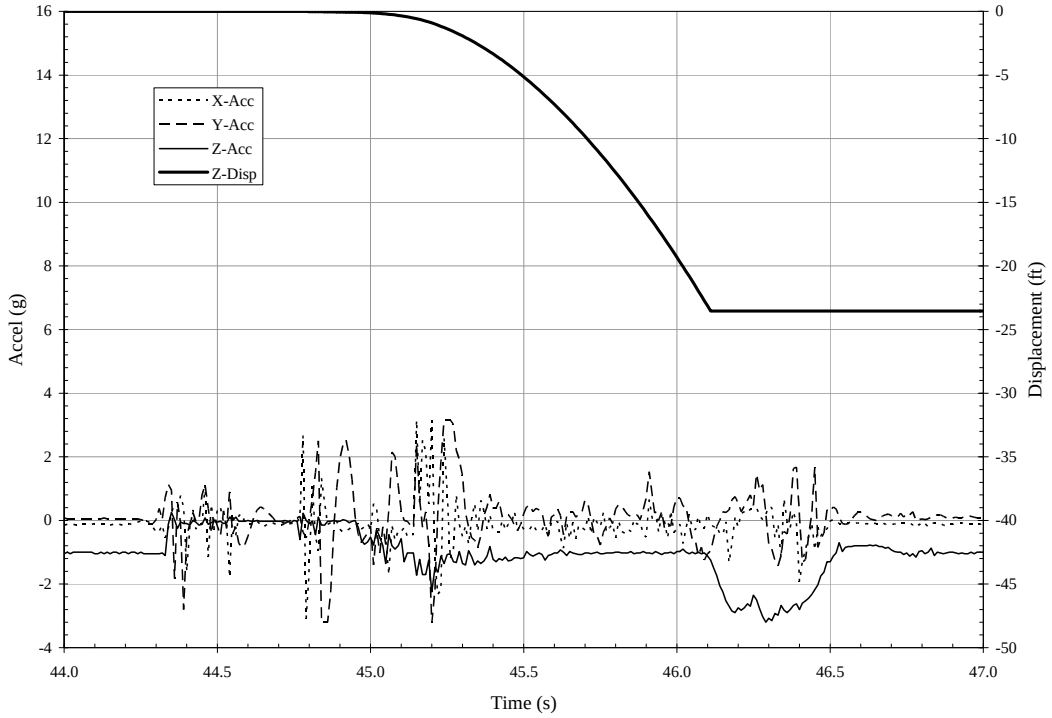
X-Acc
Y-Acc
Z-Acc
Z-Disp
Accel (g)
Displacement (ft)
Time (s)
16
14
12
10
8
6
4
2
0
-2
-4
0
-5
-10
-15
-20
-25
-30
-35
-40
-45
-50
44.0
44.5
45.0
45.5
46.0
46.5
47.0

Drop 7

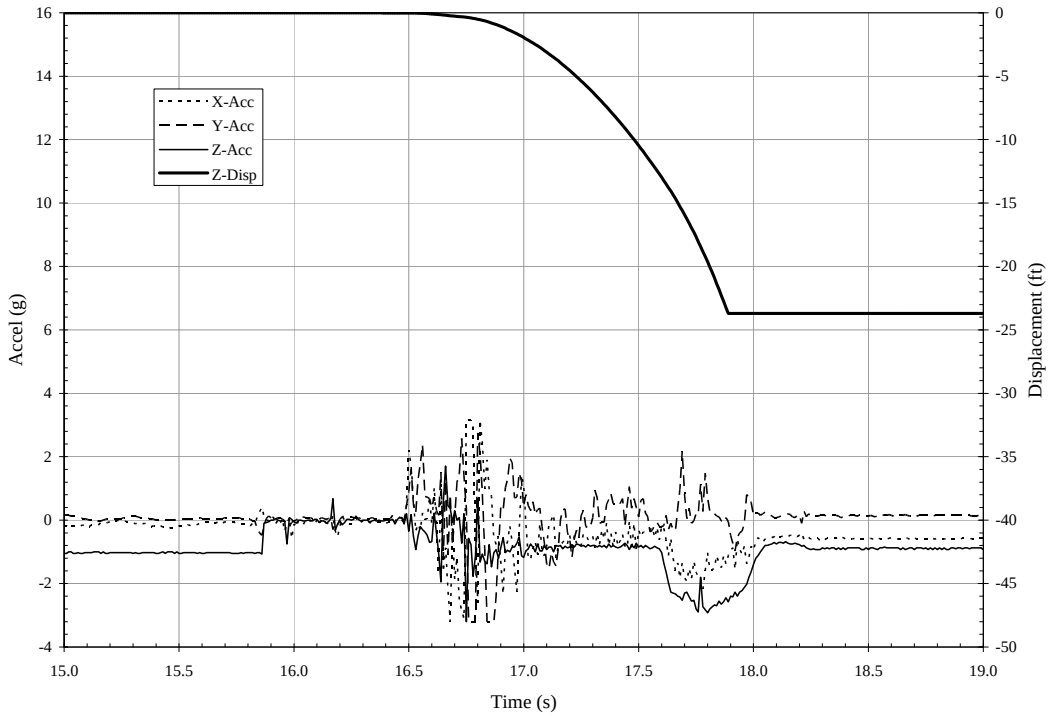
X-Acc
Y-Acc
Z-Acc
Z-Disp
Accel (g)
Displacement (ft)
Time (s)
16
14
12
10
8
6
4
2
0
-2
-4
0
-5
-10
-15
-20
-25
-30
-35
-40
-45
-50
15.0
15.5
16.0
16.5
17.0
17.5
18.0
18.5
19.0

Drop 8

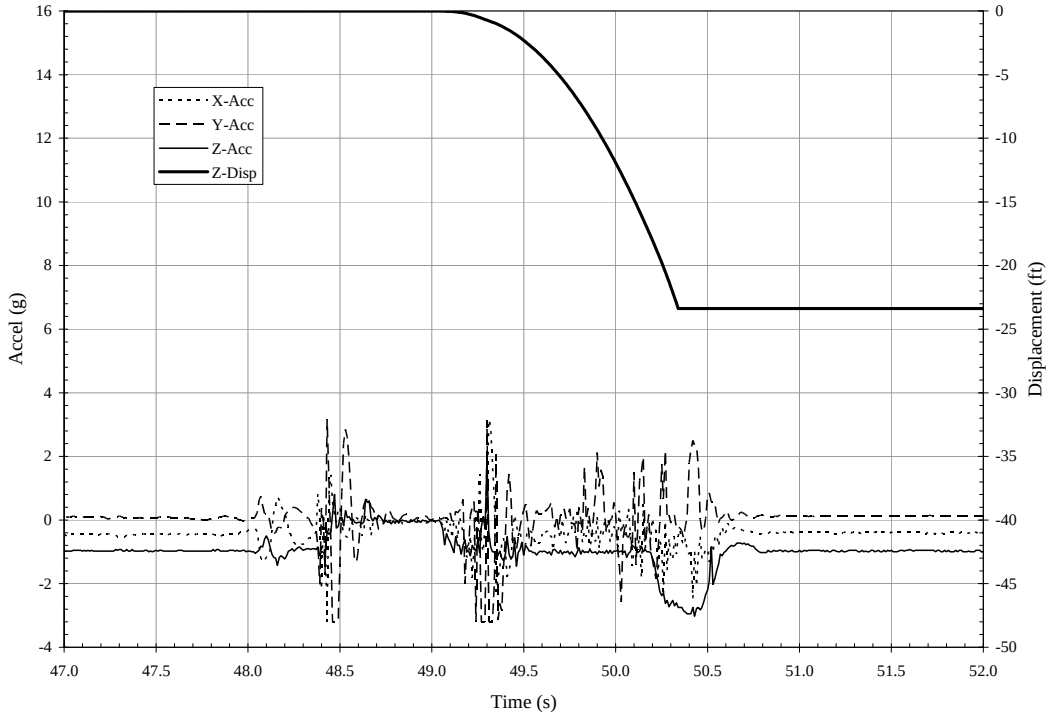
X-Acc
Y-Acc
Z-Acc
Z-Disp
Accel (g)
Displacement (ft)
Time (s)
16
14
12
10
8
6
4
2
0
-2
-4
0
-5
-10
-15
-20
-25
-30
-35
-40
-45
-50
47.0
47.5
48.0
48.5
49.0
49.5
50.0
50.5
51.0
51.5
52.0

Drop 9

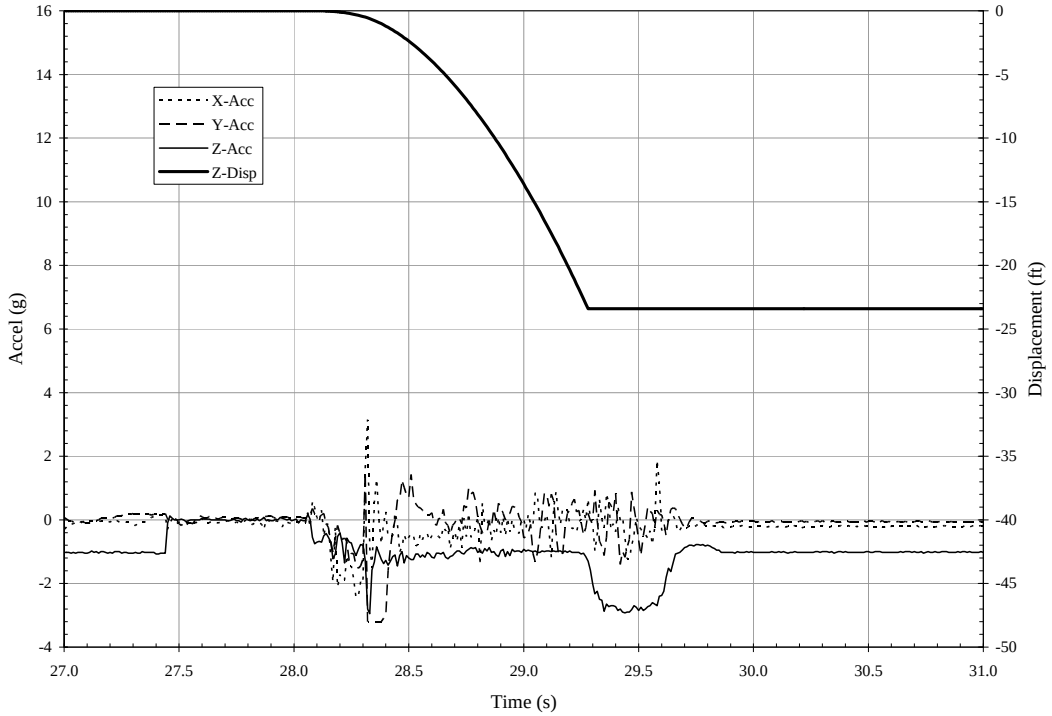


Drop 10

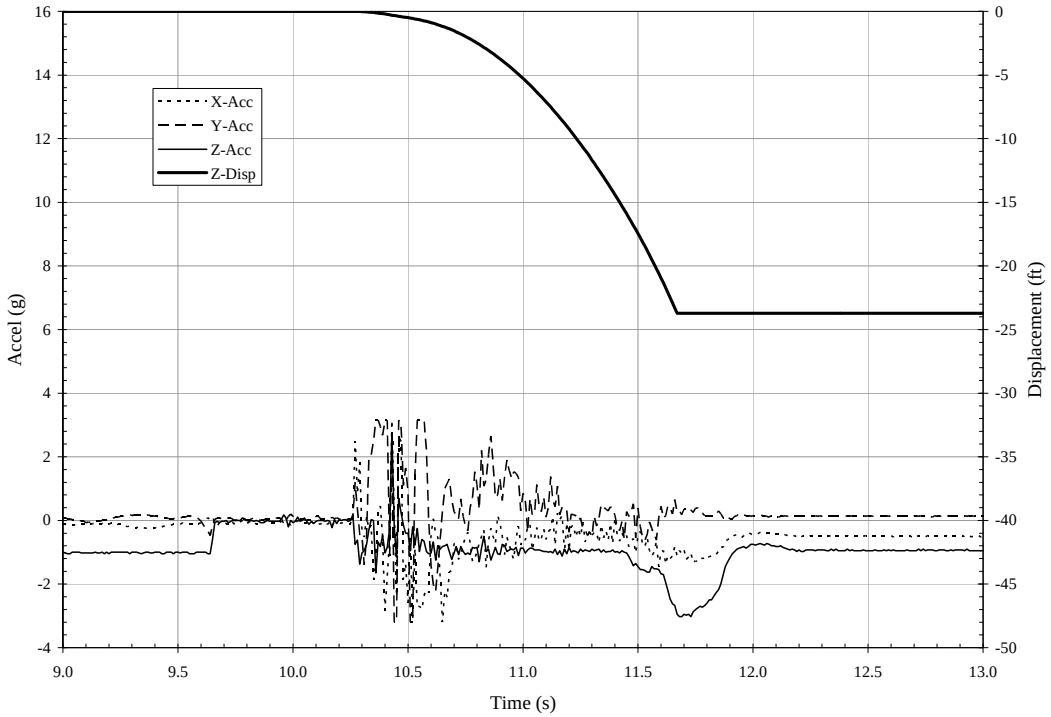

# Appendix D

## Embedment Depth for Clay Drops

| 1-Oct | Embedment Depth (ft) | in |
|---|---|---|
| Drop 1 | 1.81 | 21.72 |
| Drop 2 | 1.85 | 22.20 |
| Drop 3 | 1.92 | 23.04 |
| Drop 4 | 2.14 | 25.68 |
| Drop 5 | 1.83 | 21.96 |
| Drop 6 | 2.01 | 24.12 |
| Drop 7 | 1.89 | 22.68 |
| Drop 8 | 1.86 | 22.32 |
| Drop 9 | 2.10 | 25.20 |
| Drop 10 | 2.20 | 26.40 |
| Drop 11 | 1.88 | 22.56 |
| Drop 12 | 2.17 | 26.04 |
| Drop 13 | 1.88 | 22.56 |
| **15-Oct** | | |
| Drop 1 | 1.86 | 22.32 |
| Drop 2 | 1.94 | 23.28 |
| Drop 3 | 2.06 | 24.72 |
| Drop 4 | 1.98 | 23.76 |
| Drop 5 | 1.84 | 22.08 |
| Drop 6 | 2.02 | 24.24 |
| Drop 7 | 1.85 | 22.20 |
| Drop 8 | 2.27 | 27.24 |
| Drop 9 | 1.89 | 22.68 |
| Drop 10 | 2.02 | 24.24 |
| **15-Feb** | | |
| Drop 1 | 2.47 | 29.64 |
| Drop 2 | 2.50 | 30.00 |
| Drop 3 | 2.63 | 31.56 |
| **31-Mar** | | |
| Drop 1 | 2.36 | 28.32 |
| Drop 2 | 2.42 | 29.04 |
| Drop 3 | 2.62 | 31.44 |
| Drop 4 | 2.59 | 31.08 |
| Drop 5 | 2.51 | 30.12 |
| Drop 6 | 2.54 | 30.48 |
| Drop 7 | 2.71 | 32.52 |
| Drop 8 | 2.39 | 28.68 |
| Drop 9 | 2.41 | 28.92 |
| Drop 10 | 2.72 | 32.64 |

| | | |
|---|---|---|
| **3 in Average Embedment Depth =** | 1.97 | ft |
| | 23.64 | in |
| **9 in Average Embedment Depth =** | 2.53 | ft |
| | 30.34 | in |

# Appendix E

Strain rate constant calculations

```
Function Gamma(z)
'Specific weight of sediment as function of depth, z

   Gamma = (20 + 0.2 * z) + 64          'NC Clay, from Marine Geotechnical Handbook, Figure
2.2-4

End Function
Function Su(z)
'Undrained shear strength of sediment as function of depth, z

   Su = (1 + 0.0033 * 12 * z) * 144     'Normally-consolidated Clay, Table 5.3-2, MGT Hdbk
   Su = Su * 0.5

End Function
Function SuSideAvg(z)
'Average shear strength as function of depth, z

N = 10

delz = z / N

   For i = 1 To N

      SuSideSum = SuSideSum + Su(delz * i)

   Next i

SuSideAvg = SuSideSum / N

If z = 0 Then SuSideAvg = Su(0)

End Function
```

| | | | | | | | | | | | | | | | | | | | | | | |
|---|---|---|---|---|---|---|---|---|---|---|---|---|---|---|---|---|---|---|---|---|---|---|
| | A | B | C | D | E | F | G | H | I | J | K | L | M | N | O | P | Q | R | S | T | U | V |
| 1 | | Drop Alt: | 21.0 | ft | Diam: | 3 | in | | Penetrator Shape (From NFESC Handb | | | | | | | | | | | | | |
| 2 | | Weight: | 21.1 | lb | $L_{nose}$: | 3.25 | in | | Long, Cylindrical Penetrators | | | | | | | | | | | | | |
| 3 | | Wet Wt: | 17.6 | lb | $L_{body}$: | 33.4 | in | | | | | | | | | | | | | | | |
| 4 | | (m + a): | 0.765 | slugs | $A_{drag}$: | 7.1 | $in^2$ | | $S_e$*: | 4 | | | | | | | | | | | | |
| 5 | | $E_{impact}$: | 203.5 | ft-lb | $A_{nose}$: | 7.1 | $in^2$ | | $C_e$: | 4 | | | | | | | | | | | | |
| 6 | | $E_{soil}$: | 215.2 | ft-lb | $C_{drag}$: | 0.50 | | | $C_o$: | 0.11 | | | | | | | | | | | | |
| 7 | | $P_{nose}$: | 12.1 | psi | $C_{added\_m}$: | 1.00 | | | St: | 2 | | | | | | | | | | | | |
| 8 | | Max g: | 6.6 | g's | $\rho_{seawater}$: | 1.9879 | slug/cuft | | Max Se: | 5.000 | | | | | | | | | | | | |
| 9 | | Embed: | 20.4 | in | $V_{impact}$: | 23.1 | fps | | | | | | | | | | | | | | | |
| 10 | | Exposed: | 16.2 | in | $V_{term}$: | 26.9 | fps | | | | | | | | | | | | | | | |
| 11 | | | | | | | | | | | | | | | | | | | | | | |
| 12 | | Time | Altitude | Density | Distance | Velocity | | Drag | Acceleration | | su_nose | su_side | Se_nose | Se_side | Nt | γb | Soil Wt | Wbi | $Z_{embed}$ | $A_{nose}$ | $A_{side}$ | $Q_{nose}$ | $F_{side}$ |
| 13 | | sec | ft | slug/cuft | ft | ft/s | m/s | lb | $ft/sec^2$ | g's | psf | psf | | | | pcf | lb | lb | ft | $ft^2$ | $ft^2$ | lb | lb |
| 14 | | 0.000 | 21.000 | 1.988 | 0.000 | 0.000 | 0.000 | 0.000 | 23.019 | 0.715 | 72.356 | 72.000 | 1.000 | 1.000 | 6.168 | 0.000 | 0.000 | 17.600 | 0.000 | 0.000 | 0.000 | 0.000 | 0.000 |
| 15 | | 0.020 | 20.995 | 1.988 | 0.005 | 0.460 | 0.140 | 0.005 | 23.012 | 0.715 | 72.356 | 72.000 | 1.261 | 1.262 | 6.168 | 0.000 | 0.000 | 17.600 | 0.000 | 0.000 | 0.000 | 0.000 | 0.000 |
| 16 | | 0.040 | 20.982 | 1.988 | 0.018 | 0.920 | 0.281 | 0.021 | 22.992 | 0.715 | 72.356 | 72.000 | 1.436 | 1.437 | 6.168 | 0.000 | 0.000 | 17.600 | 0.000 | 0.000 | 0.000 | 0.000 | 0.000 |
| 17 | | 0.060 | 20.959 | 1.988 | 0.041 | 1.380 | 0.421 | 0.046 | 22.958 | 0.714 | 72.356 | 72.000 | 1.567 | 1.569 | 6.168 | 0.000 | 0.000 | 17.600 | 0.000 | 0.000 | 0.000 | 0.000 | 0.000 |
| 18 | | 0.080 | 20.926 | 1.988 | 0.074 | 1.839 | 0.560 | 0.082 | 22.911 | 0.712 | 72.356 | 72.000 | 1.673 | 1.675 | 6.168 | 0.000 | 0.000 | 17.600 | 0.000 | 0.000 | 0.000 | 0.000 | 0.000 |
| 19 | | 0.100 | 20.885 | 1.988 | 0.115 | 2.296 | 0.700 | 0.129 | 22.851 | 0.710 | 72.356 | 72.000 | 1.760 | 1.762 | 6.168 | 0.000 | 0.000 | 17.600 | 0.000 | 0.000 | 0.000 | 0.000 | 0.000 |
| 20 | | 0.120 | 20.835 | 1.988 | 0.165 | 2.752 | 0.839 | 0.185 | 22.777 | 0.708 | 72.356 | 72.000 | 1.835 | 1.837 | 6.168 | 0.000 | 0.000 | 17.600 | 0.000 | 0.000 | 0.000 | 0.000 | 0.000 |
| 21 | | 0.140 | 20.775 | 1.988 | 0.225 | 3.207 | 0.978 | 0.251 | 22.691 | 0.705 | 72.356 | 72.000 | 1.900 | 1.902 | 6.168 | 0.000 | 0.000 | 17.600 | 0.000 | 0.000 | 0.000 | 0.000 | 0.000 |
| 22 | | 0.160 | 20.706 | 1.988 | 0.294 | 3.660 | 1.116 | 0.327 | 22.591 | 0.702 | 72.356 | 72.000 | 1.958 | 1.960 | 6.168 | 0.000 | 0.000 | 17.600 | 0.000 | 0.000 | 0.000 | 0.000 | 0.000 |
| 23 | | 0.180 | 20.629 | 1.988 | 0.371 | 4.111 | 1.253 | 0.412 | 22.480 | 0.699 | 72.356 | 72.000 | 2.009 | 2.012 | 6.168 | 0.000 | 0.000 | 17.600 | 0.000 | 0.000 | 0.000 | 0.000 | 0.000 |
| 24 | | 0.200 | 20.542 | 1.988 | 0.458 | 4.559 | 1.390 | 0.507 | 22.356 | 0.695 | 72.356 | 72.000 | 2.056 | 2.058 | 6.168 | 0.000 | 0.000 | 17.600 | 0.000 | 0.000 | 0.000 | 0.000 | 0.000 |
| 25 | | 0.220 | 20.446 | 1.988 | 0.554 | 5.005 | 1.525 | 0.611 | 22.220 | 0.691 | 72.356 | 72.000 | 2.098 | 2.100 | 6.168 | 0.000 | 0.000 | 17.600 | 0.000 | 0.000 | 0.000 | 0.000 | 0.000 |
| 26 | | 0.240 | 20.342 | 1.988 | 0.658 | 5.448 | 1.660 | 0.724 | 22.072 | 0.686 | 72.356 | 72.000 | 2.137 | 2.139 | 6.168 | 0.000 | 0.000 | 17.600 | 0.000 | 0.000 | 0.000 | 0.000 | 0.000 |
| 27 | | 0.260 | 20.228 | 1.988 | 0.772 | 5.888 | 1.795 | 0.846 | 21.913 | 0.681 | 72.356 | 72.000 | 2.172 | 2.174 | 6.168 | 0.000 | 0.000 | 17.600 | 0.000 | 0.000 | 0.000 | 0.000 | 0.000 |
| 28 | | 0.280 | 20.106 | 1.988 | 0.894 | 6.324 | 1.928 | 0.976 | 21.743 | 0.676 | 72.356 | 72.000 | 2.205 | 2.207 | 6.168 | 0.000 | 0.000 | 17.600 | 0.000 | 0.000 | 0.000 | 0.000 | 0.000 |
| 29 | | 0.300 | 19.975 | 1.988 | 1.025 | 6.757 | 2.060 | 1.114 | 21.562 | 0.670 | 72.356 | 72.000 | 2.235 | 2.237 | 6.168 | 0.000 | 0.000 | 17.600 | 0.000 | 0.000 | 0.000 | 0.000 | 0.000 |
| 30 | | 0.320 | 19.836 | 1.988 | 1.164 | 7.186 | 2.190 | 1.260 | 21.371 | 0.664 | 72.356 | 72.000 | 2.264 | 2.266 | 6.168 | 0.000 | 0.000 | 17.600 | 0.000 | 0.000 | 0.000 | 0.000 | 0.000 |

Penetrometer Specifications

**3-inch Penetrometer**

Dry Weight= 21.1 lbs
Wet Weight= 17.6 lbs
Diameter= 3 in
Nose Length= 3.25 in
Body Length= 25.5 in

**9-inch Penetrometer**

Dry Weight = 146.1 lbs
Wet Weight = 104.66 lbs
Diameter = 9 in
Nose Length = 6.5 in
Body Length = 39 in